EXPERIMENTAL INVESTIGATION OF A 16 INCH DIAMETER WATERPISTON PROPULSOR AT SPEEDS UP TO 23 FEET PER SECOND AND GAS TEMPERATURES UP TO 3600° F

By

V. E. Johnson, Jr., R. A. Barr,
D. Kowalyshyn, and R. Bateman

May 1991

Prepared for

David Taylor Research Center
Bethesda, Maryland 20084

Under
Contract Number N00167-88-D-0033

Delivery Order 0008

Tracor Hydronautics, Inc. 7210 Pindell School Road Laurel, Maryland 20723

UNCLASSIFIED

SECURITY CLASSIFICATION OF THIS PAGE

REPORT DOCUMENTATION PAGE

1a REPORT SECURITY CLASSIFICATION	1b RESTRICTIVE MARKINGS UNCLASSIFIED
2a SECURITY CLASSIFICATION AUTHORITY	3 DISTRIBUTION/AVAILABILITY OF REPORT DISTRIBUTION: UNLIMITED
2b DECLASSIFICATION/DOWNGRADING SCHEDULE	
4 PERFORMING ORGANIZATION REPORT NUMBER(S) Technical Report 88006-1	5 MONITORING ORGANIZATION REPORT NUMBER(S) DTRC - SD - CR - 2[illegible]
6a NAME OF PERFORMING ORGANIZATION Tracor Hydronautics Inc.	6b OFFICE SYMBOL (If applicable)
7a NAME OF MONITORING ORGANIZATION David Taylor Research Center	
6c ADDRESS (City, State, and ZIP Code) 7210 Pindell School Road Laurel, Md. 20723	7b ADDRESS (City, State, and ZIP Code) MCPO Code 1240 Bethesda, Md. 20084-5000
8a NAME OF FUNDING/SPONSORING ORGANIZATION MCRDAC - AWT	8b OFFICE SYMBOL (If applicable)
9 PROCUREMENT INSTRUMENT IDENTIFICATION NUMBER N00167 88 D 0033 Del. Ord. 0008	
8c ADDRESS (City, State, and ZIP Code) Quantico, Va.	10 SOURCE OF FUNDING NUMBERS

PROGRAM ELEMENT NO	PROJECT NO	TASK NO	WORK UNIT ACCESSION NO
62131M	C3150		DN 978568

11 TITLE (Include Security Classification)
Experimental Investigation of a 16 Inch Diameter Water Piston Propulsor at Speeds Up to 23 Feet per Second and Gas Temperatures up to 3600° F.

12 PERSONAL AUTHOR(S)
V.E. Johnson, Jr., R.A. Barr, D. Kowalyshyn, and R. Bateman

13a TYPE OF REPORT	13b TIME COVERED	14 DATE OF REPORT (Year, Month, Day)	15 PAGE COUNT
FINAL	FROM 2/89 TO 5/91	1991 MAY	121

16 SUPPLEMENTARY NOTATION

17 COSATI CODES			18 SUBJECT TERMS (Continue on reverse if necessary and identify by block number)
FIELD	GROUP	SUB GROUP	Water Piston Propulsor Marine Propulsion Combustors Amphibian Vehicles

19 ABSTRACT (Continue on reverse if necessary and identify by block number)

The Water Piston Propulsor (WPP) is a unique device that combines prime mover, transmission, and propulsor into a single unit. High pressure heated gas is expanded directly on columns of water so as to add momentum to ingested fluid and thereby produces thrust. The water piston propulsor theoretically has a very high power per unit volumne and power per unit weight if the gas can be transmitted to the rotor with minor pressure loss and if the gas can be expanded in the water passages with only a moderate transfer of heat to the ejected water. This potentially high power-to-volume ratio makes the WPP an attactive candidate to propel Marine Corps high speed amphibians. This repot describes the investigation carried out using a full-scale water piston rotor and its fuel oil gas generator. The main results of this study are that the heat lost to the expelled water during its expulsion when the input gas temperature is about 3000°F is approximately 67% of the input heat and that the thrust produced by the WPP was substantially less than predicted. Consequently, the power-to-unit volume ratio of the system tested will be significantly greater than that for a conventionally propelled amphibian vehicle.

20 DISTRIBUTION/AVAILABILITY OF ABSTRACT	21 ABSTRACT SECURITY CLASSIFICATION
☐ UNCLASSIFIED/UNLIMITED ☒ SAME AS RPT ☐ DTIC USERS	

22a NAME OF RESPONSIBLE INDIVIDUAL	22b TELEPHONE (Include Area Code)	22c OFFICE SYMBOL
Richard Swanek	(301) 227-1852	MCPO

DD FORM 1473, 84 MAR 83 APR edition may be used until exhausted. All other editions are obsolete.

SECURITY CLASSIFICATION OF THIS PAGE
UNCLASSIFIED

Although the water piston propulsor is shown to be unattractive as applied to a Marine Corps amphibian with an air breathing fuel oil gas generator; it is believed that the water piston propulsor may be attractive for high speed underwater missiles with other types of gas generators. The report also discusses a typical Marine Corps amphibian propulsion requirement and the reason that water piston propulsion is potentially attrative. It further describes the water piston propulsor envisioned for application to an amphibian vehicle and summarizes the research and development program that has preceded the present investigation.

TABLE OF CONTENTS

TABLE OF CONTENTS (CONCLUDED)

LIST OF FIGURES

LIST OF FIGURES (CONTINUED)

LIST OF FIGURES (CONCLUDED)

LIST OF TABLES

1.0 INTRODUCTION

The Water Piston Propulsor (WPP) is a unique device that combines prime mover, transmission, and propulsor into a single unit. High pressure heated gas is expanded directly on columns of water so as to add momentum to ingested fluid and thereby produces thrust. As described in References 1 through 13 the water piston propulsor theoretically has a very high power per unit volume and power per unit weight if the gas can be transmitted to the rotor with minor pressure loss and if the gas can be expanded in the water passages with only a moderate transfer of heat to the ejected water. This potentially high power-to-volume ratio made the WPP an attractive candidate to propel Marine Corps 20 ton high speed amphibians, and since 1983 the David Taylor Research Center has sponsored a research and development program at Tracor Hydronautics to study the feasibility of a water piston propelled amphibious vehicle for the Marine Corp.

References 5 through 13 describe the work that has led to the tests of a full scale propulsor designed for a 20 mph amphibian. This report describes the investigation carried out using a full-scale water piston rotor and its fuel oil gas generator.

The main results of this study are that the heat lost to the expelled water during its expulsion when the input gas temperature is about 3000°F is approximately 67 percent of the input heat and that the thrust produced by the WPP was substantially less than predicted. Consequently, the power-to-unit volume ratio of the system tested will be significantly greater than that for a conventionally propelled amphibian.

Although the water piston propulsor is shown to be unattractive as applied to the Marine Corps amphibian with an air breathing fuel oil gas generator; it is believed that the water piston propulsor may be attractive for high speed underwater missiles with other types of gas generators.

The following background section discusses the Marine Corps amphibian propulsion requirement and the reason that water piston propulsion is potentially attractive. It describes the water piston propulsor envisioned for application to the amphibian and summarizes the research and development program that has preceded the present investigation.

1.1 Background

1.1.1 General

The mission of Marine Corps amphibious vehicles typically includes transits from ship to shore, shore to shore, and shore to ship. If an assault is made on a fortified shore, it may be necessary for the ships launching the amphibians to remain well offshore to achieve an over the horizon launch. Long waterborne transits at slow speeds can seriously reduce the combat effectiveness of the vehicle occupants. For this reason, technologies required to increase the speed in water of future Marine Corps amphibious vehicles are being explored. The effort in this report is focused on applying the water-piston propulsor to a 20 ton amphibious vehicle with a waterborne speed of 20 miles per hour.

Marine Corps amphibious vehicles are designed to spend only 20 percent of their operating life cycle in water. During the remaining 80 percent of their operating life, the vehicles must provide an overland capability that will meet the projected threat. The two operating modes have power requirements that are quite different. The overland power for a 20 ton amphibian varies from idle to approximately 400 HP. The required power in water is about 1500 HP if 20 plus miles per hour speeds are to be sustained.

Various engine options to meet the two power levels associated with the land and water operations are as follows:

1. A single engine capable of operating in two power regimes,

2. A combination of engines, one of which may be secured when operating ashore, or

3. A land propulsion engine augmented by an in-water propulsor that may not meet the conventional description of an engine. This report focuses on the third option.

The ideal source of in water propulsive thrust for Marine Corps amphibious vehicle is one that converts a high energy density fuel into hydrodynamic thrust within a minimum volume and weight, with reduced complexity and reasonable overall efficiency. The water piston propulsor, an unconventional propulsive device, has been shown to meet this objective if the mechanical, hydraulic and internal heat losses are not excessive.

This section describes briefly the working of the water piston propulsor and the tests that have been conducted during recent years to determine its operating characteristics (References 1 through 13).

These experimental and analytical results were used to design four 16 inch diameter propulsors suitable for propelling a 20 ton tracked amphibious vehicle at a speed of 20 plus mph in water (References 6 through 13). In these design studies the power required of the prime mover (air compressor) varies from 625 to 750 HP depending on the gas pressure and temperature values selected for the propulsors. The propulsion system when operating with moderate heat loss offers large weight and volume savings compared with more conventional propulsion systems (diesels and waterjets, etc.) because of the elimination of a large diesel or gas turbine engine with their associated water drive trains.

1.1.2 Water Piston Propulsor Description

The Water Piston Propulsor (WPP) was originally conceived to propel underwater weapons at high speeds. The device eliminates the majority of the process steps that occur between the generation of the working fluid and the production of thrust. In a conventional propulsion system, the hot, high pressure gas is expanded in a piston or a turbine engine. The shaft power produced is conditioned in a gear box and transmitted to the propeller or waterjet which produces thrust by imparting momentum to a stream of sea water. The same effect is accomplished in the water piston propulsor by having the gas expand directly against columns of sea water entrained in helical channels or passages within the water piston rotor.

The complete water piston propulsor system shown in Figure 1 consists of an air compressor and its drive which supplies high pressure air to a combustion chamber where heat is added. The resulting hot gas is then expanded through the propulsor. The total heat energy delivered to the system is the sum of that delivered to the compressor prime mover and that delivered to the combustion chamber. In a typical WPP design, the energy supplied to the compressor is substantially less than half the total energy, the combustion chamber is small and light and the rotor is similar in size and weight to a waterjet pump or a propeller. Therefore, the volume and weight of the complete system is much less than for a conventional water jet system or a propeller system if the WPP ideal performance is not greatly reduced by real fluid losses and heat losses from the gas to the water.

The propulsor rotor, which is the heat of the WPP consists of a cylindrical thruster which has many helical channels. When the thruster rotates about a shaft, the channels are blocked and unblocked alternately. As shown inFigure 1-1, water enters through the open face of the rotor, into the channels is the rotor. The closed face has a gas port connected to the high pressure, hot gas source. As the channel passes the gas port, the gas enters the channel and imparts momentum to the mass of water as it enters and completes its expansion after the port closes. Because the interfacial area between the gas and the water is small, energy loss is kept to a

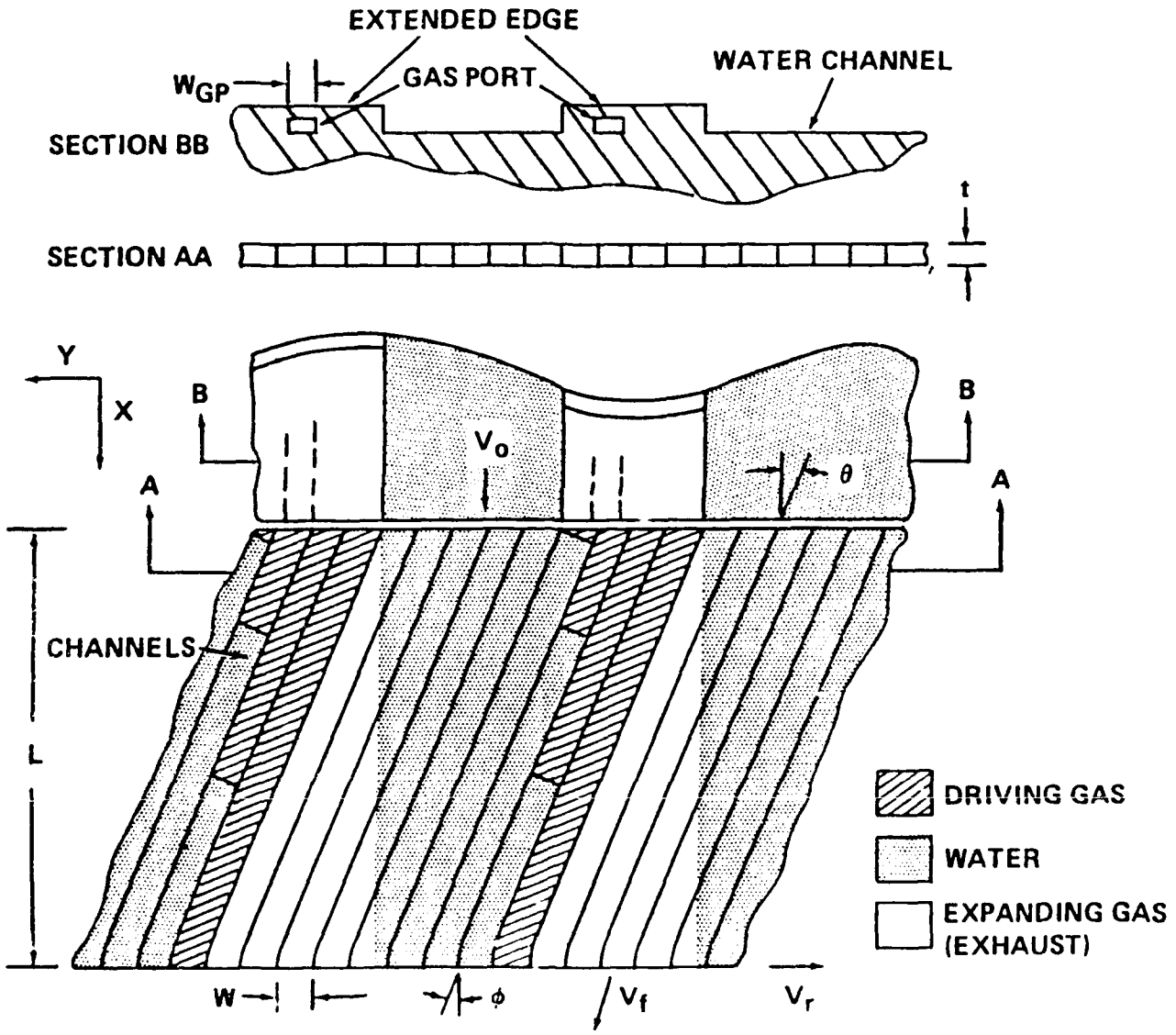

Figure 1-1. A Developed Schematic View of the Water Piston Propulsion System

minimum; thus, a large mass of water is accelerated by a small quantity of gas. After expulsion of the water, the channel is filled with water again when its opening has emerged from behind the closed face or obturator. The incoming water scavenges the expanded gas. The cycle is repeated for each channel, each time it passes a gas port. Each cycle produces an axial and a tangential impulse because of the change in momentum between the exiting and the incoming flow in both axial and tangential directions. The total thrust in the axial direction equals the product of the number of cycles per second and the axial impulse per fill cycle; the number of cycles per second is the product of numbers of channels, the number of gas ports, and the thruster rotative speed in revolutions per second. The device can produce thrust and tangetial force (torque) at the same time, if needed. If the device is used solely to produce thrust, the exit angle is set so as to produce the torque necessary to provide the required rpm (against seal and bearing friction, and external hydrodynamic friction) for the most critical operating condition. Fine control of the RPM at other conditions may then be provided by a control device such as a brake.

1.2 Previous Studies

In 1983 the David Taylor Research Center (DTRC) funded a small study by Tracor Hydronautics, Inc. to determine whether water piston propulsor technology was applicable to the propulsive requirements of a Marine Corps amphibious assault vehicle. This study (Reference 6) indicated that the water piston propulsor was potentially applicable to Marine corps requirements.

Conceptual design of a water piston propulsion system for a 20-ton Marine Corps tracked amphibian was conducted by Tracor Hydronautics, Inc. between September 1983 to January 1984 under a DTRC competitive procurement. The preliminary design and performance analysis (Reference 6) showed that an ideal water piston propulsion system offered large weight and volume savings because of the elimination of a large diesel or gas turbine engine with its associated water drive trains. Since land power requirements are approximately one third of the water power requirements, the land power can be provided by a relatively small diesel engine coupled to either a conventional land drive train or the compressor of a water piston propulsor.

Upon completion of this second study, it was determined that a significant amount of design work would be required to translate the initial design into hardware suitable for water tunnel or tow tank testing to confirm the performance predictions. DTRC developed a task in which Tracor Hydronautics, Inc. was required to establish the hardware and labor needs of both a full-scale rotor test in a model basin and a half-scale rotor test in a water tunnel. This work (Reference 8) was completed in April 1984 and provided important insight into the areas where information was lacking or where technological problems existed. In particular, the following key problem areas were identified:

1. Maintenance of a stable gas-water interface at high gas temperature.

2. Heat transfer rate to the water in the passage during gas expansion.

3. Combustor/rotary seal interface design.

4. Rotary seal life at elevated temperature (2,000 to 3,000°F).

5. Effect of channel aspect ratio on the complete filling of the passages with water.

6. Rotor construction cost and rotary seal cost.

Cost estimates included in the Tracor Hydronautics effort indicated that cost of full-scale rotor tests in a model basin could exceed $600K while the high speed channel model tests would cost about $500K. At this point, it was determined that DTRC would pursue the combustor procurement through alternate avenues. Concurrently, a less expensive yet technically acceptable method of determining the stability of the gas-water interface and the heat loss to the water as the hot gas expanded through the passage was desired. To meet this need, DTRC issued a task in June 1984 to Tracor Hydronautics, Inc. for the design, construction, and initial testing of a single channel device. The significant advantage of testing the non-rotating, single channel device was that it allowed direct observation of the gas-water interface. By proceeding with the less expensive single channel tests, it was felt that it might be possible to deduce the heat transfer effects and to determine the stability of the interface at high temperatures before a commitment was made to the full-scale rotor test. Such a developmental approach also provided opportunity for the optimization of the gas injection scheme of the full-scale rotor by varying the gas port shape, size, and the port opening time in the single channel tests.

Such single channel tests were carried out and the results reported in Reference 5 and 10. The single channel test results reported in Reference 5 indicated that the gas-water interface inside the trapezoidal channel remained stable and intact during the entire cycle of operation at gas temperatures up to the highest test value of 685°F. The preferred gas port configuration was trapezoidal with a shape that just matched the passage cross section. In Reference 10, it was concluded that the heat loss, based on he data obtained, would be about 45 percent at the design temperature of 3000°F, but this conclusion was not considered convincing because of the large extrapolation required from data obtained at only 700°F maximum.

Since the Marine Corps found the water piston propulsor so advantageous (if the heat loss were substantially less than 45 percent) and since the high estimate of heat loss might be in error; DTRC decided to proceed with tests of a full scale rotor at full scale temperature (3,000°F) in the Tracor Hydronautics High Speed Channel.

Reference 11 described in detail the model, the combustor and the instrumentation and controls required for the HSC tests. Reference 11 also outlined a preliminary test program and presented estimated costs to accomplish the goals of the program. Figures 1-2, 1-3 and 1-4 show various aspects of the proposed test equipment. Figure 1-2 shows two proposed test setup for the full scale propulsor installed in the test section of the Tracor Hydronautics High Speed Water Channel. Figure 1-3 shows a schematic of the proposed instrumentation for the tests. Figure 1-4 shows the Solar gas turbines combustor and seal assembly designed and built for the tests. More details of this combustor and seal assembly are given in Reference 14. Figure 1-5 shows the bronze seal with trapezoidal gas port built for and used in the fluid set of tests.

In 1988 DTRC issued Task Order 0308 under Contract No. N00167-88-D-0033 to carry out the program described in Reference 11. This present report describes the work carried out, including the objectives of the study, the means used to accomplish these objectives, and the results obtained.

1.3 Program Objectives

It is apparent from the foregoing background discussion that the principal purpose of the present investigation was to determine the water piston propulsor performance when driven with hot gas so that the results obtained could be used to confidently assess the feasibility of the propulsor applied to the Marine Corps amphibian.

Clearly the performance measurements that are of principal interest in assessing feasibility are the thrust and efficiency at design conditions. If the propulsor produces less than design thrust at its design speed and rpm when supplied with the design pressure, the thrust cannot be increased except by increasing the pressure, because the rotor diameter and length cannot be easily increased. Increased pressure demands increased compressor power. If the required thrust is produced but the mass flow is higher than the design value because of leakage or heat loss, the compressor power must again be increased and additional fuel will be required. If the overall volume required for the larger compressor and its prime mover (plus the additional fuel) equals or exceeds the values required for a conventional propulsion system the water piston propulsor will lose any advantage. It was shown in Reference 13 that

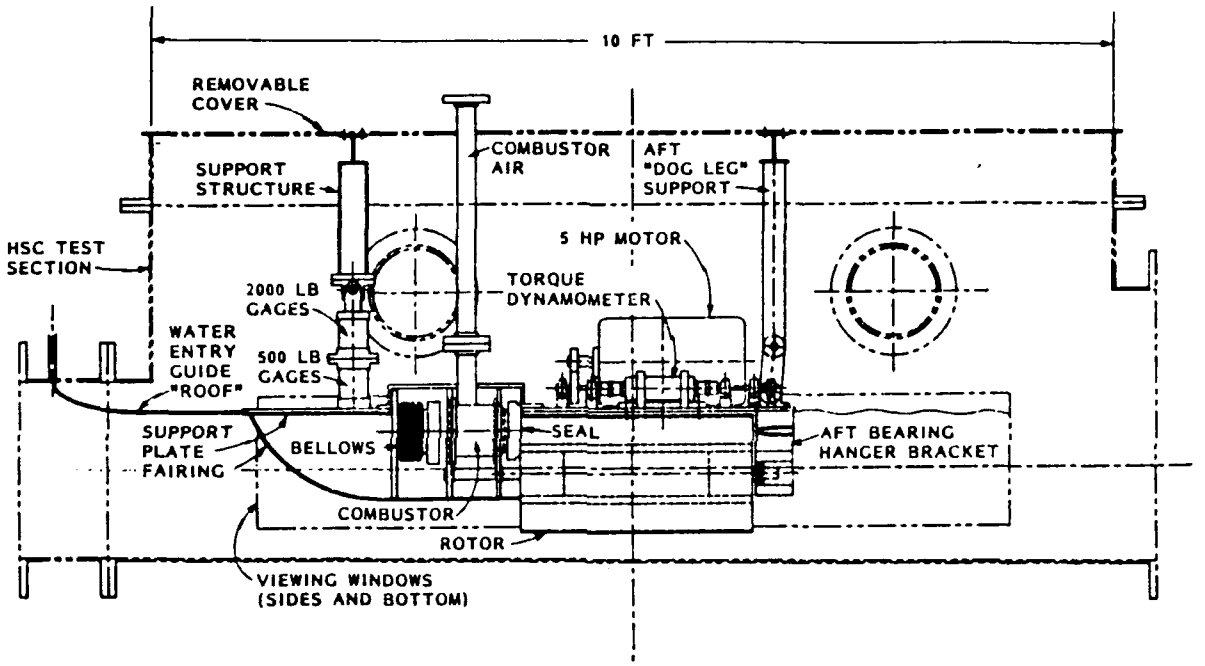

Figure 1-2. Full-Scale Test Setup

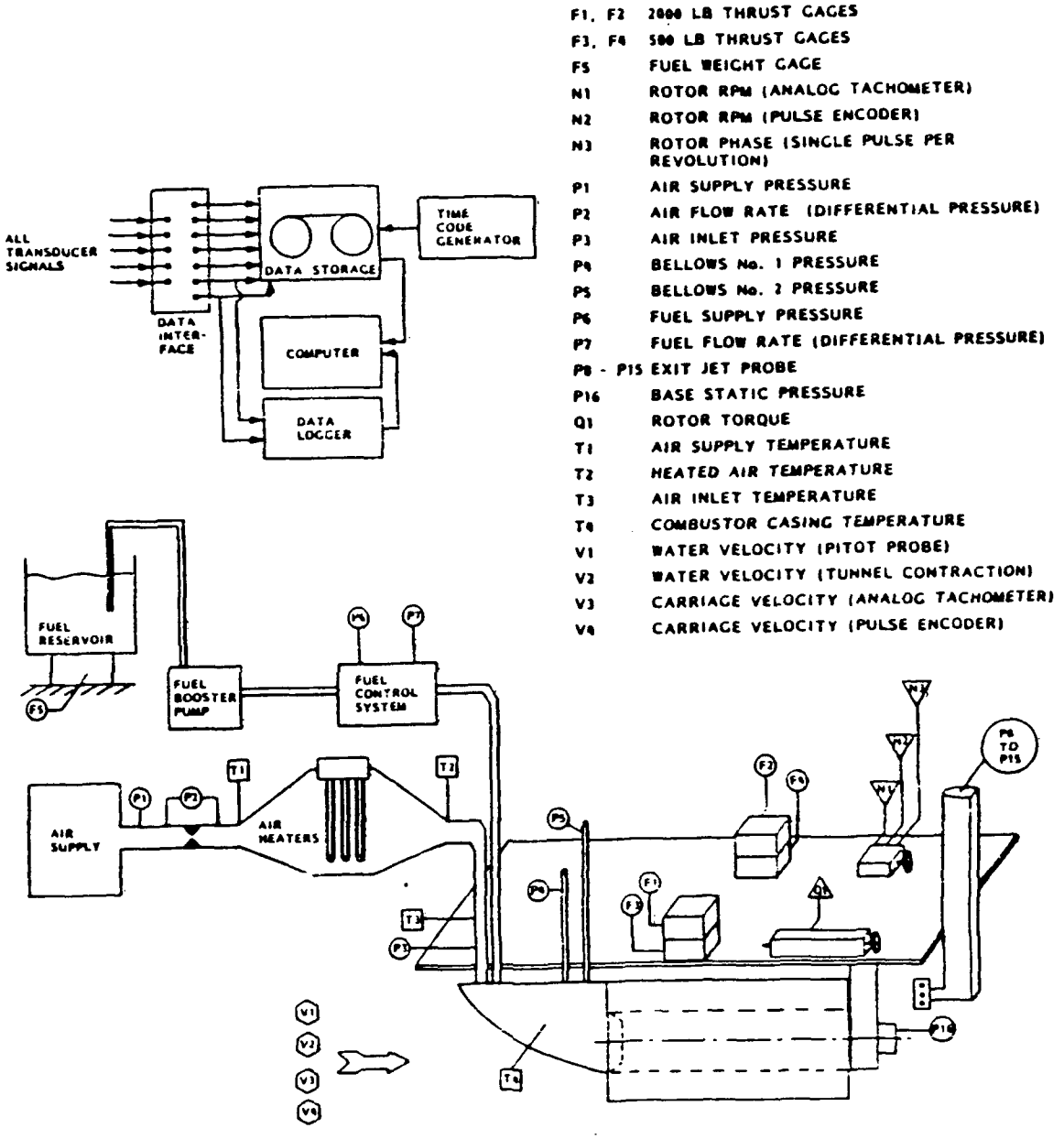

Figure 1-3. Test Setup and Instrumentation Schematic

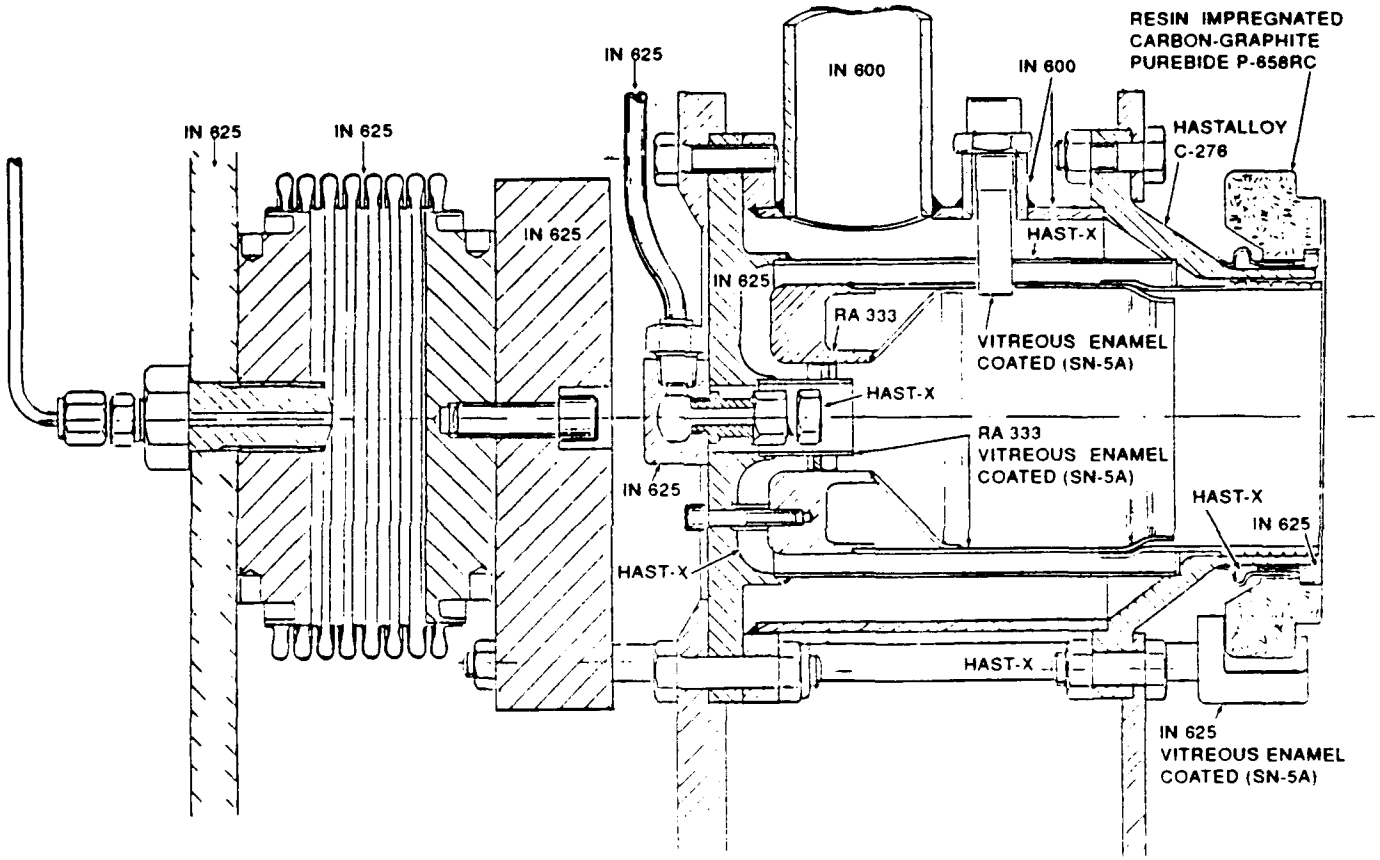

Figure 1-4. Cross-Section View of Solar Combustion Chamber Used for Water Piston Tests

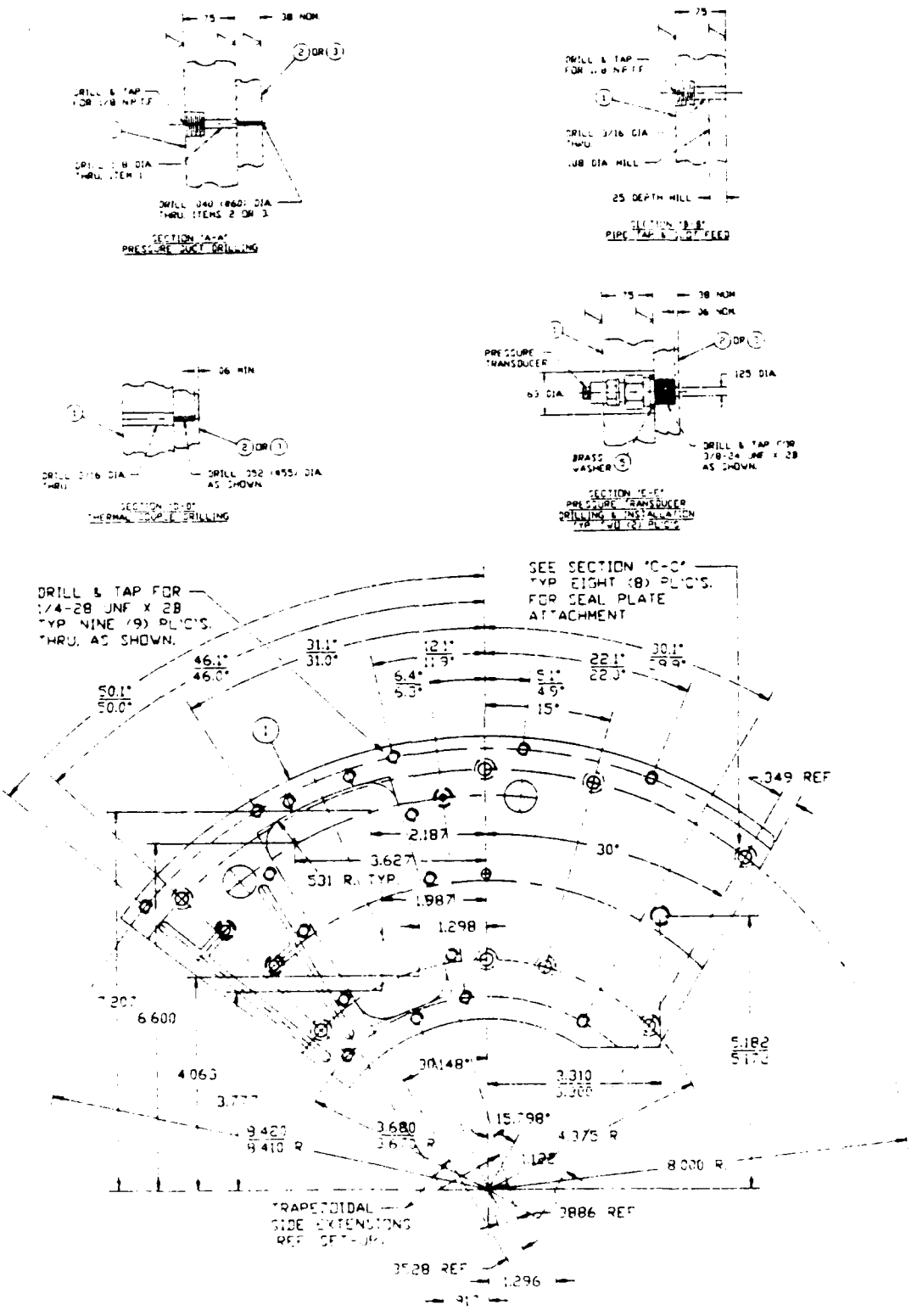

Figure 1-5. Bronze Seal with Trapezoidal Gas Port
Built for and Used in Final Tests

the actual efficiency of the WPP must exceed 50% of the adiabatic overall efficiency in order to be considered competitive.

The objective of the present study is to conduct tests at various operating conditions that can be used to convincingly predict prototype values of thrust and energy input and thus overall efficiency so that the feasibility of the water piston propulsor as applied to the Marine Corps amphibian may be confidently assessed. The following sections of this report review the theoretical predictions of thrust and efficiency and the various scaling parameters involved in the water piston propulsion performance.

2.0 DESCRIPTION OF WATER PISTON TEST SETUP AND EQUIPMENT

A special set up was developed for testing the water piston propulsion system in the Tracor Hydronautics High Speed Water Channel (HSC). The test setup was designed to reproduce as closely as possible, within the constraints imposed by the limited HSC test section dimensions, all external and internal arrangements of the proposed amphibian water piston propulsion system.

2.1 Description of Water Piston Propulsion System

The test setup consisted of nine major components which were:

1. Water Piston Rotor and Support Bearings
2. Combustion Chamber/Seal Assembly
3. Inlet Fairing and Cover
4. Surface Plate and Thrust Gage Assemblies
5. Rotor Motor Drive and Torque Dynamometer
6. Fuel Supply System
7. Compressed Air Supply System
8. Additive Injection System
9. Variable Area Exit Nozzle
10. Instrumentation

These components are described in this section. Figure 2-1 shows two views at the complete WPP test setup.

2.1.1 Water Piston Rotor, Support and Drive Systems

The water piston rotor was 16 inches in diameter and 32 inches long. The full scale rotor was the Tracor Hydronautics design described in Reference 11. This rotor was designed using requirements specified by the Marine Corps. The primary characteristics of this rotor are given in Table 2-1 which was taken from Reference 11. Figure 2-1 shows two views of the rotor and Figure 2-2 shows dimensions of the rotor.

Table 2-1. Water Piston Propulsor Geometry

Outside diameter	16.0	inches
Length	32.0	inches
Number of helical channels	16	
Number of gas supply ports	1	
Entrance helix angle	40.9	degrees
Exit helix angle	14.2	degrees
Channel width at entrance	2.18	inches
Channel height	4.0	inches
Wall thickness of channel	0.125	inches
Gas supply port width	1.66	inches
Gas supply port length	3.0	inches
Radial location of gas supply port	6.0	inches
Width for fill	27.7	inches
Ratio of entrance to exit area of the channel	0.9	

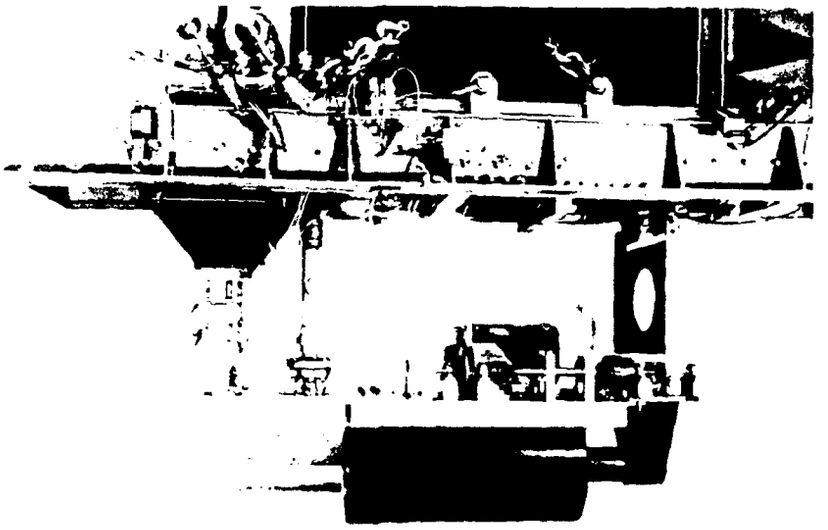

a. Profile View

b. Bow Quarter View - Original Fairing

Figure 2-1 Overall Views of Water Piston Test Setup

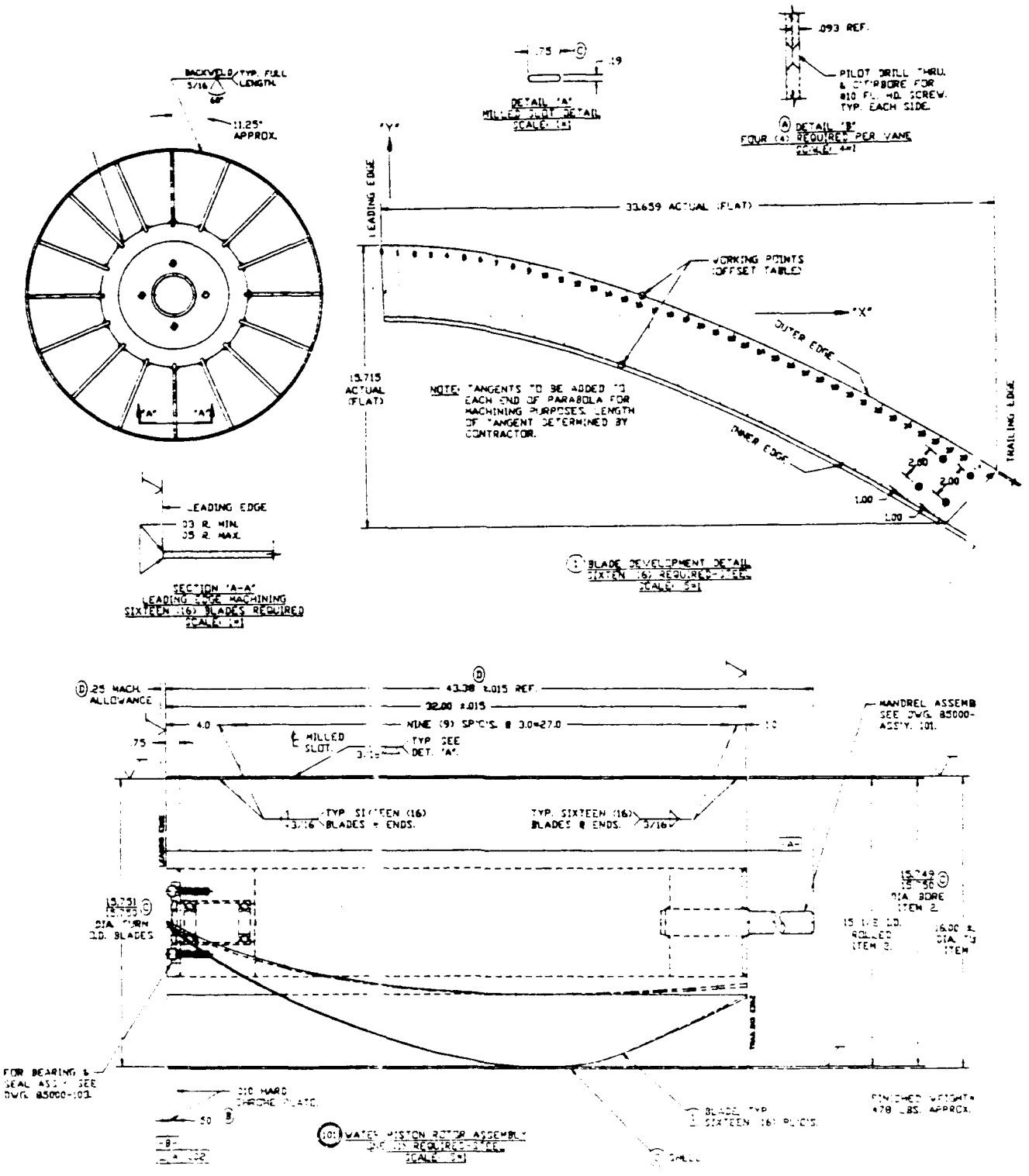

Figure 2-2. Drawing of Water Piston Rotor

2.1.2 Combustion Chamber/Seal Assembly and Fuel Supply System

The combustion chamber and seal assembly was designed and initially built by Solar Gas Turbines. The assembly as delivered by Solar consisted of the following components:

1. Combustion chamber
2. Fuel and air supply pipes
3. Obturator seal with carbon seal face
4. Two seal positioning bellows
5. Support structure and tie rods

Figure 2-3 shows several views of the combustion chamber/seal assembly. This figure shows the assembly as received from Solar and the assembly after installation of the new seal and transition. All of the above components can be identified in these photographs. The design and geometry of this system are described in Solar reports to DTRC. Figure 2-4 shows the assembly installed ahead of the rotor. Figure 1-4 shows a cross-section drawing of this assembly.

Air was supplied to the combustion chamber through a vertical pipe which was connected to the air compressor and heater through several flexible pipes. The inlet pipe contains an orifice type flow meter used to determine the air mass flow rate and a thermocouple used to determine the air temperature upstream of the combustion chamber inlet. Figure 2-5 shows the large Atlas Copco air compressor and air supply pipe used in these tests.

Fuel (diesel oil) was supplied to the combustion chamber using a pressurized fuel tank and regulating valve. Figure 2-6 shows the fuel pump and metering system. A Solar designed microprocessor system was used to control fuel mass flow rate. The microprocessor used inlet air mass flow rate and temperature and commanded gas combustion temperature to determine required fuel mass flow rate. Instrumentation was provided by Solar to measure air inlet temperature and fuel mass flow rate and these data were used by a microprocessor feedback loop to establish and maintain the desired combustion temperature.

In the first set of tests an alcohol injection system was used to facilitate initiation of combustion. Initially, alcohol was injected into the combustion chamber and ignited; once ignition was established, the fuel oil supply system was turned on and fuel oil combustion initiated. Once fuel oil ignition occurred, alcohol flow was terminated. For the second set of tests no alcohol injection was used and direct ignition of fuel oil was used successfully.

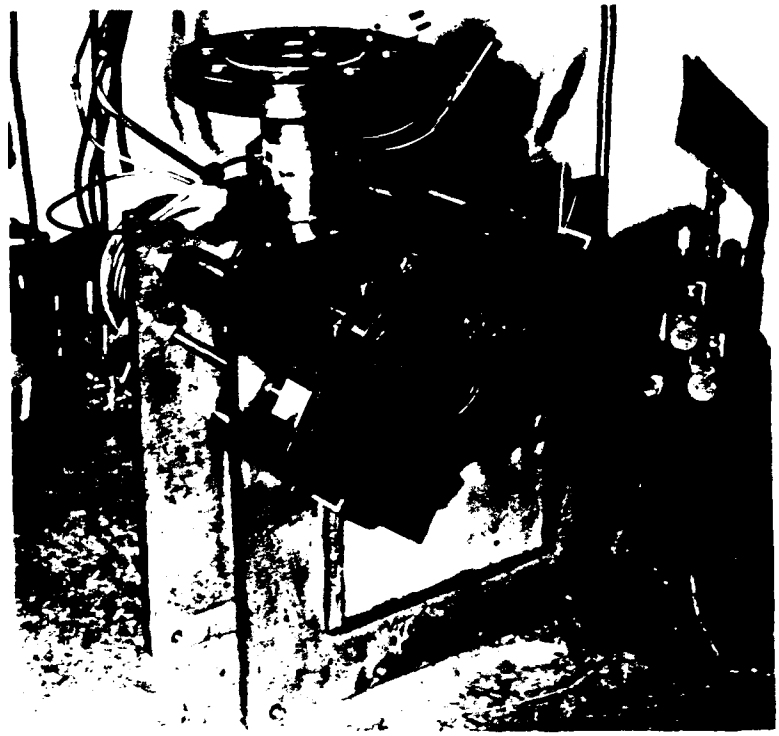

a. View Looking Forward Showing Seal (As Received from Solar)

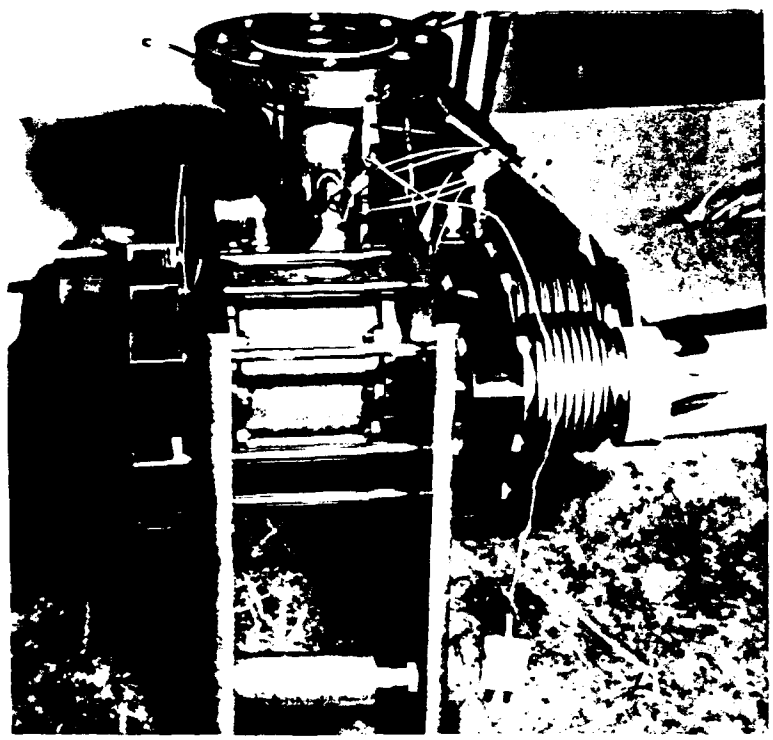

b. Profile View Showing Combustion Chamber, Air Supply Manifold and Seal Positioning Bellows Assembly

Figure 2-3. Two Views of Seal Combustion Chamber Assembly

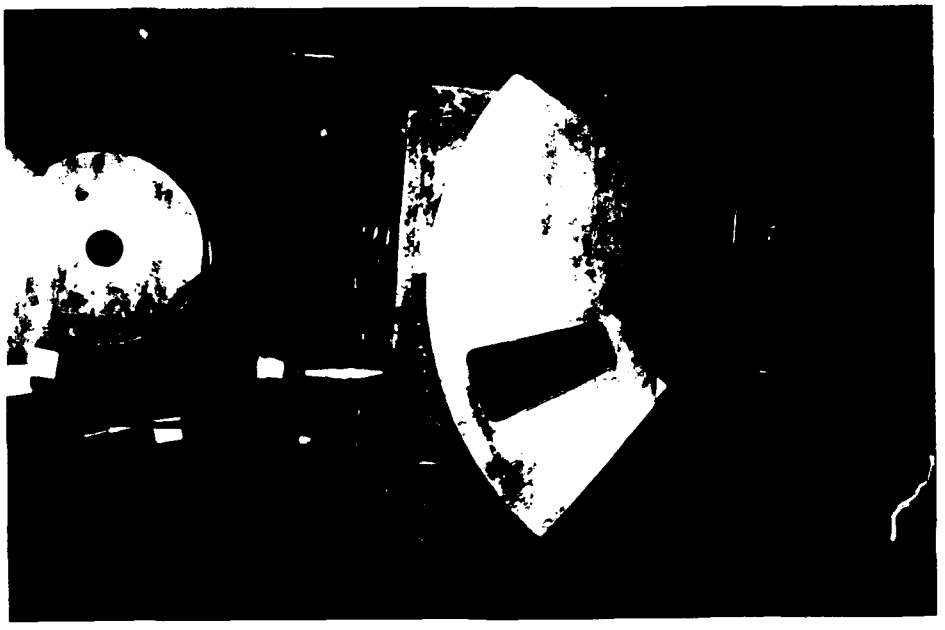

c. View Looking Forward Showing Bronze Seal and Trapezoidal Gas Port

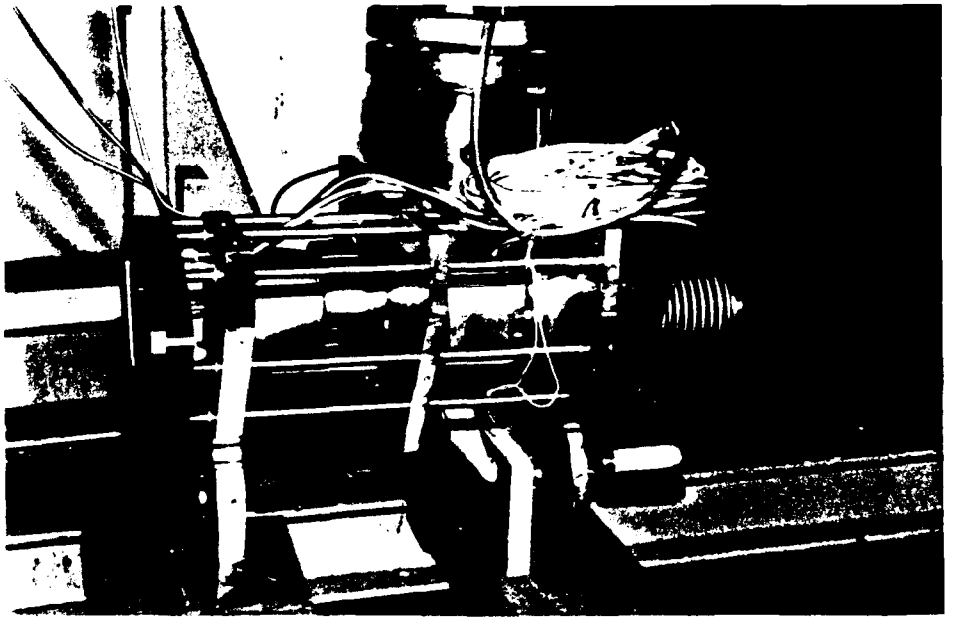

d. Profile View Showing Transition Used with Bronze Seal

Figure 2-3 (Concluded)

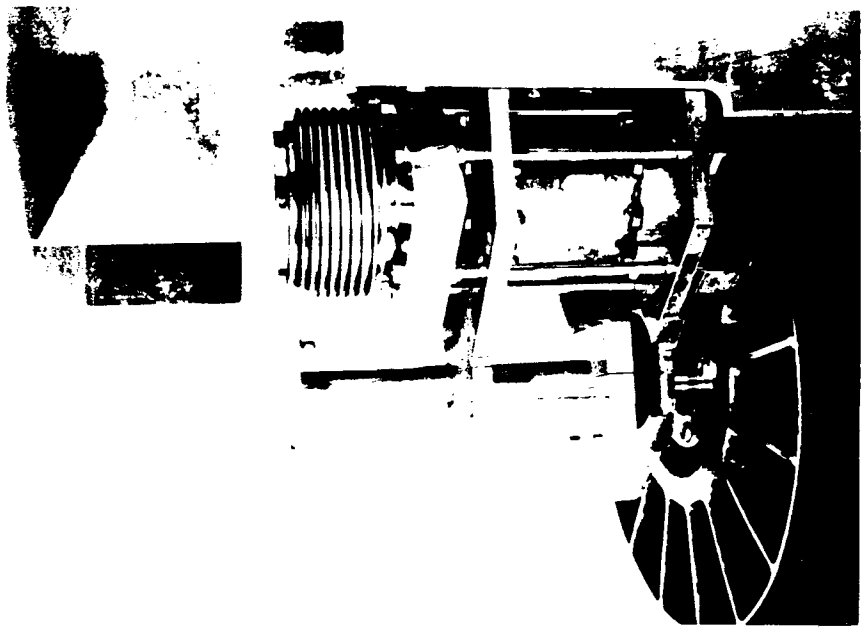

a. Installation for Initial Tests with Graphite Seal

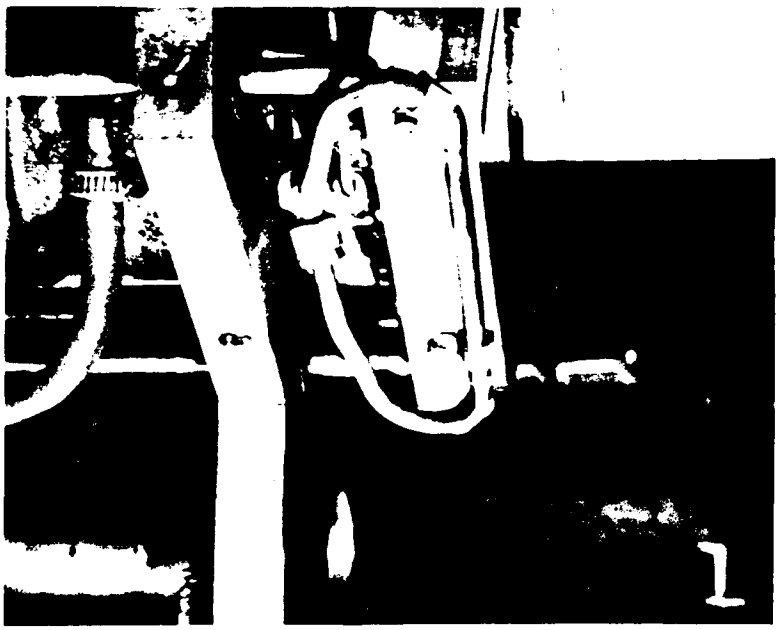

b. Installation for Initial Tests with Bronze Seal
(Showing Chemical Additive Supply Manifold)

Figure 2-4. Two Views of Seal/Combustion System Installation

a. Atlas Copco Mobile Compressor

b. Air Heater Mounted on Wall

Figure 2-5. Compressed Air Supply System

a. System as Received from Solar

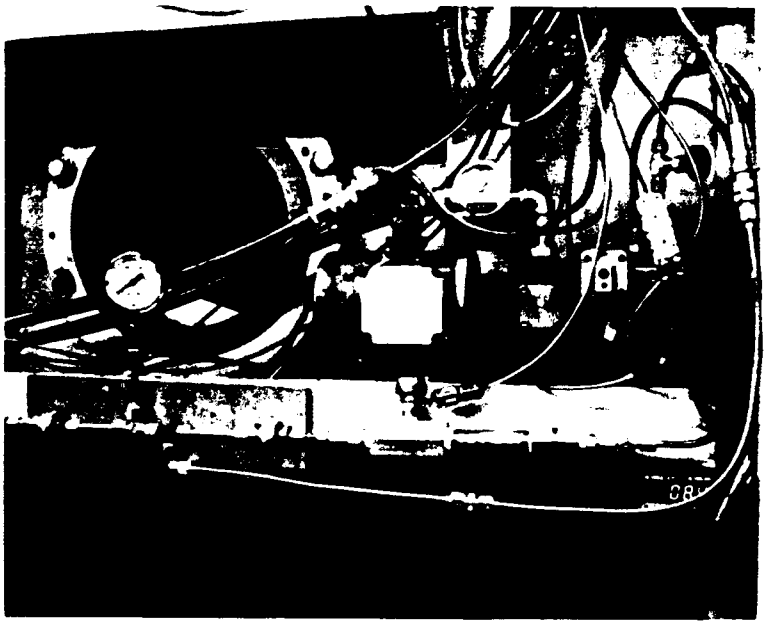

b. System Installed at High Speed Water Channel

Figure 2.6. Fuel Pumping and Metering System

Combustion temperature was not measured in the first set of tests, but was calculated by the Solar microprocessor using standard combustion equations. For the second set of tests a thermocouple was placed in the transition section and used to measure gas temperature near the middle of the transition cross-section.

The system was designed to allow axial and rotational motions of the seal in order to minimize the gap between the seal and rotor and resulting gas leakage through this gap. The two bellows, whose internal pressures could be adjusted, provided the axial force required to push the seal, which was attached to the free to slide tie rods, against the rotor. Bellows pressure was provided by high pressure bottled nitrogen and a differential pressure regulator and was typically set to be 10 to 20 psi greater that the chamber gas pressure.

The initial combustion chamber/seal assembly delivered by Solar included a carbon block seal with the combustion chamber termination in an o-ring seal within the circular gas port in the seal. After the initial tests it was decided to build a new seal with a trapezoidal gas port that approximately matched the shape of the rotor flow passages. This gas port had a radial length of 3.75 inches and a mean width of 1.75 inches.

It was necessary to build a transition piece for use between the round combustion chamber exit and the trapezoidal seal gas port. In order to avoid gas flow separation in the transition, a minimum transition length of 5.5 inches was selected. Transition geometry, which is shown in Figure 2-7, was selected to minimize adverse pressure gradients and the danger of gas flow separation. In order to accommodate this transition piece, it was necessary to relocate the combustion chamber and to lengthen by 5.5 inches the tie rods which hold together the combustion chamber/seal assembly. The transition piece which was cast of stainless steel, can be seen in the photograph in Figure 2-3.

For the new seal with trapezoidal gas port it was decided, as a result of the problems experienced with the carbon seals, to use a bronze seal face with an aluminum backing. This seal was fitted with several pressure taps and with a narrow radial slot for injecting additives into the flow passages. Figure 2-3 shows several views of this new bronze obturator seal. The additive injection slot located near the leading edge of the seal can be seen in these photographs.

2.1.3 Base Plate, Thrust Gage Assemblies and Inlet Fairing

The complete water piston propulsion system was mounted on an aluminum base plate which also acted as a roof for the HSC test section. This base plate, which was actually a rigid beam structure

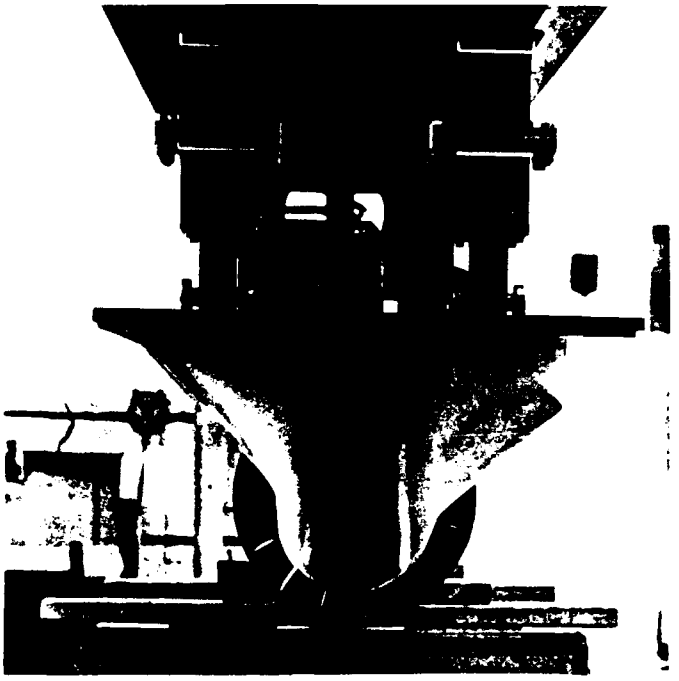

a. Bow View

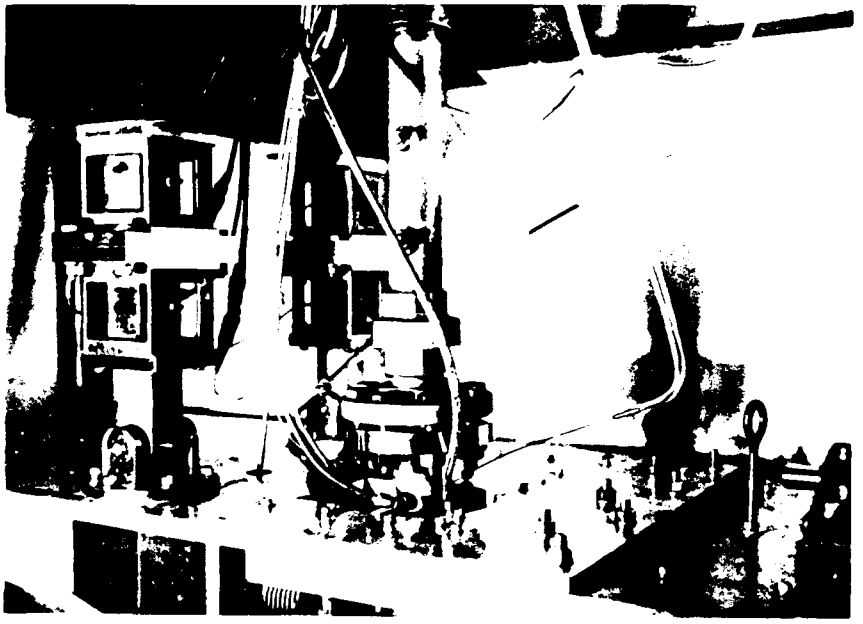

b. Stern Quarter View

Figure 2-7 Two Views of Test Setup Showing Four Modular Force Gages Used to Measure Axial Force

approximately six inches deep, 23 inches wide and seven feet long, was attached to the HSC cover through two forward and one aft vertical members, as shown in Figures 2-1 and 2-7. The two forward, rigidly attached members each contained two block gages used to measure total system thrust. The single after member was free to rotate so that total axial force was transmitted through the block gages and measured. Two pairs of block gages of different capacity were used to insure that thrust force was accurately measured over a wide range of thrust forces.

The electric drive motor used to set desired rotor RPM and the shaft torque dynamometer were mounted on the top of the base plate. The rotor shaft support bearings were mounted from the base plate - the after bearing support can be clearly seen in Figure 2-8 The rotor shaft timing belt drive runs between the V-supports for the after bearing.

The flow fairing used to cover the combustion chamber/seal assembly was mounted on the bottom of the base plate as shown in Figure 2-1. This fairing is also used to direct the flow into the proper fill area of the rotor. It was necessary to make the width of this fairing about 0.625 inches wider than the seal due to the geometry of the combustion chamber/seal assembly provided by Solar. The fairing shape was designed to minimize the forebody drag and thrust tare.

2.1.4 Compressed Air System

One component of the proposed propulsion system not modeled in these tests was the air compressor and air heating system. For these tests a large trailer mounted Atlas Copco compressor which could provide maximum air mass flow rates up to one pound per second and maximum air pressure up to about 200 psi (with less mass flow) was used. The compressor has a pressure regulating system which permits accurate control of outlet pressure with varying mass flow (discharge) rate. Figure 2-5 shows this compressor.

Air from the compressor passed through a Chromolox electric heater, which could be used to heat the air to 900 to 1000 deg. F. The heater was used to obtain test data for air at temperatures of 400 to 1000 deg. F and to preheat air for combustion tests in order to facilitate initiation of combustion. For cold air tests the heater was turned off. The heater is shown in Figure 2-5.

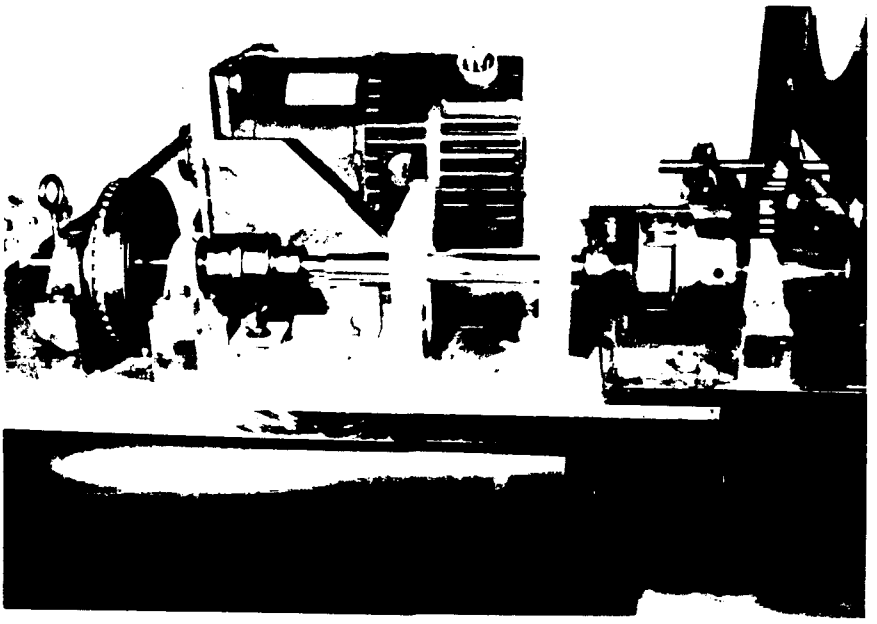

a. Five Horsepower Motor and Drive (Torque Balance Not Shown)

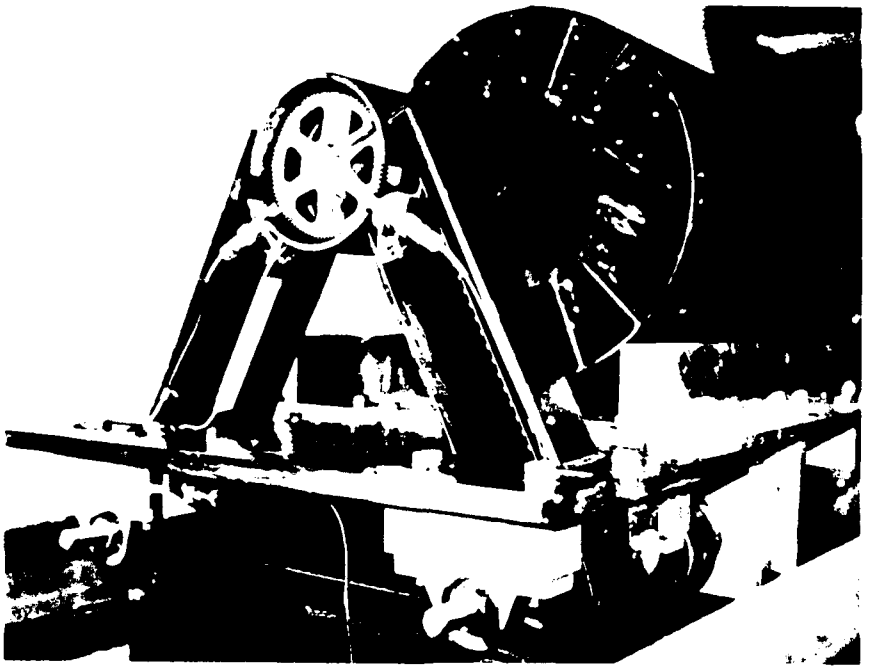

b. Timing Belt Drive to Rotor (Showing Magnetic RPM Pickup)

Figure 2-8 Rotor Motor Drive System

2.1.5 Additive Injection System

Based on the large heat losses (75% or more) observed in the initial set of tests, it was concluded that a large volume of bubbles, mist or foam was being generated in the flow passage as it sealed. It was expected that the injection of chemical additives, such as anti-foaming agents or long-chain polymers, into the flow passage as it was sealing might inhibit the formation of such flows, and thus reduce the effective area for heat transfer from the gas to the water.

A system was provided in the second set of tests for injecting various additives into the flow passage as the passage was sealing. This system consisted of a narrow radial slot in the seal located approximately 0.375 inches form the seal leading edge. Flow of the diluted additive to this slot was supplied by a line connected through a flow regulating valve to a pressurized supply bottle containing the additive. The additive injection system is shown in Figure 2-4.

2.1.6 Instrumentation

Instrumentation was provided to measure all important water, air, fuel and gas flow and thermodynamic properties and net thrust, torque and RPM of the water piston.

Measured water, air and gas properties included:

1. Water flow free stream velocity and temperature
2. Atmospheric pressure and temperature
3. Compressed air pressure, temperature and mass flow rate
4. Fuel supply pressure, temperature and mass flow rate
5. Combustion gas temperature (second set of tests only)
6. Chemical additive mass flow rate

The temperature of the combustion gas was calculated for both sets of tests using NASA combustion equations supplied by Solar and imbedded in the Solar microprocessor. The pressures in the flow passages were also measured at two points on the seal using small static pressure taps and Kistler dynamic pressure transducers.

HSC water flow velocity was measured using a standard pitot static probe located. The differential pressure from this probe (total pressure minimum static pressure) was determined using a Pace

variable reluctance pressure transducer with a 10 psi range. Water temperature was measured using a (TBD).

Air temperature, pressure and mass flow rate were measured in the supply pipe just above the combustion chamber. Mass flow rate was measured using a standard ASME orifice plate and two static pressure taps connected to Pace variable reluctance pressure gages. The tap downstream of the orifice plate was also used to determine the air supply pressure. The air supply pressure was also measured by pressure taps provided by Solar in the air flow portion of the combustion chamber and these pressures and Solar steady flow calibrations were used by the microprocessor to determine air mass flow rate.

Fuel mass flow rate was measured using two flow meters, one supplied by Solar and connected to the microprocessor and, one supplied by Tracor Hydronautics. Fuel temperature and pressure were measured using instrumentation supplied by Solar and connected to its microprocessor.

In the second set of tests the gas or air temperature was measured using a thermocouple in the transition piece between the combustion chamber and the seal. For the air and combustion tests, K and B type thermocouples with a maximum temperature ratings of 2200 and 3500 deg. F., respectively, were used.

The differences between the pressures in both bellows and the pressure in the air supply was measured using pace variable reluctance pressure gages.

Measured water piston operating parameters were thrust (net axial force), shaft torque and RPM or rotative speed. These were measured as follows:

1. Thrust: Total axial force was measured using variable reluctance block or force gages located near the forward end of the base plate, as shown in Figure 3-7. These gages, which have minimal cross-talk with other modes of motion, were oriented to measure axial force (thrust). Each vertical pair of gages contained gages with 500 and 1000 pound capacities to insure accurate results over the widest possible force range.

2. Torque: Shaft torque was measured in the motor output shaft using a Tracor Hydronautics manufactured variable reluctance torque dynamometer. This dynamometer measured the rotor torque plus the frictional torques in the rotor bearings, the motor output shaft bearing and the timing belt drive.

3. RPM: The water piston rotor RPM was measured using a magnetic pickup located on the shaft at the after end of the rotor.

2.2 Description of Test Facility

All tests were conducted in the Tracor Hydronautics High Speed, Variable Speed Free Surface Water Channel (HSC). The HSC is described in detail in the paper included as Appendix A of the report.

For these tests the channel was operated at a fixed water depth of 20 inches and with atmospheric pressure in the test section. All water piston tests equipment including the rotor, combustion and seal assembly, drive motor, instrumentation and hydrodynamic fairing were mounted on a base plate as described earlier. This plate acted as a roof for the test section, although there was some flow around the edges of the plate, particularly at higher tests speeds. Figure 1-2 shows a schematic view of the full-scale test setup in the test section of the HSC.

The HSC Data Acquisition System was used to acquire, integrate and process all data except the data from the Solar microprocessor. The HSC data loggers integrated all data for the specified period of three seconds. These time averaged data was then transmitted to data files in a MicroVAX, which was used to accomplish all data reduction. The test number and data from the Solar microprocessor were input by hand into these MicroVAX data files. Figure 1-3 shows a schematic of the proposed instrumentation. The actual instrumentation used in the tests was essentially the same as that shown in Figure 1-3.

3.0 OVERVIEW OF PROJECT

The project included two sets of tests of the prototype water piston propulsor. The second or final set of tests was undertaken as a result of the poor performance found in the first or initial set of tests. Major modifications were made to the seal and gas port in response to results of the initial tests. The final set of tests were similar to but more extensive than the first set of tests.

3.1 Initial Test Program

During the initial test program, three types of tests were carried out:

1. Tare tests to determine system tare forces

2. Gas leakage and bellows pressure tests

3. Propulsion tests with cold and warm compressed air and hot gas produced by combustion.

A set of tare tests were carried out in an attempt to determine any correction to the measured model thrust required to determine correct prototype thrust for the same operating conditions.

A set of leakage tests were carried out to determine the effect on thrust of gas leakage caused by an inadequate difference between the pressure in the two seal bellows and the propellant gas pressure. The bellows pressures were systematically varied to determine the minimum pressure difference at which thrust became independent of pressure difference. This pressure difference was used in all tests to minimize gas leakage and friction between the rotor and seal.

A number of propulsion tests were carried out to determine the effect on performance of important test variables. During these tests the primary test variables were channel flow velocity, propellant gas temperature and pressure, and rotor RPM. During individual tests one or more of these variables was varied in a systematic manner to determine the effect of important operating parameters such as pressure ratio, pressure coefficient or advance coefficient on water piston performance. Test velocities were limited to values at 12 to 17 feet per second, with most tests conducted at 15 feet per second. Tests were not conducted at higher velocities due to the large amounts of water thrown out of the HSC test section at these speeds.

3.1.1 Initial Test Plan

The carefully designed original test plan for the tests was presented in Reference 11. While this plan guided the conduct of all tests, it was neither desirable nor practical to follow it in detail. The actual test plan evolved during testing and reflected the increasing knowledge base achieved with each test and the capabilities of the air compressor and HSC.

3.1.2 Test Scope

Table 3-1 summarizes the test conditions for all tests conducted during the initial test program. This table indicates that gas temperature and pressure and advance coefficient (RPM) were typically varied during each test. However, important variations were made in only one or two of these principal test variables.

3.1.3 Mechanical Problems Encountered

The principal mechanical problems encountered in these tests were the failure of the rotor shaft soon after the start of tests and the failure of one graphite seal about half way through the tests. The rotor shaft failure was attributed primarily to defective shaft material. The massive damage sustained by one seal and the damage observed on two other seals were felt to be due primarily to the inability of the seal graphite material to resist the cyclic thermal shock. Minor, and probably not significant, failure of part of the internal structure of the combustion chamber was observed after completion of testing.

Significant and progressive oil or soot fouling of the HSC water occurred during the tests. After completion of tests much of the internal structure of the HSC was found to be coated with an oily/sooty mixture and some fouling of the inside of the combustion chamber was observed. It was thus concluded that combustion efficiency was significantly lower than predicted by Solar, perhaps due to the much lower than design gas pressures used in the reduced velocity tests.

3.1.4 Performance and Conclusions

The principal conclusions arising from these tests were:

1. Performance (thrust and efficiency) were worse than predicted.

2. Heat losses were much greater than the estimated 50 percent with 3000 deg F gas.

3. The graphite seals appear unsuitable for extended at-sea operation.

4. Use of the variable area nozzle led to somewhat degraded rather than improved performance, probably due to the significant axial gap between the nozzle plate and rotor and the resulting radial deflection of the exit flow from the passages.

It was concluded that the poor performance achieved in these tests could be significantly improved by using a trapezoidal gas port with length equal to the passage length rather than a round gas port.

3.1.5 Configuration Modifications

As a result of this initial set of tests it was decided to modify the propulsor by:

1. Replacing the graphite seal with a bronze seal

2. Replacing the round gas port with a trapezoidal gas port with a 3.75 inch length and providing a transition between the combustion chamber and the seal that minimized the danger of flow separation.

3. Reducing the fairing width to reduce its blockage of inflow to and filling of the rotor.

4. Provision of a thermocouple in the new transition just ahead of the seal to measure gas temperature just before it entered the rotor flow passages.

All of these modifications were made before the start of the final set of tests.

3.2 Final Test Program

During the final test program, using the trapezoidal gas port two types of tests were carried out:

1. Gas leakage and bellows pressure tests.

2. Propulsion tests with cold and warm compressed air and hot gas produced by combustion.

For this series, no new tare tests were conducted.

A set of leakage tests were carried to determine the effect on thrust of gas leakage caused by an inadequate difference between the pressure in the two seal bellows and the propellant gas pressure. Bellows pressures were systematically varied to determine the pressure difference at which thrust became independent of this difference. As a result of these tests, a pressure differential of 10 psi was used in all tests to minimize gas leakage and friction between the rotor and seal.

A large number of propulsion tests were carried out to determine the effect on performance of channel flow velocity, propellant gas temperature and pressure, and rotor RPM. During individual tests one or more of these variables was varied in a systematic manner to determine the effect of important operating parameters such as pressure ratio, pressure coefficient or advance coefficient on water piston performance. Tests were carried out between velocities of 10 and 23 feet per second. Velocities greater than 17 feet per second were permitted by modifications which greatly reduced water thrown out at the test section at higher velocities.

3.2.1 Test Scope

Table 3-2 summarizes the test conditions for all tests conducted during the final test program. This table indicates that gas temperature and pressure and/or advance coefficient (RPM) were varied during each test. In these tests systematic variations were typically made in only one of these variables.

3.2.2 Mechanical Problems Encountered

The primary mechanical problem encountered during these tests was the failure, toward the end of testing, of four of the 16 vanes which separate the rotor flow passages. The bronze seal experienced significant wear after 30 to 35 hours of operation but was not in any immediate danger of failure. The thermocouple just upstream of the seal failed twice during the tests, probably due to the high gas temperatures and generally hostile operating environment.

Severe fouling of the water in the HSC occurred soon after the start of testing. This fouling was much worse than that which occurred during the initial set of tests. This fact, coupled with the severe fouling of the combustion chamber fuel oil spray nozzle and the HSC structure observed at the end of testing, indicated poor combustion efficiency.

3.2.3 Performance and Conclusions

The principal conclusions arising from these tests were:

1. Performance (thrust and efficiency and heat loss) were much worse than predicted and were similar to those found in the initial tests.

2. The use of the new gas port and seal resulted in a only a modest improvement in performance.

3. The use of additives had minimal positive effect on heat losses.

4. The serious failure of four rotor vanes indicated that the present system was not robust for at-sea operation at higher speeds and pressures.

It was therefore concluded that the present water piston propulsor design was not suitable for its planned use on a high speed amphibian.

Table 3-1. Test Conditions for Initial Set of Tests

Test	Gas Temperature Range – deg F	Test Velocity Ft/sec	Advance Coefficient Range	Chamber Pressure Range–psia
101	warm, 80° – 780°	15	2.59 – 2.62	70 – 74
	warm, 420° – 600°	12	2.46 – 2.63	47 – 49
102	warm, 135° – 313°	15	2.63 – 2.66	69 – 71
	warm, 130° – 770°	16.6	2.62 – 2.65	72 – 91
208	warm, 130° – 810°	15	3.80 – 3.86	71 – 73
209	warm, 60° – 780°	12	3.77 – 3.83	47 – 50
400	warm, 547° – 581°	12	2.75 – 3.99	47 – 72
203	hot, 2700° – 3370°	15	2.46 – 3.08	40 – 80
204	hot, 3060° – 3640°	12	2.60 – 3.00	36 – 78
205	hot, 2710° – 3300°	12	2.64 – 4.49	37 – 66
206	hot, 2840° – 3210°	15	2.54 – 3.37	36 – 81
207	hot, 2780° – 3240°	15	2.57 – 3.39	33 – 85
208	hot, 3055° – 3251°	15	2.96 – 4.16	59 – 87
209	hot, 3048° – 3253°	12	2.99 – 3.80	49
210	hot, 2273° – 3226°	15	3.25 – 3.92	69 – 72
400	hot, 3538° – 3197°	12	2.50 – 3.34	42 – 74

Table 3-2. Test Conditions for Final Set of Tests

Test	Gas Temperature Range – deg F	Test Velocity Ft/sec	Advance Coefficient Range	Chamber Pressure Range – psia
101	cold, 120° – 142°	15	2.41 – 2.93	58 – 74
103	cold, 126° – 143°	15	2.86 – 2.89	58 – 79
104	cold, 130° – 138°	15	3.19 – 3.21	58 – 78
106	cold, 128° – 160°	16	3.10 – 3.11	44 – 96
107	cold, 124° – 160°	10	3.12 –3.16	34 – 75
108	cold, 139° – 479°	17	3.12 – 3.17	55 – 93
109	cold, 116° – 145°	15	3.09 – 3.16	81 – 166
201	warm, 375° – 382°	19	3.14 – 3.19	53 – 94
202	warm, 376° – 377°	18	2.84 – 3.48	87– 96
203	warm, 380° – 387°	18	2.28 – 3.34	88 – 96
204	warm, 376° – 382°	15	2.39 – 2.86	68 – 79
205	warm, 524° – 640°	15	3.12 – 3.14	44 – 86
206	warm, 876° –1036°	15	3.14 – 3.15	43 – 87
207	warm, 862° – 939°	15	3.13 – 3.18	55 – 74
208	warm, 477° – 561°	15	3.12 – 3.15	54 – 76
209	cold, 117° – 142°	15	3.10 – 3.14	55 – 77
210	cold, 133° – 162°	15	3.12 – 3.16	75 – 166
301	hot, 2360° – 3135°	15	3.08 – 3.14	53 – 132
302	hot, 2471° – 3592°	15	3.09 – 3.15	55 – 128
303	hot, 2240° – 3243°	15	3.09 – 3.14	73 – 75
304	hot, 2732° – 3421°	10	3.08 – 3.13	34 – 75
305	hot, 2622° – 2969°	17	3.11 – 3.15	55 – 133
306	hot, 2487° – 2871°	19–23	3.13 – 3.46	62 – 131
307	hot, 2370° – 2642°	23	3.12 – 3.20	73 – 128
308	hot, 2687° – 2762°	15	3.10 – 3.12	75
309	hot, 2737° – 2880°	18	2.51 – 3.47	93 – 97
310	hot, 2560° – 2734°	22	2.70 – 3.51	125
311	hot, 2875° – 3056°	18	3.10 – 3.14	74 – 119
312*	hot, 2173° – 3532°	22	3.09 – 3.18	122 – 143
313*	hot, 2582° – 3870°	22	3.04 – 3.16	114 – 119
314*	hot, 3801° – 4670°	18	3.12 – 3.17	96 – 99
315*	hot, 3168° – 4445°	18	3.12 – 3.14	94 – 97

* Higher temperature data in these tests appear to be in error.

4.0 PREDICTION OF WATER PISTON PERFORMANCE

Two methods were used to predict water piston performance. The first was the use of a computer program developed initially by Dr. Carl Zovko of NSWC and later modified by Tracor Hydronautics. The second was an analytical approach based on the use of first principles, using the methods presented in the Appendix of Reference 4 and on empirical constants to be determined from the test data. This latter approach was invoked when it became clear that the computer program significantly overpredicted both thrust and efficiency, even when ambient temperature air was used and heat losses were not present.

4.1 Initial Performance Predictions Using Computer Program

Performance was calculated for the water piston propulsor during its design using the Zovko performance analysis program as modified by Tracor Hydronautics. The principal rotor design parameters and corresponding performance, including thrust and gas mass flow rate for the 20 mile per hour design speed, are summarized in Table 4-1. This table was taken from the water piston propulsor design report, Reference 8.

4.1.1 Water Piston Performance Analysis Program

The performance analysis program described above carries out a time domain calculation of the coupled water and gas flow in a single passage for one complete operating cycle (one revolution for the single gas port design used here). This cycle is divided into four phases. The program then determines total performance by multiplying the results for a single passage by the number of passage operating cycles per unit time.

In the calculation for a single passage, the program first determines the flow of water into the passage from the time it emerges from behind the obturator until it again passes behind the obturator at the end of the fill cycle. The program then calculates the behavior of the fluid and pressure during the time the passage is sealed behind the obturator (before it uncovers the gas port and gas begins to flow into the passage). The program next calculates the coupled flow of the gas into the passage and the motion of the water in the passage during the time that the passage is open to the gas port. Finally, the program calculates the flow (ejection) of the water due to adiabatic expansion of the fixed volume of gas that has entered the passage during the third phase, assuming no gas heat or leakage losses.

Table 4-1. Water Piston Propulsor Design Characteristics from Reference 8

Design Speed	20 miles per hour (29.3 feet per second)
Design Thrust	3000 pounds
Design Gas Temperature	3000°F
Design Gas Flow Rate	0.83 pounds per seond
Design Gas Pressure	220 psia
Rotor Characteristics	
Length	32 inches
Outside Diameter	16 inches
Mean Passage Diameter	11.75 inches
Number of Passages	16
Passage height (radial length)	4.0 inches
Passage Inlet Area	8.0 square inches
Passage Exit Area	7.2 square inches
Passage Inlet Angle	40.9 degrees
Passage Exit Angle	14.2 degrees
Gas Port Characteristics	
Height (radial length)	3.0 inches
Width	1.66 inches
Shape	trapezoidal
Obturator Width	90 degrees
Fill Width	270 degrees

4.1.2 Initial Design Performance Calculations

The predicted thrust and gas mass flow rate given in Table 4-1 for the design gas chamber pressure of 220 psia were based on the following assumptions:

1. Rotor inlet losses were negligible and rotor effective inlet velocity was equal to free stream velocity of 20 miles per hour or 29.3 feet per second

2. Flow passage head losses were neglected

3. The rotor flow passages had an exit area equal to 90 percent of the passage inlet area

4. The gas port had a trapezoidal shape similar to the rotor flow passage shape

5. The rotor had a mean vane inlet angle of 39.3 degrees.

As discussed later in this report, the test data indicate that rotor inlet and passage flow head losses were significant and the rotor (as built) has an effective inlet angle of 36 degrees or less. Also, the rotor was built with essentially equal passage inlet and exit areas, and the seal was built with a round rather than a trapezoidal gas passage.

4.1.3 Performance Calculations for the Water Piston Propulsor as Built and Tested

In order to determine the expected performance of the rotor as built and tested, new performance calculations were made as part of the test effort. These calculations were made using the program used to obtain the results in Table 4-2. Calculations were made for both round and trapezoidal gas ports, for equal flow passage inlet and exit areas, and for passage head losses corresponding to both smooth and very rough passage walls.

Calculations were also made for a case with only two-thirds of water in the passage being ejected by the gas due to gas flow channeling caused by use of a round gas port; flow channeling was observed in the tests described in Reference 5, particularly for the case with a round rather than a trapezoidal gas port. Finally, calculations were made for a case with a 36 degree rotor inlet angle. Results for these cases are presented in Table 4-2.

Table 4-2. Summary of Results of Calculated Performance

Velocity Ft/Sec	Pressure psi	Exit Area Ratio	Friction Factor *	Gas Port Width-in	Dimension Height-in	Passage Height-in**	Thrust Pounds	Gas Mass Flow-lb/sec
29.3	220	1.0	1.0	1.66	3.0	4.0	2796	0.81
29.3	220	1.0	1.0	2.26	2.26	4.0	3376	1.22
29.3	220	1.0	1.0	2.26	2.26	2.67	2287	0.85
29.3	220	0.9	1.0	1.66	3.0	4.0	2814	0.80
29.3	220	0.9	1.0	2.16	2.16	4.0	3447	1.21
29.3	220	0.9	5.0	2.26	2.26	4.0	2742	1.06
29.3	220	0.9	5.0	2.26	2.26	2.67	1806	0.73
29.3	220	0.9	5.0	1.66	3.0	4.0	2142	0.70
15.0	69	1.0	1.0	2.26	2.26	2.67	552	0.13
15.0	69	1.0	1.0	1.75	3.80	4.0	588	0.15
15.0	69	1.0	5.0	2.26	2.26	2.67	400	0.12
15.0	69	0.9	1.0	2.26	2.26	4.0	819	0.19
15.0	69	0.9	5.0	2.26	2.26	4.0	596	0.17
15.0	69	0.9	5.0	1.66	3.00	4.0	340	0.11

* 1.0 represents smooth pipe friction

** 4.0 is geometric height of passage

The results in Table 4-2 indicate the significant effect that factors such as gas port geometry, passage friction, passage height and exit area ratio can have on predicted thrust, mass flow rate and overall efficiency. It should be noted that for a given operating speed, gas pressure and temperature, efficiency is essentially proportional to the ratio of thrust to gas mass flow rate.

4.2 Theoretical Performance Predictions and Scaling Parameters for the Water Piston Propulsor

Performance predictions and scaling requirements are most readily understood when performance factors such as thrust and mass flow are normalized in terms of other relevant factors such as geometry, speed, and pressure. Furthermore, the value of these non-dimensional performance parameters will vary as operating conditions are changed. If these independent variables are also formed into non-dimensional parameters the scaling requirements usually become totally revealed.

4.2.1 Performance Parameters

Thrust

The most useful parameter containing the thrust, T_h, produced by the water piston propulsor is denoted at K_t and defined as

$$K_t = \frac{T_h}{(p_o - p_a) A} \qquad (1)$$

where p_o is gas supply pressure
p_a is ambient exhaust pressure
A is characteristic area

The value of K_t is thus the ratio of the thrust per unit area or mean effective pressure (relative to the ambient pressure) acting over the area, A, to the supply value $(p_o - p_a)$.

The net thrust (exclusive of internal and external friction which produce a negative thrust) is produced by pressures acting over the obdurator (thrust) and internal pressures and frictional stresses acting on the rotor that produce a drag or negative thrust on the system. Clearly the most useful characteristic area in defining the thrust is the obdurator area, A_o. When K_t is defined using A_o it is denoted at $K_{t,o}$, thus

$$K_{t,o} = \frac{T}{(p_o - p_a) A_o} \tag{2}$$

If the total thrust is divided into the axial forces on the obdurator, F_o, and the axial force on the rotor, F_r, Equation (2) becomes

$$K_{t,o} = \frac{F_o}{(p_o - p_a) A_o} - \frac{F_r}{(p_o - p_a) A_o} \tag{3}$$

Some insight into the expected value of $K_{t,o}$ is gained by examining these components.

$$\frac{F_o}{(p_o - p_a) A_o} = \frac{\overline{(p_1 - p_a)} A_1 + \overline{(p_2 - p_a)} A_2 + \overline{(p_3 - p_a)} A_3}{(p_o - p_a) A_o}$$

where $\overline{p_n - p_a}$ is mean value over the interval, n

A_n is area of the obdurator in the interval, n

n=1 is interval during passage closure

n=2 is interval during gas injection

n=3 is interval during gas expansion

As discussed in detail in the Appendix of Reference 4 the pressures during the first interval are negative and may be expressed as

$$\frac{\overline{p - p_a}}{p_o - p_a} = - K_a \frac{p_a}{p_o - p_a} \tag{4}$$

where K_a is a factor less than unity that denotes the portion of the interval during which the pressure is equal to vapor pressure. The area A_1 is half the area of a passage plus the area of a web.

During the second interval (when gas is injected) the area A_2 as discussed in the Appendix of Reference 4 is the area of the gas port, a web, and a passage. The maximum value of the second interval pressure ratio is unity. However, as discussed in the Reference 4 Appendix, the actual value may be significantly less than unity. The single channel "blow down" tests described in References 5 and 11 indicate that the pressure ratio during injection is approximately 0.7 for the conditions tested. However, the blow down tests were supplied by a reservoir of fixed volume and a major portion of the pressure reduction is accounted for as the mass flow reduces the driving pressure in the supply reservoir.

In the third interval the area A_3 is 3/2 the area of the obdurator available for the expansion phase. The pressure ratio in the third interval depends on the nondimensional location of the gas water interface (denoted as ℓ_{12} in Reference 4 and the pressure ratio p_o/p_a. Figure 4-1 presents the approximation for the third interval pressure ratio as given by Equation (48) in Reference 4. For the propulsor tested, the interface location, ℓ/L is about 0.45 and Figure 4-1 shows that the mean effective pressure for this interval is generally less than about 0.45 of the driving pressure.

It is pointed out in the Reference 4 Appendix that there is a negative thrust generated on the rotor that is approximately $(\sin^2 \beta) \cdot F_o$, where β_1 is rotor web inlet angles. If the rotor internal and external friction and the passage nozzle pressure drags are neglected the value of $K_{t,o}$ may be deduced from the preceding discussion to be approximately

$$K_{t,o} = \left[K_a \frac{p_a}{p_o - p_a} \frac{A_1}{A_o} + \frac{\overline{p_2 - p_a} A_2}{p_o - p_a A_o} + \frac{\overline{p_3 - p_a)} A_3}{(p_o - p_a) A_o} \right] \cos^2 \beta_i \tag{5}$$

An approximate upper bound may be obtained by neglecting the first term and taking the second and third interval pressure coefficients as 1.0 and 0.45 respectively. That is,

$$(K_{t,o})_{max} \equiv \left(\frac{A_2}{A_o} + 0.45 \frac{A_3}{A_o}\right) \cos^2 \beta_i \tag{6a}$$

For the propulsor tested with trapezoidal gas port

$$\frac{A_2}{A_o} = 0.44$$

$$\frac{A_3}{A_o} = 0.5$$

$$\beta_i = 40°$$

Equation (5) then gives

$$(K_{t,o})_{max} = [0.44 + 0.5\ (0.45)]\ 0.586 = 0.38 \tag{6b}$$

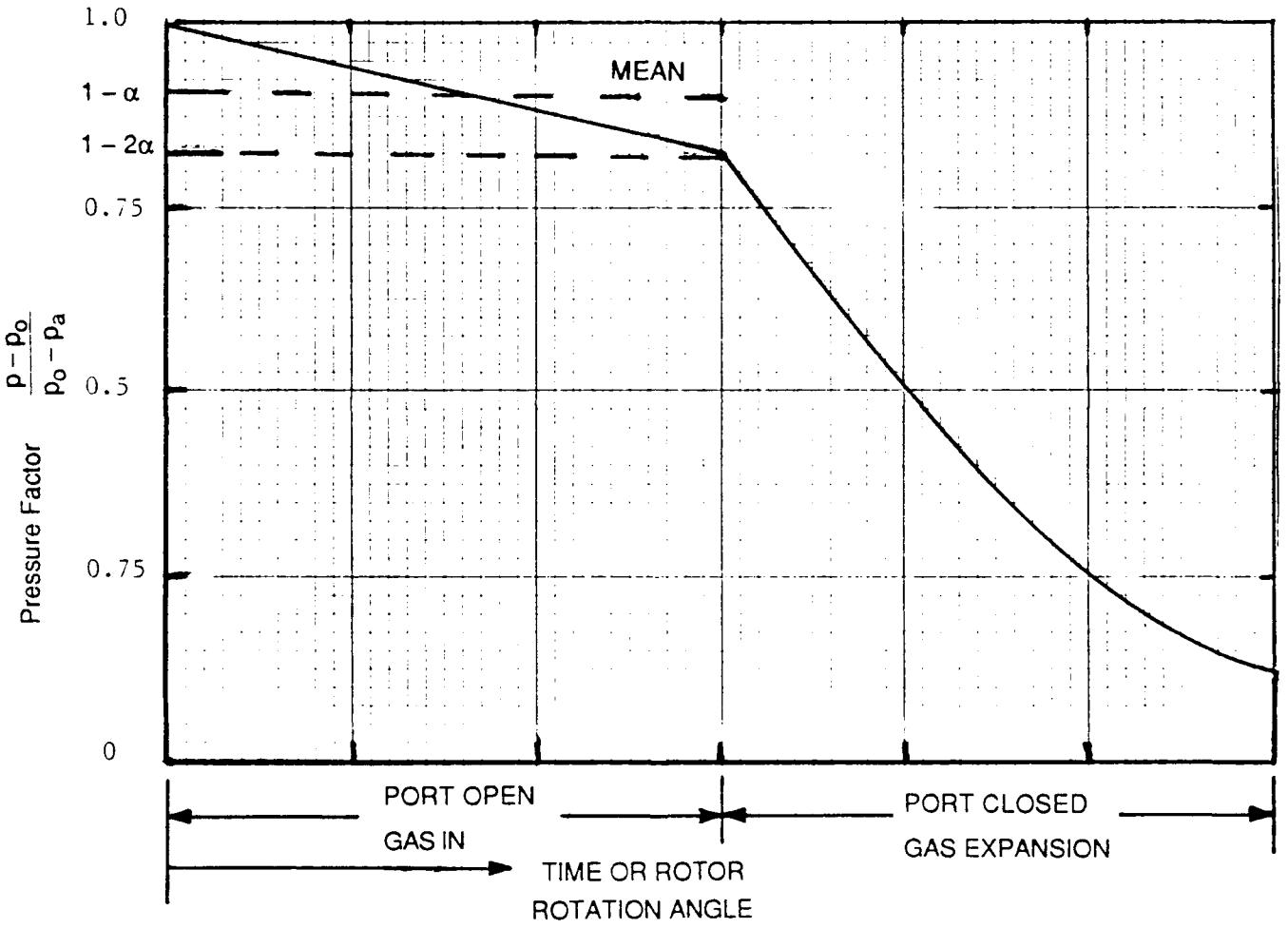

Figure 4-1. Sketch Defining the Pressure Loss Parameter, α

The process that occurs in a water piston propulsor involves the unsteady thermodynamics and fluid dynamics of a compressible gas and the hydrodynamics of the water upon which the gas acts. The foregoing discussion of thrust is a simplification developed to provide a ready comprehension of the complex process.

As discussed in Section 4.1 more, detailed numerical analysis of the propulsor performance has been developed for computer solution by Zovko (Reference 2). This program has been revised by THI to include the influence of internal friction. This basic program assumes that the gas injection and expansion processes are without heat transfer from the gas to its surroundings and that there is no loss in the total pressure of the gas during injection and expansion. Such an isentropic process is nearly achievable in the flow of gas up to the gas port exit. However, there clearly must be an increase in entropy during the portion of the gas injection when the velocity head in the inlet area is a significant portion of the total pressure and the inlet area is significantly less than the passage area (near opening and near closure of the gas port). No attempt to modify the computer program for this effect was made prior to the present study because the early tests described in Reference (4) showed fair agreement between measured thrust and the values predicted by the program. Furthermore, all of the studies conducted subsequent to Reference (4) were directed toward determining the transfer of heat from the hot gas to the water rather than the pressure loss during gas injection. It should be noted that thrust was not directly measured in the Reference (4) study because adequate funds were not available. Thrust was deduced from a jet impact apparatus.

The water piston propulsor system designed for the Marine Corps amphibian completely fills the dimensional envelope specified for the craft. The water piston rotor diameter (16 inches) and length (32 inches) are the maximum allowable. Furthermore, the design pressure of 220 psia was selected as the maximum available from known compressors not requiring significant further development. The computer code (with smooth friction) predicted that this design could produce a thrust of 3,000 pounds per rotor at a pressure of 220 psia and a craft speed of 30 mph. For an obdurator area of 36 square inches, the predicted value of $K_{t,o}$ at the design condition was

$$K_{t,o}\,(\text{design}) = \frac{3000}{(205)(36)} = 0.406 \qquad (7)$$

Note that this value of $K_{t,o}$ is slightly higher than the maximum value of 0.38 given by Equation (6b). Consequently, measured values of $K_{t,o}$ in the present investigation are expected to be substantially less than the original design value of 0.4 when pressure losses and external drag effects are included.

The effects of viscosity on the net thrust of the water piston propulsor system are the skin friction drag on the forebody fairing and the external rotor. The rotor internal skin friction also contributes to the drag, reduces the mean inlet velocity from the free stream and reduces the fluid acceleration within the passage during water expulsion. An additional drag is produced by the unbalanced hydrostatic pressure acting over the forebody fairing of the water piston propulsor system.

A general equation for each of these drag components which must be subtracted from the basic value of $K_{t,o}$ is presented below:

$$(1)\ \delta K_{t,o}\ (\text{Forebody}) = \frac{C_{f,1}\, s_f \frac{1}{2} \rho V_o^2}{(p_o - p_a)\, A_o} \tag{8a}$$

$$(2)\ \delta K_{t,o}\ (\text{Hydrostatic}) = \frac{\rho g h_{cg} A_b}{(p_o - p_a)\, A_o} \tag{b}$$

$$(3)\ \delta K_{t,o}\ (\text{External Rotor}) = \frac{C_{f,3}\, \pi D L \frac{1}{2} V_o^2}{(p_o - p_a)\, A_o \cos \beta_j} \tag{c}$$

$$(4)\ \delta K_{t,o}\ (\text{Int. Rotor Eject}) \approx \frac{C_{f,4}\, (w\, t\, h) \cdot L \cdot N_{p,o} \frac{1}{2} \rho \overline{V_e^2}}{(p_o - p_a)\, A_o} \tag{d}$$

$$(5)\ \delta K_{t,o}\ (\text{Int. Rotor Fill}) \approx \frac{C_{f,5}\, (w\, t\, h) \cdot L\ N_{p,f} \frac{1}{2} \rho \overline{V_i^2}}{(p_o - p_a)\, A_o} \tag{e}$$

$$\delta K_{t,o}\,((1) + (3) + (4) + (5)) = \frac{C_{f,1} \frac{S_f}{A_o} + \frac{C_{f,3}\, \pi DL}{\text{Cos}\, \beta_j\, A_o} + \frac{C_{f,4}\, \pi DL (w\, t\, h)\, L\, N_{p,o}}{A_o} \left(\frac{V_e}{V_o}\right)^2}{\overline{P}} + \frac{\frac{C_{f,5}\, \pi DL (w\, t\, h)\, L\, N_{p,f}}{A_o} \left(\frac{V_i}{V_o}\right)^2}{\overline{P}} \tag{9}$$

where

$$\overline{P} \equiv \frac{p_o - p_a}{1/2\, \rho\, V_o^2}$$

$C_{f,n}$ = skin friction coefficient for appropriate Reynolds number

The value of the numerator in Equation (9) for the rotor tested in the present study at a nominal velocity of 15 fps is approximately 1.09. The estimated total reduction in net thrust when the hydrostatic (2) drag is included is therefore estimated to be

$$\delta K_{to} \approx -\left[\frac{1.09}{\bar{P}} + \frac{50}{p_o - p_a}\right] \text{ for } V_o \approx 15 \text{ fps} \tag{10}$$

At speeds of 10, 15, and 17 fps and a value of $p_o - p_a = 2$ atmospheres ($p_o/p_a = 3$) Equation (9) gives $\delta K_{t,o} = -0.035, -0.065$, and -0.080 respectively. At a value of $p_o - p_a = 7$ atmospheres ($p_o/p_a = 8$ the values of $K_{t,o}$ for 10, 15, and 17 fps are -0.010, -0.019, and -0.023. Thus the influence of the negative thrust contributors is more significant at low values of p_o/p_a.

Based on the foregoing discussion, an estimate of the value of $K_{t,o}$ for the water piston propulsor tested at velocities around 15 fps may be written, using Equation (5) as

$$K_{t,o} \approx \cdot 586\left[-\cdot 1\left[K_a \frac{1}{\frac{p_o}{p_a} - 1}\right] + (\cdot 44)\left(\frac{p_2 - p_a}{p_o - p_a}\right) + \cdot 50\left(\frac{p_3 - p_a}{p_o - p_a}\right)\right] - \left[\frac{1.09}{\bar{P}} + \frac{50}{p_o - p_a}\right] \tag{11}$$

The manufacturer of the combustion chamber through which all gas passes (hot or cold) has estimated that there is a total pressure loss through the chamber of approximately 17%. The measured inlet pressure to the WPP for the amphibian is taken upstream of the combustion chamber. There is an additional loss of a portion of the kinetic energy entering the passage particularly during opening and closure. For the purpose of this simplified analysis, it is assumed that the pressure history in the passage is linear with time from the beginning of gas injection until the end as shown in Figure 4-1. This empirical pressure history is defined by the coefficient α so that the mean level is $(1 - \alpha)(p_o - p_a)$ and the level at the beginning of the expansion after the port closure is $(1 - 2\alpha)(p_o - p_a)$.

If the pressure coefficient during gas injection is assumed to decline linearly from 1 to $(1-2\alpha)$ at the gas port closure, then the coefficient in the second term will be $1-\alpha$ and the pressure coefficient in the third interval will be that given in Figure 4-1 for p_a/p_o replaced by $1 + (1-2\alpha)(p_o/p_a - 1)$ and $\overline{p_3 - p_a}/(p_o p_a)$ multiplied by $(1-2\alpha)$ so that Equation (11) becomes

$$K_{t,o} \approx \cdot 586\left[-\cdot 056\,\frac{p_a/p_o}{1 - \frac{p_a}{p_o}} + \cdot 44(1 - \alpha) + .33\left(1 - \frac{2\alpha}{1 - \frac{p_a}{p_o}}\right)\left(\frac{p_3 - p_a}{p_o - p_a}\right)\right] - \frac{1.09}{\bar{P}} - \frac{50}{p_o - p_a} \tag{12}$$

As shown in Figure 3, the contribution to the value of $K_{t,o}$ during the gas expansion (third term in Equation (12)) depends on the nondimensioßnal location of the interface ℓ/L as well as the effective pressure ratio. An approximate value of the interface location given in Equation (48) of the Appendix of Reference 4 is presented in the following equation.

$$\ell/L \approx \left[\frac{2\theta_p + \theta_{gp}}{\theta_f} + \frac{\bar{P}\, K_{t,o}}{\bar{V}_i} \left(\frac{\theta_p + \theta_{gp}}{\theta_f} \right)^2 \frac{A_o}{A_{p,t}} \right] \frac{J}{J_D} \tag{13}$$

where θ_p is angle subtended by a passage an web

θ_{gp} is angle subtended by the gas port

θ_f is angle subtended by the fill passage

$\bar{V}_i$ is V_j/V_o, inlet velocity ratio

$A_{p,t}$ is total area of all passages and webs

J is V_o/nD

J_D is minimum value of J to fill - - the design value

For the propulsor tested Equation (13) becomes

$$\ell/L \approx \left[.27(1 + .01\bar{P}) \right] \frac{J}{J_D} \tag{14}$$

where L is the rotor length

It is clear from the foregoing analysis that the nondimensional parameters that influence the thrust developed by the water piston propulsor may be expressed by the following equation

$$K_{t,o} = \text{fcn}\ (\bar{P},\ p_o/p_a,\ A_n/A_o,\ \beta_i,\ L/D,\ w/h,\ N_p,\ N_{gp},\ J/J_D,\ R_e,\ \alpha) \tag{15}$$

where

A_n is various areas, e.g., base area, A_b, passage area A_p, etc.

R_e is water Reynolds Number VL υ that determines the value of C_f in $\delta K_{t,o}$ and $\bar{V}_i$.

N_p is number of passages

N_{gp} is number of gas ports

The effect of gas inlet temperature T_o, has been omitted from Equation (15). If there is no heat transfer from the hot gas to the rotor or water while the gas is inside the rotor passage, temperature can influence the thrust only by the effect on the pressure ratios during gas injection and expansion and thus temperature effects must appear as changes in the parameter, α. The blow down tests described in Reference 5did find that the pressure history was slightly less for 600° gas. Reference 5 did find large effects of the gas temperature on the expected gas mass flow rate.

Gas Mass Flow Rate

The gas mass flow rate, $\dot{m}$, for a water piston propulsor may be written in terms of the interface location when the gas port closes, ℓ, and the density of the gas, ρ_i, at this instant.

$$\dot{m} = N_{gp}\, \rho_i\, N_p\, A_p\, \ell\, n \tag{16}$$

A useful mass flow parameter, $\dot{m}^*$, is formed by the following division.

$$\dot{m}^* \equiv \frac{\dot{m}}{N_{gp}\, \rho_o\, N_p\, A_p\, L\, n} = \frac{\rho_i}{\rho_o}\,\frac{\ell}{L} \tag{17}$$

where

$\rho_o = p_o/RT_o$, the inlet gas density at inlet pressure, p_o, and temperature, T_o.

If the process of gas injection is without a transfer of heat from the gas to the water then

$$\frac{p}{\rho^n} = \text{constant} \tag{18}$$

where $1 \le n \le \gamma$

$\gamma \equiv$ ratio specific heats c_p/c_v

n is 1, pure throttling

n is γ, isentropic

Thus,

$$\dot{m}^* = \left(\frac{p_i}{p_o}\right)^{\frac{1}{n}}\,\frac{\ell}{L} \text{ (adiabatic)} \tag{19}$$

In terms of the parameter, $\alpha = 0.28$, discussed in the previous section

$$\frac{p_i}{p_o} = (1 - 2\alpha) + 2\alpha\frac{p_a}{p_o} = .44 + .56\frac{p_a}{p_o} \text{ for } (\alpha = .28) \tag{20}$$

Combining Equations (14), (20), and (17) gives

$$\dot{m}^* = \left[.44 + .56\frac{p_a}{p_o}\right]^{1/2}\left[.27\,[1 + .01\,\overline{P}]\right]\frac{J}{J_D} \tag{21}$$

For an ideal gas, Equation (17) may also be written for any process in terms of the pressure and temperature ratios; that is,

$$\dot{m}^* = \left(\frac{p_i}{p_o}\right)\left(\frac{T_o}{T_i}\right)\frac{\ell}{L} = \left(\frac{p_i}{p_o}\right)\left(\frac{T_o}{T_{i,a}}\right)\left(\frac{T_{i,a}}{T_i}\right)\frac{\ell}{L} \tag{22}$$

where $T_{i,a} = T_i$ for an adiabatic process

thus

$$\left(\frac{T_o}{T_{i,a}}\right) = \left(\frac{p_i}{p_a}\right)^{\frac{1-n}{n}} \tag{23}$$

Equation (20) shows that for any adiabatic process, the pressure ratio, p_i/p_o is determined by the value of α. Equations (17). (19) and (23) show that the values of m^*, $T_o/T_{i,a}$, ahd ℓ/L are then also determined.

The evidence presented in Reference 5 for temperatures up to 700°F shows that if the process involves heat loss, there is no significant change in the value of α defining p_i/p_o as the inlet temperature, T_o, is changed. With the rotor geometry fixed, Equation (19) shows that the value of ℓ/L is also expected to be independent of temperature. However, if there is heat loss in the process, the temperature at gate closure, T_i, must be less than the temperature at gate closure without heat loss, $T_{i,a}$. Thus, Equation (17) becomes

$$\left(\frac{L}{\ell}\right)\dot{m}^* = \frac{p_i}{p_o}\,\frac{T_o}{T_i} = \left(\frac{p_i}{p_o}\,\frac{T_o}{T_{i,a}}\right)\left(\frac{T_{i,a}}{T_i}\right) = \left(\frac{p_i}{p_o}\right)^{\frac{1}{n}}\left(\frac{T_{i,a}}{T_i}\right) \tag{24}$$

The values of ℓ/L and p_i/p_o are expected to be independent of temperature, T_o. We now define $\dot{m}^*_c$ as the value of m^* at room temperture (cold) that is, $T_o \approx 70°F$. The ratio of $\dot{m}^*_h$ at any temperature T_o (hot) to m_c is then

$$\left(\frac{\dot{m}^*_h}{\dot{m}^*_c}\right) = \left(\frac{T_{i,a,h}}{T_{i,h}}\right)\left(\frac{T_{i,c}}{T_{i,a,c}}\right) = \left(\frac{T_{o,h}}{T_{i,h}}\right)\left(\frac{T_{i,c}}{T_{o,c}}\right) \tag{25}$$

Thus,

$$\frac{T_{i,h}}{T_{i,c}} = \frac{\dot{m}^*_c}{\dot{m}^*_n} \cdot \left(\frac{T_{o,h}}{T_{o,c}}\right) = \frac{T_{o,h,effective}}{T_{o,c,effective}} \tag{26}$$

and

$$\frac{T_{o,h,effective}}{T_{o,h}} = \frac{\dot{m}^*_c}{\dot{m}^*_n}\left(\frac{T_{o,c}}{T_{o,c,eff}}\right) \approx \frac{\dot{m}^*_c}{\dot{m}^*_n} \tag{27}$$

Efficiency

Equation (27) is clearly a measure of the heat loss from the gas to the water. In fact, if the pressure history is independent of temperature, the energy conversion efficiency within the rotor, η_r, may be calculated as

$$\eta_r \equiv \frac{\text{Workout}}{\text{Energy in}} = \frac{\dot{m}_c c_p T_{o,c}\left[1 - \left(\frac{p_o}{p_a}\right)^{\frac{\gamma-1}{\gamma}}\right]}{\dot{m}_n c_p T_{o,h}\left[1 - \left(\frac{p_o}{p_a}\right)^{\frac{\gamma-1}{\gamma}}\right]} = \frac{\dot{m}^*_c}{\dot{m}^*_n} \tag{28}$$

The heat loss fraction α_L is defined as

$$\alpha_L \equiv \frac{\text{heat loss}}{\text{Energy in}} \tag{29}$$

An expression for α_L may then be formed as

$$\alpha_L = \frac{\text{Energy in} - \text{Workout}}{\text{Energy in}} = 1 - \eta_r = 1 - \frac{\dot{m}^*_c}{\dot{m}^*_n} \tag{30}$$

The overall efficiency of the water piston propulsor may be expressed as

$$\eta_o = \frac{T_h V_o}{\text{Power in}} = \frac{T_h V_o}{P_1 + P_2} \tag{31}$$

The energy rate into the propulsor is composed of the power supplied to the compressor, P_1, and the heat added in the combustor, P_2. In a real system the total rate of energy supplied to the combustor is the energy rate supplied to the compressor prime mover. This energy rate is the product of the prime mover fuel rate and the fuel heat of reaction.

For the present tests we define the power supplied to the compressor as

$$P_1 = \frac{\dot{m} c_p T_{in} \left[1 - \left(\frac{p_a}{p_o} \right)^{\frac{\gamma-1}{\gamma}} \right]}{\eta_{supply} \equiv 1/3} \tag{32}$$

This compressor power is taken to be equal to the power available by adiabatic expansion from the input pressure and temperature divided by the overall efficiency of the compressor drive system, n_c, taken to be equal to 1/3.

The power supplied in the combustion process is taken to be

$$P_2 = \dot{m}_f \, Q(\text{reaction}) \tag{33}$$

where $\dot{m}_f$ *is fuel mass rate of flow*

Q_r is heat of reaction x (combustion efficiency)

If it is assumed that the efficiency measured for a gas temperature approximately equal to the water temperature is the adiabatic efficiency, η_a, then

$$\eta_a = \frac{T_h V_o \eta_c}{\dot{m}_c c_p T_{o,c}\left[1-\left(\frac{p_a}{p_o}\right)^{\frac{\gamma-1}{\gamma}}\right]\eta_h} \tag{34}$$

where η_c is efficiency of the compressor system ≈ 1/3.

η_h = hydraulic efficiency $\frac{T_n V_o}{\text{Workout}}$ ≈ (.3 to .5)

Equation (34) may be written in terms of $\dot{m}^*_c$ as

$$\frac{\eta_a}{\eta_c} = \left(\frac{K_{t,o}}{\dot{m}_c^*}\right)\left(\frac{\gamma-1}{\gamma}\right)\left(\frac{A_o}{A_{p,t}}\right)\left(\frac{D}{L}\right) J \frac{1-\frac{p_a}{p_o}}{\left[1-\left(\frac{p_a}{p_o}\right)^{\frac{\gamma-1}{\gamma}}\right]}\eta_h \tag{35}$$

Noting that

$$\frac{A_o}{A_{pt}}\frac{D}{L} J_o = \frac{1}{\overline{V}_i}\left(\frac{A_o/A_{pt}}{1-A_o/A_{pt}}\right) \tag{36}$$

Equation (35) may be written as

$$\frac{\eta_a}{\eta_c} = \left[\frac{K_{t,o}}{\overline{V}_i \dot{m}_o^* \cdot \frac{J_o}{J}}\right]\left[\frac{A_o/A_{p,t}}{1-A_o/A_{p,t}}\right]\left(\frac{\gamma-1}{\gamma}\right)\frac{1-\frac{p_a}{p_o}}{1-\left(\frac{p_a}{p_o}\right)^{\frac{\gamma-1}{\gamma}}}\eta_h \tag{37}$$

Now using Equations (21) and (37) the adiabatic efficiency for the propulsor studied may be written as

$$\frac{\eta_a}{\eta_c} = \left(\frac{K_{t,o}}{\overline{V}_i(.26+.002\overline{P})}\right)\left[\frac{A_o/A_{p,t}}{1-A_o/A_{p,t}}\right]^{\frac{\gamma-1}{\gamma}}\left(\frac{\left(1-\frac{p_a}{p_o}\right)}{\left(.44+.56\frac{p_a}{p_o}\right)^{\frac{1}{n}}\left[1-\left(\frac{p_a}{p_o}\right)^{\frac{\gamma-1}{\gamma}}\right]}\right)\eta_h \tag{38}$$

The last term in Equation (38) is plotted in Figure 4-2 where it may be seen that the function (denoted as f_2)has a nearly constant value of 3.4 for a very wide range of the pressure ratio. Since the values of $A_o/A_{p,t}$ and r are also fixed an approximate value of the adiabatic efficiency may be written, with $\overline{V}_i$ taken as 0.8, as

$$\frac{\eta_a}{\eta_c} \approx \frac{\bullet 4\, K_{t,o}\, \eta_h}{.27(1 + .01\, \overline{P})} \quad (J = J_D) \tag{39}$$

When the gas temperature is increased and there is a loss of heat from the gas to the water, the value of $K_{t,o}$ is not expected to change. However, the mass flow will increase with heat loss and thus temperature. Consequently, the adiabatic efficiency will be reduced by the ratio of the mass flows. Therefore,

$$\eta = \frac{\dot{m}_c^*}{\dot{m}^*}\, \eta_a \tag{40}$$

Heat Loss

It is desirable to deduce from the experiments as much information as possible concerning the laws covering the heat transfer from the hot gas to the cold water so that the experimental results may be scaled to other dimensions and conditions. The following analysis is presented to aid in the analysis of the hot gas experiments.

Heat will be transferred from the hot gas to the cold water by convection and radiation. The rate of heat loss may be expressed by the following equation:

$$\dot{Q}_\ell = C_s\, N_o\, A_s \left[h\,(T_o - T_w) + \varepsilon\sigma(\overline{T_o^4 - T_w^4}) \right] N_{gp} \tag{41}$$

where $\dot{Q}_\ell$ is the total rate of heat loss

C_s is a coefficient defined as the ratio of the actual water surface area exposed to the gas to total surface area of one passage A_s

A_s is the product of the passage perimeter and length

N_o is the number of passages covered by one obturator

h is the convective heat transfer coefficient

T_o is the inlet gas temperature

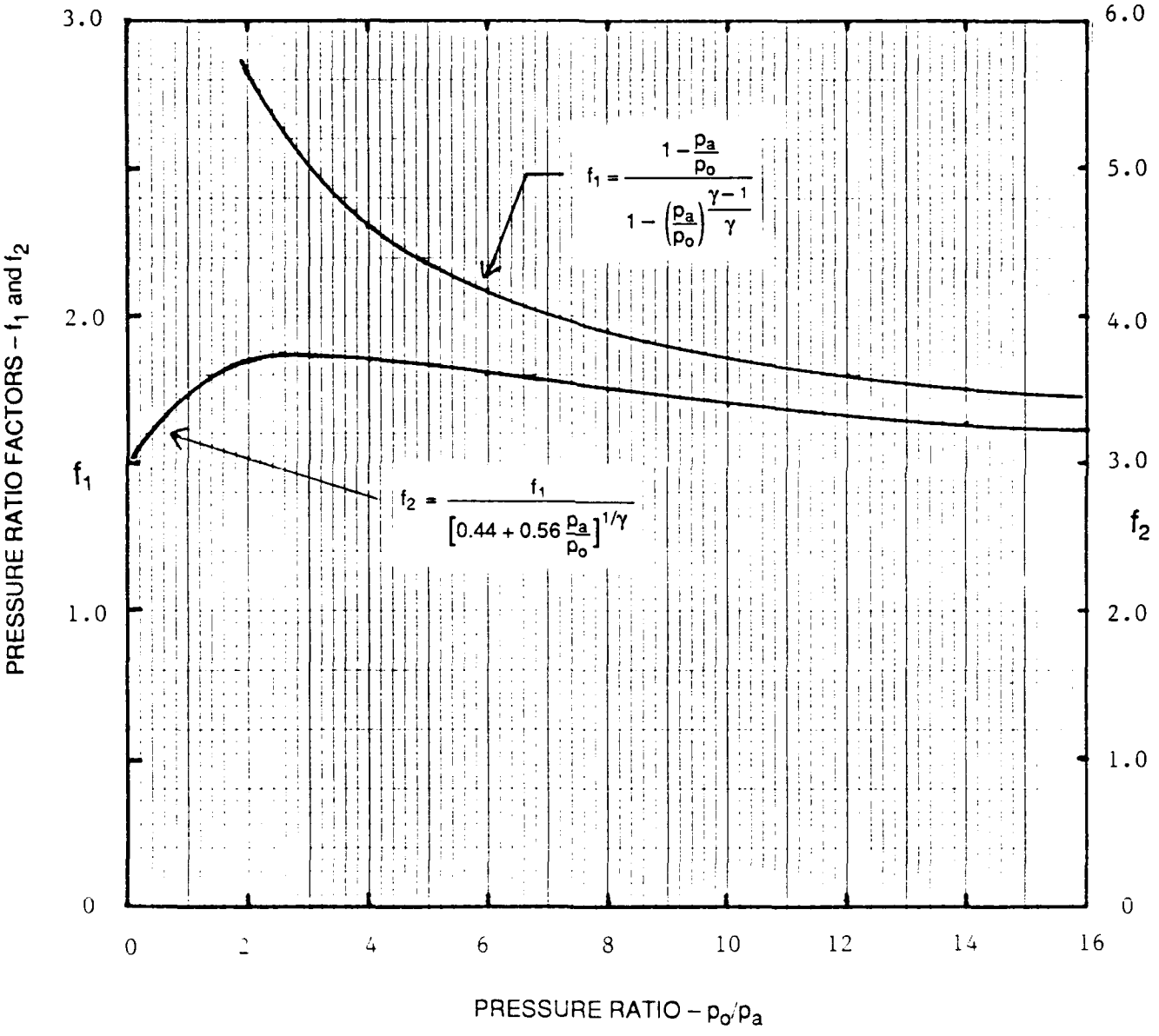

Figure 4-2. Pressure Ratio Functions, f_1 and f_2 (Equation 38)

T_w is the water temperature

ε is the radiant emissivity of the hot gas'

σ is the Stefan Baltzman constant = $.03 \times 10^{-8}$ ft–lb/ft^2 (° R)^4 sec

N_{gp} is the number of obdurators or gas ports

$$\dot{Q}_L = C_s N_o A_s h(T_o - T_w)\left[1 + \frac{\varepsilon\sigma(\overline{T_o^4 - T_w^4})}{h(T_o - T_w)}\right] N_{gp} \tag{42a}$$

Defining the last term in brackets as Ω, Equation (42a) becomes

$$\dot{Q}_L = C_s N_o A_s N_{gp} h(T_o - T_w)\left[1 + \Omega\right] \tag{42b}$$

The magnitude of Ω is simply the ratio of radiative to convective heat loss. Clearly, the temperature at which the value of Ω becomes significant depends on the ratio $\varepsilon\sigma/h$ and σ is a fixed constant. Thus, Equation (42) may be used to note the value of the temperature above which the value of $\dot{Q}_L$ increases exponentially with temperature rather than linearly.

When the value of Ω is small relative to unity and the heat loss is dominated by convection, the following analysis is helpful.

The convective heat transfer coefficient , h, expressed in the Nusselt Number (hd/k) is dependent on the gas Reynolds Number ($V_g d/\nu$) and the Prandtl Number ($c_p\mu/k$). It is useful to assume this relationship to be given by the following equation

$$N_a = C_h R_e^a P_r^b \tag{43a}$$

$$\frac{hd}{k} = C_h\left(\frac{V_g\, d}{\nu}\right)^a \left(\frac{c_p\mu}{k}\right)^b \tag{43b}$$

where C_h, a, and b are constants

V_g = gas velocity in the passage

$d \equiv 4\dfrac{A_p}{P_{er}}$

ν = kinematic viscosity, μ/ρ_g

c_p= gas specific heat

μ = dynamic gas viscosity

k = gas conductivity

It is useful to note that Reference 11 gives the following approximate equation

$$\mu_o \approx \left(\frac{T,°R}{460°}\right)^n \mu_o \tag{44}$$

where $\mu_o \approx 3.4 \times 10^{-7}$ (lb–sec/ft) for air

independent of pressure for $p_o \leq 5000$ psi

$\approx .5\mu_o$ (air) for H_20 vapor

$\approx .8\mu_o$ (air) for $C0_2$

Reference 11 gives the following approximate equation for the Prandtl number, P_r,

$$P_r \approx 4/\left(9-5\frac{c_v}{c_p}\right) = .74 \text{ for } \frac{c_p}{c_v} = 1.4 \tag{45}$$

independent of temperature and pressure.

The conductivity, k, may be determined from the viscosity, μ, and the Prandtl number as follows

$$\text{or } P_r = \frac{c_p\, Ru}{R\, k} \tag{46a}$$

$$P_r = \left(\frac{\gamma}{\gamma - 1}\right)\frac{Ru}{k} \tag{b}$$

$$\text{and } k = \left(\frac{\gamma}{\gamma - 1}\right)\frac{Ru}{P_r} \tag{c}$$

where R = gas constant

We now define and formulate the ratio of the heat input required if the process is without heat loss or adiabatic, Q_a, to the total heat loss as, β, that is;

$$\beta \equiv \frac{Q_{ad}}{Q_{\ell,c}} = \frac{T_h V_o / \eta_a \eta_h}{h C_s A_s T_o \left(1 - \frac{T_w}{T_o}\right) N_o N_{gp} (1 + \Omega)} \tag{47}$$

where A_s = Perimeter x L

using Equations (41), (43) and (46) Equation (47) becomes

$$\beta \equiv C_\beta \left(\frac{V_o}{V_g}\right)\left(\frac{A_p}{P_{er}\, L}\right)\left[\frac{1 - p_a/p_o}{1 - (p_a/p_o)^{\frac{\gamma-1}{\gamma}}}\right]\frac{(K_{t,o})}{1 - \frac{T_w}{T_g}}\,\frac{R_e}{(1+\Omega)} \tag{48}$$

where

$$C_\beta = (C_s C_h \eta_h)^{-1} P_r^{1-b}$$

Per = Passage Perimeter

$$\Omega = \frac{\varepsilon \sigma d\, T_w^3}{C_n k R_e^a P_r^b}\left(\frac{T_o}{T_w}\right)^3\left[\frac{1 - \left(\frac{T_w}{T_o}\right)^4}{1 - \frac{T_w}{T_o}}\right] \tag{49}$$

The gas Reynolds may be written in terms of the inlet pressure and temperature, p_o, T_o and water speed, V_o, as

$$R_e = \frac{V_g d}{\nu} = \frac{\rho V_o d}{\mu}\left(\frac{V_g}{V_o}\right) = \frac{V_g}{V_o}\,\frac{p_o V_o d}{R T_w \left(\frac{T_o}{T_w}\right) \mu_o \left(\frac{T_o}{T_f}\right)^n} \tag{50}$$

where T_f = 460°, R = 0° F

Thus

$$R_e = \left(\frac{V_g}{V_o}\right)\left(\frac{d}{R T_w\, \mu_o}\right)\frac{p_o V_o}{\left(\frac{T_w}{T_f}\right)^n \left(\frac{T_o}{T_w}\right)^{1+n}} \tag{51}$$

Taking $\mu_o = 3.4 \times 10 \times 10^{-7}$ for all cases tested

$n = .768$ for cold or warm air

$n = .81$ for combustor gas

$V_g/V_o \approx 1$

The Reynolds number for the present tests using R = 1716 ft-lb/slug°F and Tw = 525°R, d = .222 ft may be determined as

$$R_e \approx .65 \frac{p_o V_o}{(T_o/T_w)^{1+n}} \tag{52}$$

Thus Equation (48) becomes

$$\beta = C_\beta \left(\frac{V_o}{V_g}\right)\left(\frac{A_p}{P_{er} L}\right)\left[\frac{1 - p_a/p_o}{1 - (p_a/p_o)\frac{\gamma-1}{\gamma}}\right]\frac{K_{t,o}}{1 - \frac{T_w}{T_o}}\left[\frac{(.65)\, p_o V_o}{\left(\frac{T_o}{T_w}\right)1+n}\right]^{1-a}\frac{1}{(1+\Omega)} \tag{53}$$

And Equation (49) for the radiation effect may be further developed using Equations(44) and (51).

The Prandtl Number for cold or warm air or the combustion gas has a nearly constant value of .75. Using the definition of the Prandtl Number, the conductivity k may be obtained as

$$k = \frac{c_p \mu}{P_r} \approx \left(\frac{c_p}{R}\right)\frac{R_\mu}{P_r} = \left(\frac{\gamma}{\gamma-1}\right)\left(\frac{R}{P_r}\right)\mu \tag{54}$$

where R is the gas constant

and γ= ratio of specific heats c_p/c_v

Using the previous expression for μ, the value of the gas conductivity may then be written as

$$k \approx \frac{\gamma}{\gamma-1}(P_r)^{-1}\left(\frac{T_w}{T_f}\right)^n\left(\frac{T_o}{T_w}\right)^n R\mu_o \tag{55}$$

Equation (49) for Ω then becomes

$$\Omega = C_\Omega \left[\frac{(T_o/T_w)^{a+3-n(1-a)}}{(p_o V_o)^a \left(1-\frac{T_w}{T_a}\right)} \right] \tag{56}$$

where

$$C_\Omega \equiv \frac{\varepsilon \sigma d T_w^3 P_r^{1-b}}{C_n \left(\frac{\gamma}{\gamma-1}\right) R \mu_o \left(\frac{T_w}{T_f}\right)^n (.65)^a} \tag{57}$$

There are four basic unknown coefficients involved in Equation (56). The two exponents a and b and the coefficients C_β and C_Ω. The value of b is relatively unimportant - - the assumption of b =1 can introduce only a minor effect (assuming $b \leq 1$).

The coefficient C_β is the product of $C_s C_h \eta_h$ and P_r^{1-b} and if b = 1, P_r^{1-b} is unity. The value of η_h can be estimated from the ideal efficiency reduced by internal losses ($\eta_h \approx .3$ to .5). Thus an empirical value of C_β deduced from measured values of β gives an estimate of the product of its components $C_s C_h \eta_h$.

The coefficient C_Ω also includes two other coefficients, the ratio of ε/C_h. The value of the emissivity may be deduced from references such as Reference 14. It follows that an estimate of C_h may be determined if the coefficient $C_\Omega$can be obtained empirically from the measurements.

It is therefore important to analyze the measured values of β with guidance from Equation (53) and a search for empirical values of C_β, a, and C_Ω.

It may be noted that the value of the parameter β is related to the heat loss fraction, α_L, and the efficiency ratio η_r in accordance with the following equations

$$\alpha_L \equiv \frac{Q_{loss}}{Q_{in}} = \frac{Q_{loss}}{Q_a + Q_{loss}} = \frac{1}{1+\beta} \tag{58}$$

$$\eta_r \equiv \frac{\eta}{\eta_a} = \frac{\frac{TV_o}{\eta_a}}{\frac{TV_o}{\eta}} = \frac{Q_a}{Q_a + Q_{loss}} = \frac{\beta}{1+\beta} \tag{59}$$

Consequently $\alpha_L = 1 - \eta_r$ (60a)

$$\beta = \frac{1 - \alpha_L}{\alpha_L} \quad (b)$$

$$\beta = \frac{\eta_r}{1 - \eta_r} \quad (c)$$

In the analysis of experimental data, the value of η_a is approximately the measured value when the gas temperature is the same as the water temperature. Thus the measured values of η_r may be obtained as the ratio of $\eta/(\eta)_{cold}$. Measured values of α_L and β may then be deduced from Equation (60).

Although the foregoing analyses are approximate, they are useful in uncovering the important non-dimensional parameters and their inter-relationships. These relationships are used in the following section where the experimental results are presented and discussed.

5.0 RESULTS FOR FINAL TEST SERIES

In defining the attainable performance of the WPP, reliance was placed primarily on data from the final set of tests with the bronze seal and trapezoidal gas port. Results from these tests are discussed in this section. A less extensive presentation of and discussion of data from the initial set of tests with the graphite seal and round gas port are presented in Section 6. This section also presents comparisons of results from the two sets of tests.

5.1 Results and Discussion

As pointed out in a previous section, two different gas port configurations were tested. The first configuration was a 2.6 inch diameter round gas port, as shown in Figure 3-3. Although the round gas port design was simple and minimized stress and temperature concentrations in the gas supply, Reference 10 showed that this type of gas port did not "cleanly" remove the water in the rotor passages. The results in Reference 10 indicated that a trapezoidal gas port configuration was better than a round one in removing the water from the passages. Figure 3-3 shows such a design in the second configuration tested in the current study.

5.1.1 Thrust

Cold Gas

Figures 5-1and 5-2 present the measured cold gas thrust coefficients for various values of $\overline{P}$ and p_o/p_a for the three principal test speeds, 10, 15, and 17 fps. Also shown on these figures are the results obtained using the predicted estimates given by Equation (12) with a = 0.28 and ℓ/L = 0.4. It is apparent from Figures 5-1 and 5-2 that good agreement is obtained for the higher velocities but the lowest velocity, (10 fps), results are underestimated by Equation (12) for the constant value of ℓ/L= 0.4. Possibly better agreement would obtain if actual values of ℓ/L were available. Figures 4-1 and 4-2 show that the measured trends of $K_{t,o}$ with $\overline{P}$ and p_o/p_a are correctly predicted by Equation (12) with a constant value of $\alpha = 0.28$

Figure 5-3 shows predictions of $K_{t,o}$ for various values of α for the Marine Corps propulsor at its design condition (V_o = 20 mph, p_o = 220 psia). This figure shows that the required thrust of 3,000 lbs cannot be achieved even for $\alpha = 0$. The dashed line shown in Figure 5-3 is the estimated value of $K_{t,o}$ for the original design gas port that exactly matches a rotor passage. This dashed curve shows the WPP meeting the required thrust for $\alpha = 0$ except for the forebody and external rotor friction drag.

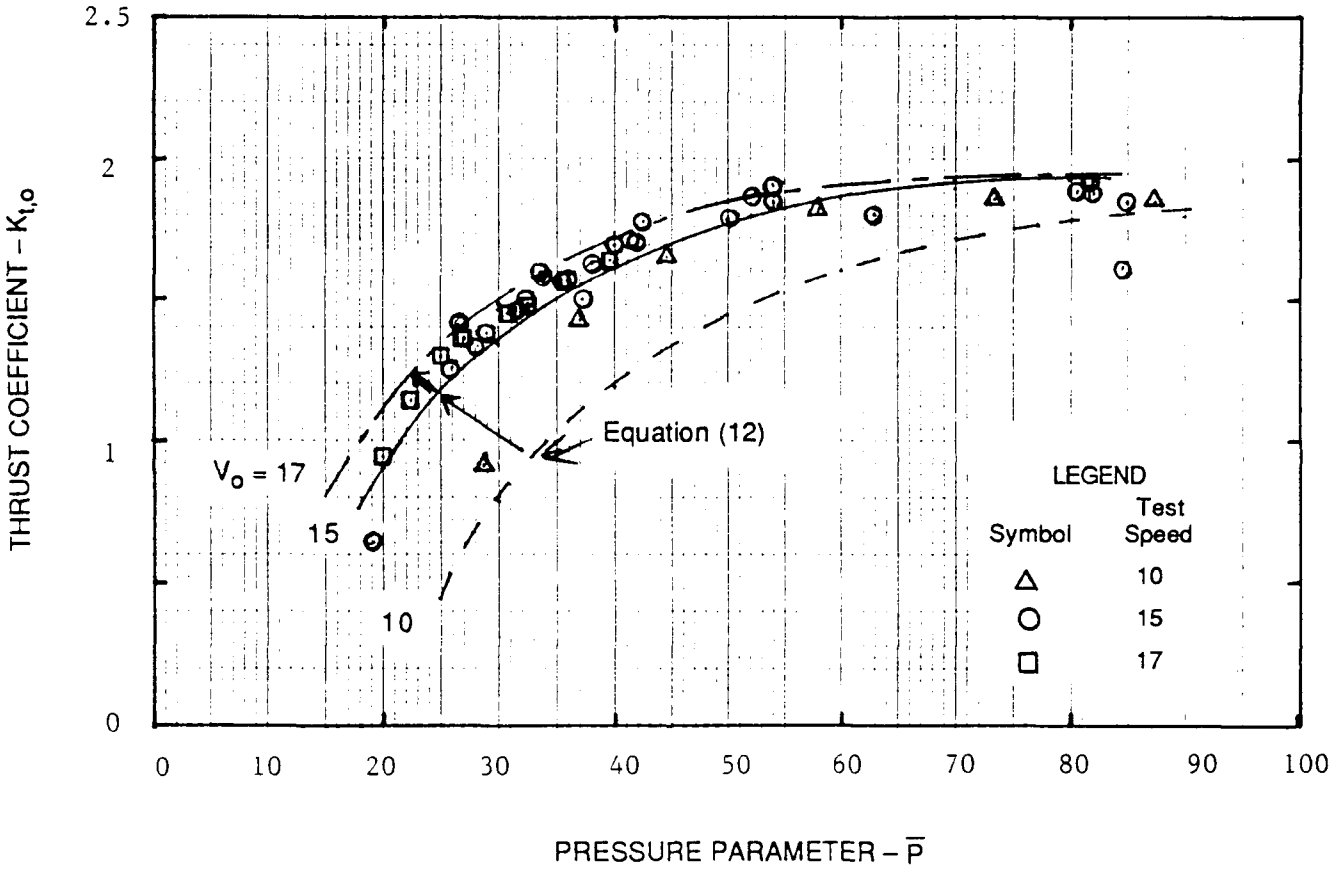

Figure 5-1. The Influence of the Pressure Parameter $\overline{P}$, on the Thrust Coefficient, $K_{t,o}$ – Theory and Experiment for Cold Gas ($T_o \cong 65°F$, $J = J_{Design} \cong 3.15$)

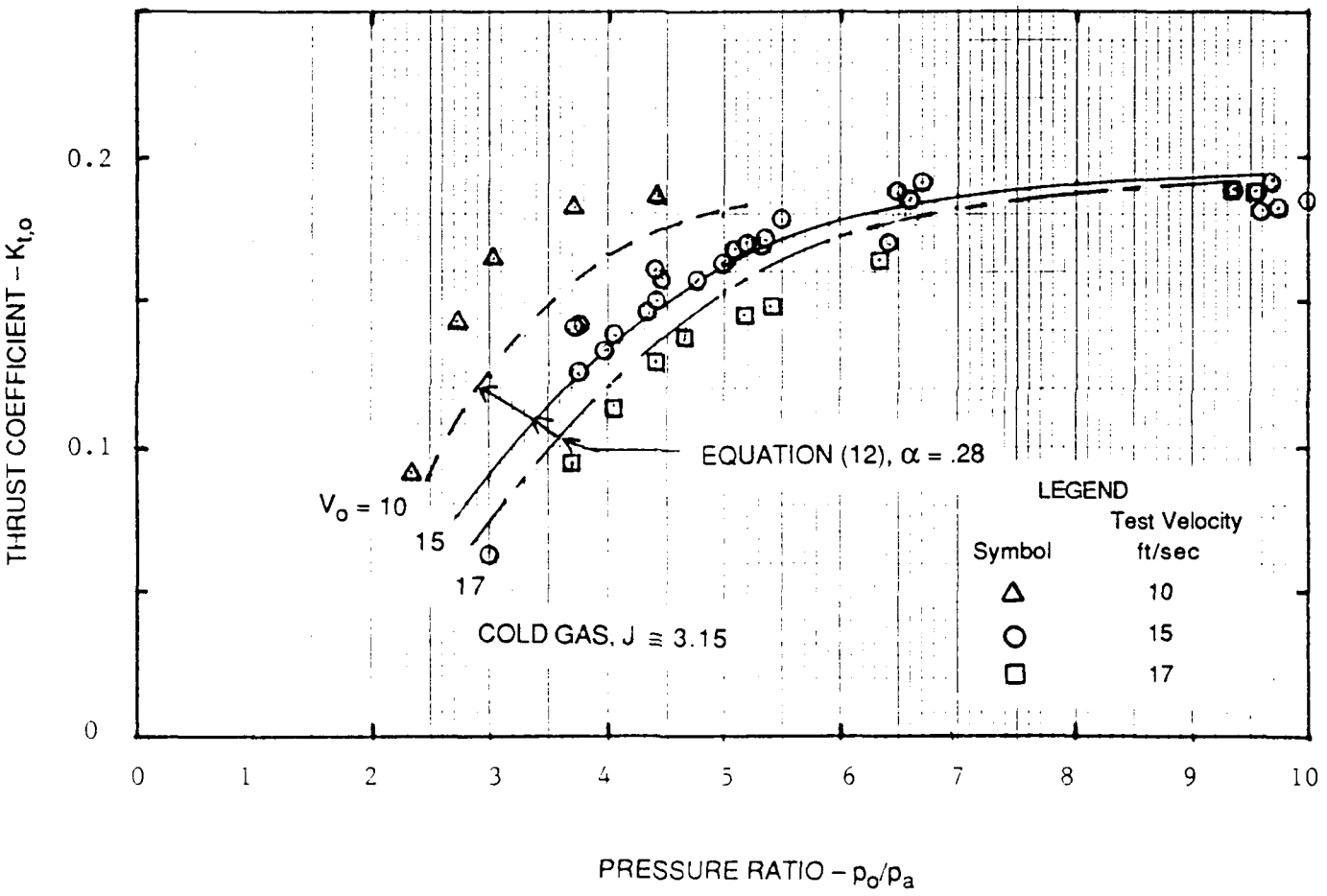

Figure 5-2. The Influence of Pressure Ratio, p_o/p_a on the Thrust Coefficient, $K_{t,o}$ – Theory and Experiment

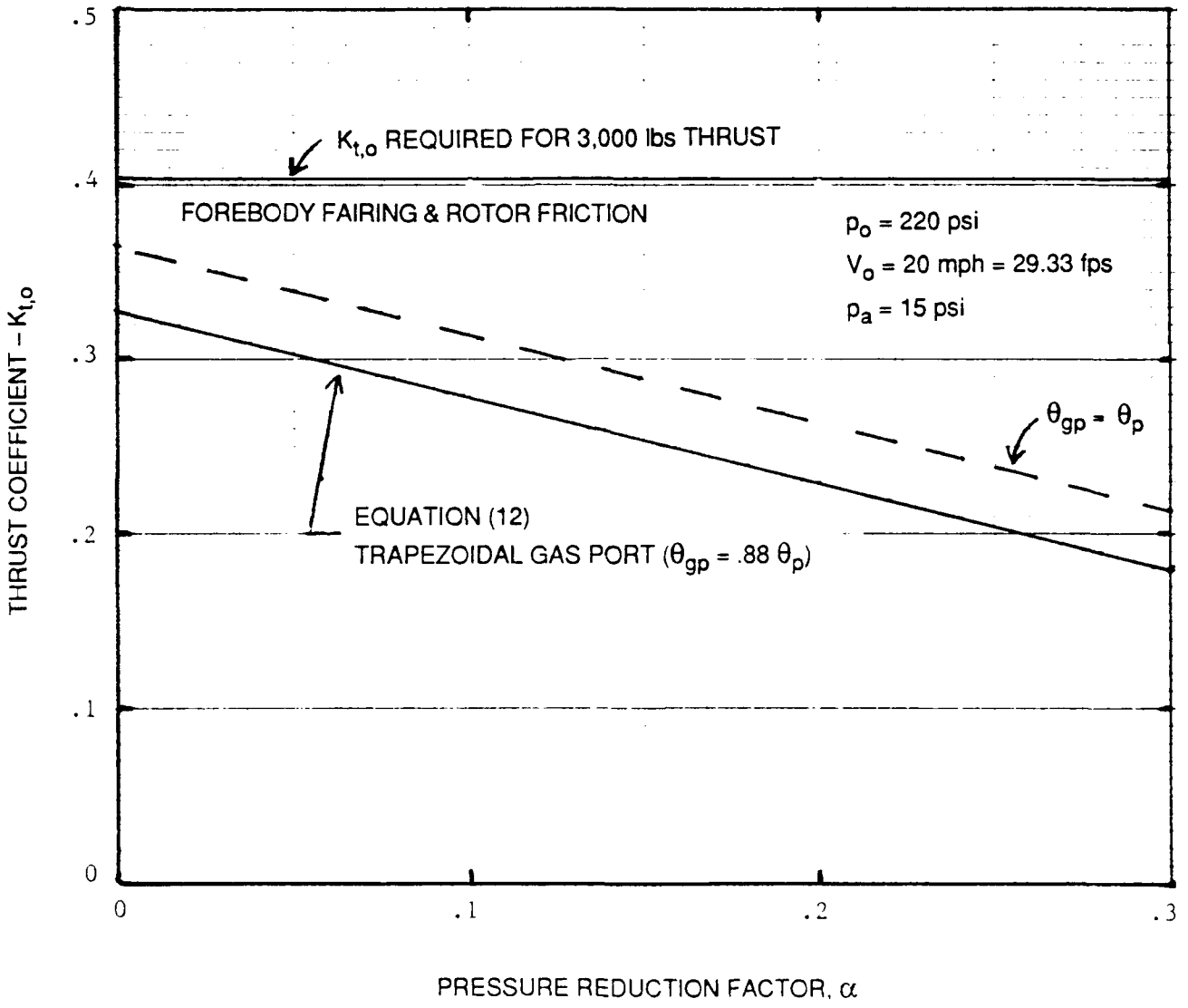

Figure 5-3. The Influence of the Pressure Reduction Factor, α, on the Thrust Coefficient $K_{t,o}$

Figure 5-4 shows measured variation of thrust coefficient with advance coefficient for a pressure ratio, $\overline{P}$, of approximately 38, the design value. This figure indicates that maximum thrust, and also efficiency is obtained at an advance coefficient of about 3.1, rather than the original design value of 2.77.

Hot Gas

Figure 5-5 presents measured values of $K_{t,o}$ for various forward speeds and values of $\overline{P}$ when the combustor was operated and the gas temperature was, on average, 3,000° F. Also shown on this figure are the predicted curves for 10, 15 and 17 fps (α = .28, ℓ/L= .4). These are the same predicted curves shown for the cold gas tests in Figure 5-1. Figure (5-5) shows that the measured values of $K_{t,o}$ at the same values of $\overline{P}$ are essentially identical for the cold gas and for the hot combustion gas.

Figure 5-6 shows the effect of varying the combustion gas temperature (between about 2600° R to 3800° R) with $\overline{P} \approx 38$ for forward speeds of 15 and 17 fps. The predicted values of $K_{t,o}$ (α = .28, ℓ/L) are also shown on the figure. Clearly, the hot combustion gas thrust coefficients are essentially identical to the values obtained with cold gas.

Figure 5-7 shows a comparison of the predicted values of $K_{t,o}$ with the measured values of $K_{t,o}$ with $\overline{P} \sim 38$ over the entire temperature range. The data in this figure show that the values of $K_{t,o}$ obtained with heated air (not combustion) in the temperature range of 300° to 800° F are about 10% less than those obtained for the cold gas and the very hot combustion gas. This anomaly for the moderate temperature range is not understood.

Figure 5-8 presents measured values of $K_{t,o}$ using combustion gas ($T \approx 3000°$ F) for a fixed value of $\overline{P} \sim 36$ as the advance ratio is varied. This figure also shows the measured curve for cold gas presented previously in Figure 5-4. The figure shows a clear if modest variation of $K_{t,o}$ with J with a maximum value of $K_{t,o}$ occurring at $J \approx 3.15$. The cold and combustion gas values are essentially identical.

5.1.2 Mass Flow Rate

Cold Gas

Measured values of the non-dimensional gas flow rate, $\dot{m}^*$, using room temperature gas ($T_o \approx 525°$ F) are presented for speeds of 10, 15 and 17 fps for various values of p_o/p_a in Figure 5-9 and

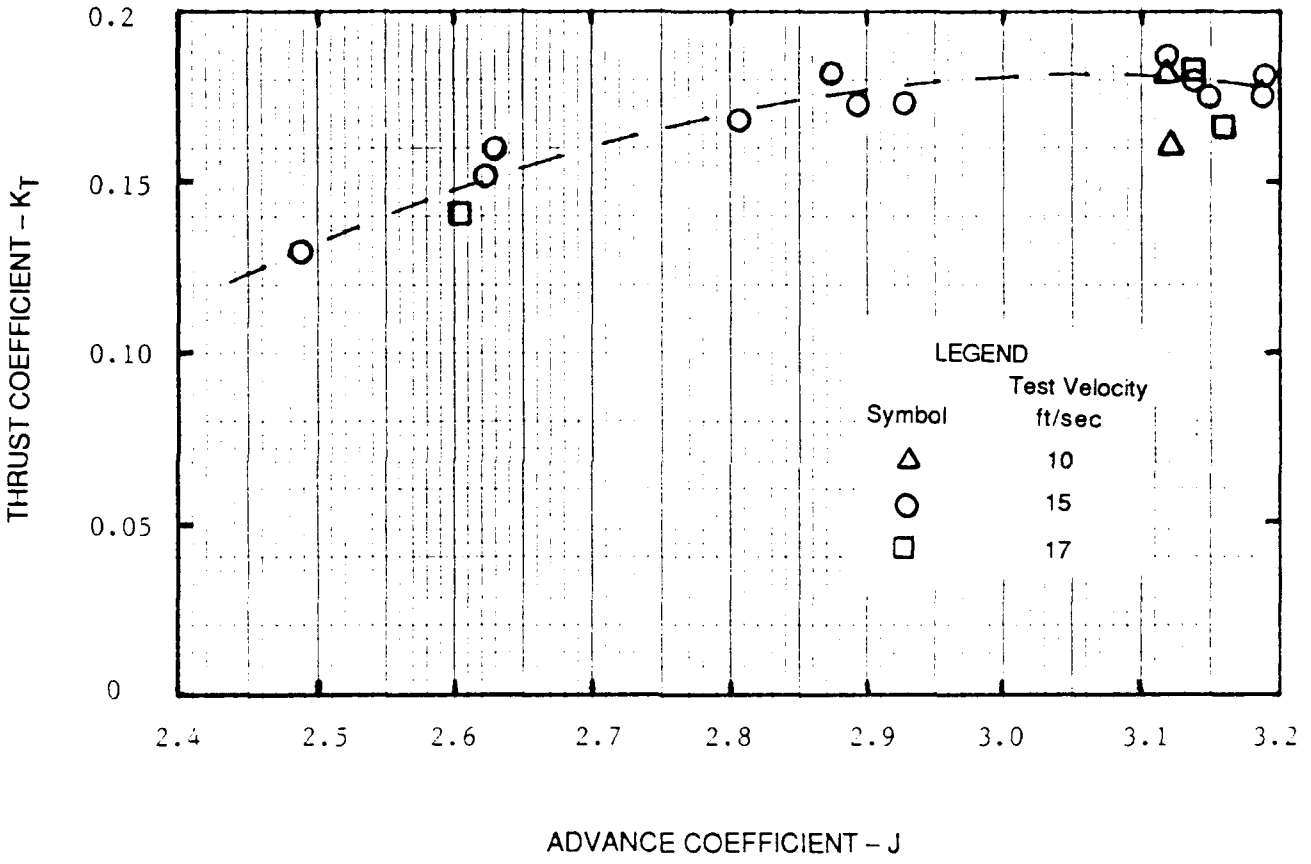

Figure 5-4. The Influence of Advance Ratio, J, on the Thrust Coefficient, $K_{t,o}$ for Cold Gas ($T_o \cong 65°F$, $\bar{P} \approx 30 - 35$)

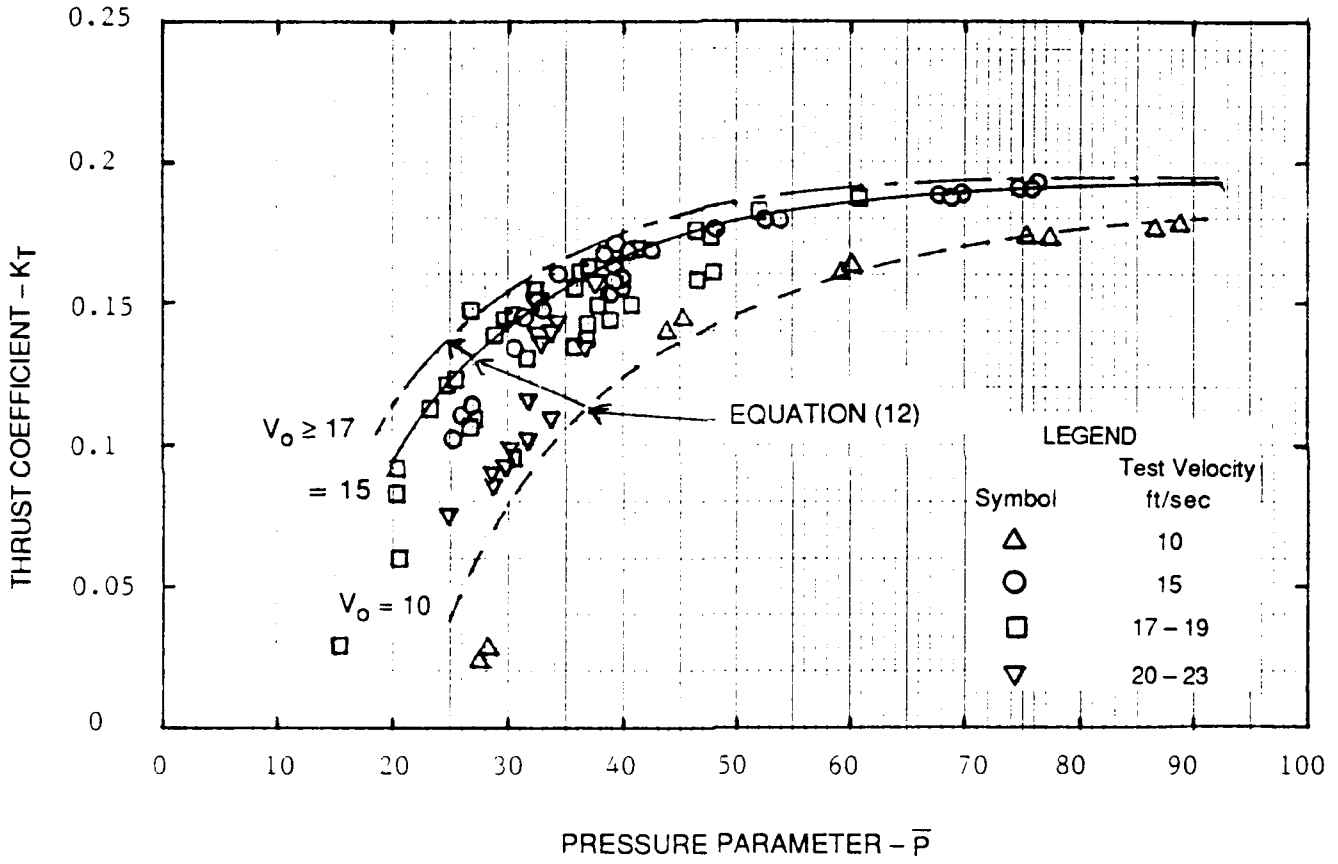

Figure 5-5. The Influence of the Pressure Parameter $\overline{P}$, on the Thrust Coefficient, $K_{t,o}$ – Comparison of Hot Gas (T_o = 3,000°F) Measurements with Adiabatic Theory, Advance Coefficient of 3.15

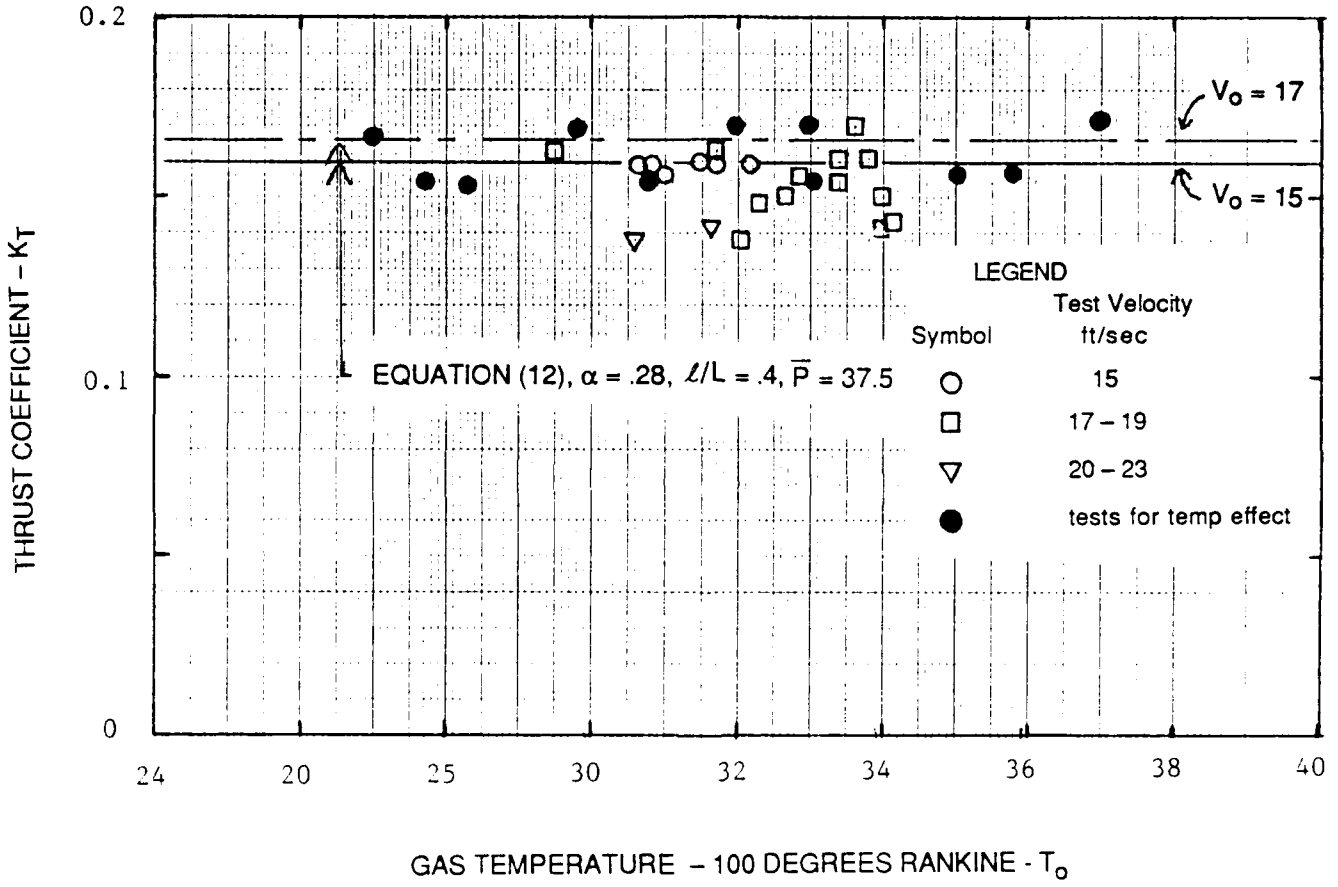

Figure 5-6. The Influence of Combustion Gas Temperature on the Thrust Coefficient – Theory and Experiment, $\bar{P}$ = 35 – 40

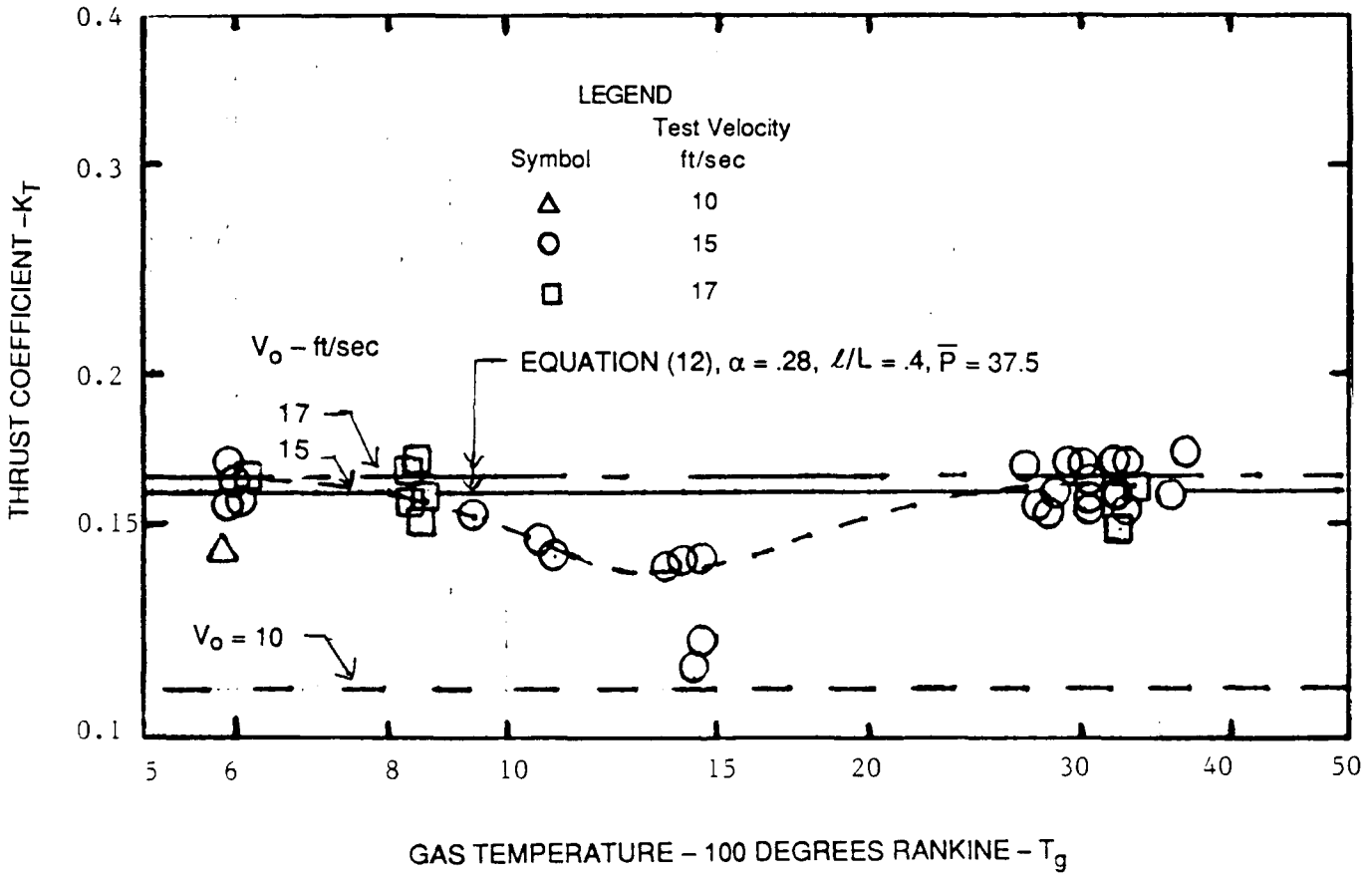

Figure 5-7. The Influence of Gas Temperature (Cold, Heated and Combustion Gas) on the Thrust Coefficient, $K_{t,o}$ - Theory and Experiment, $\overline{P}$ = 34 - 40

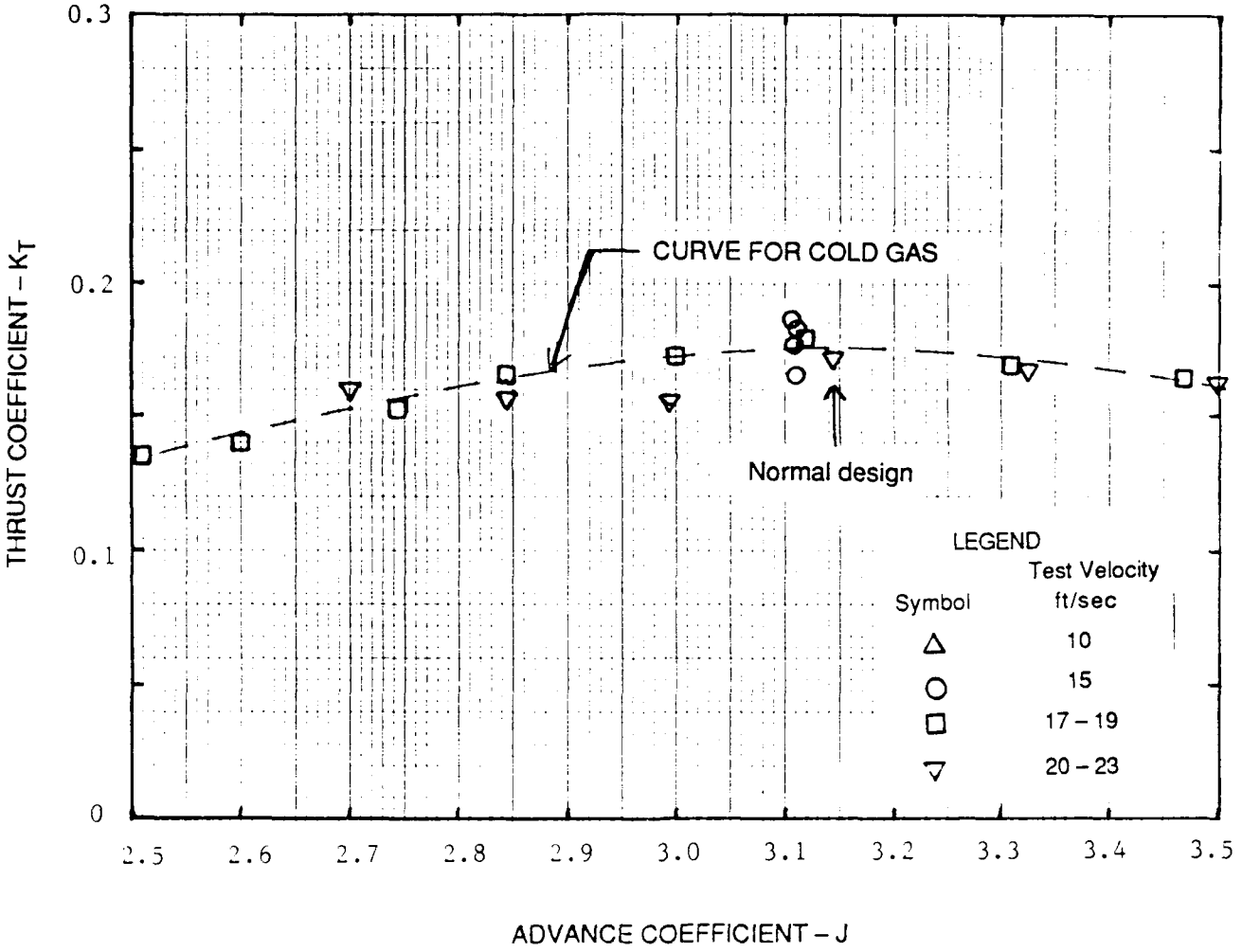

Figure 5-8. Comparison of Thrust Coefficient Versus Advance Coefficient Using Data for Cold and Combustion Gases

for various values of $\bar{P}$ in Figure 5-10. These figures show that $\dot{m}^*$ does not vary greatly with $\bar{P}$ but does vary with the pressure ratio p_o/p_a particularly for the low velocity (10 fps) case.

Figure 5-11 presents the same data as shown in Figures 5-9 and 5-10 but in the form of the parameter $\dot{m}^*/.27(1+.01\bar{P})$ plotted against the pressure ratio. This choice is based on the analysis leading to Equation (21). Figure 5-11 does collapse the data for all speeds. The predicted values given by Equation (21) are also shown in Figure 5-11. Equation (21) underestimates the measured values particularly at the lower values of the pressure ratio, but it is clearly functionally correct.

Figure 5-12 presents the measured influence of the advance ratio, J, on the mass flow parameter, $\dot{m}^*$. It should be noted that Equation (21) predicts that $\dot{m}^*$ will increase linearly as J is increased above the value required to just fill the rotor passage, J_D. As noted in the previous discussion of the effect of J on $K_{t,o}$ (Figure 5-4), the measurements show that the effective value of J_D is approximately 3.1 to 3.2. The apparent lack of any dependence of $\dot{m}^*$ on J shown in Figure (12) must result from incomplete filing of the rotor at all values of J less than 3.2. Presumably if measurements were made at values of J greater than 3.2, an increase of $\dot{m}^*$ should result.

The results shown in Figure 5-4 indicate that the rotor probably just fills when J = 3.15. This means that the mean fill velocity V_i as obtained from noting that $V_i\,\delta_{t\,fill} = L$ and therefore

$$\frac{V_i}{V_o} \equiv \bar{V}_i = \frac{L/D}{J_o\left(1-\frac{\theta_o}{\theta_{gp}}\right)} = \frac{2}{3.15\left(1-\frac{4.5}{16}\right)} = .88$$

Thus, friction within the passages causes the advance ratio for optimum $K_{t,o}$ to be 3.15 rather than 2.77 when friction is neglected and $\bar{V}_i = 1.0$.

Hot Gas

The most important measurements made in the present study are those used to determine the influence of gas temperature on the mass flow rate. Since the non-dimensional thrust coefficient is essentially independent of gas temperature, the relative increase of the parameter, $\dot{m}^*$, with temperature is inversely proportional to the efficiency.

Figure 5-13 presents measured values of $\dot{m}^*$ for a speed of 15 fps for a range of values of $\bar{P}$ and for gas inlet temperatures, T_o, of 940, 1200, and 3500° R. Also shown in the Figure is a curve

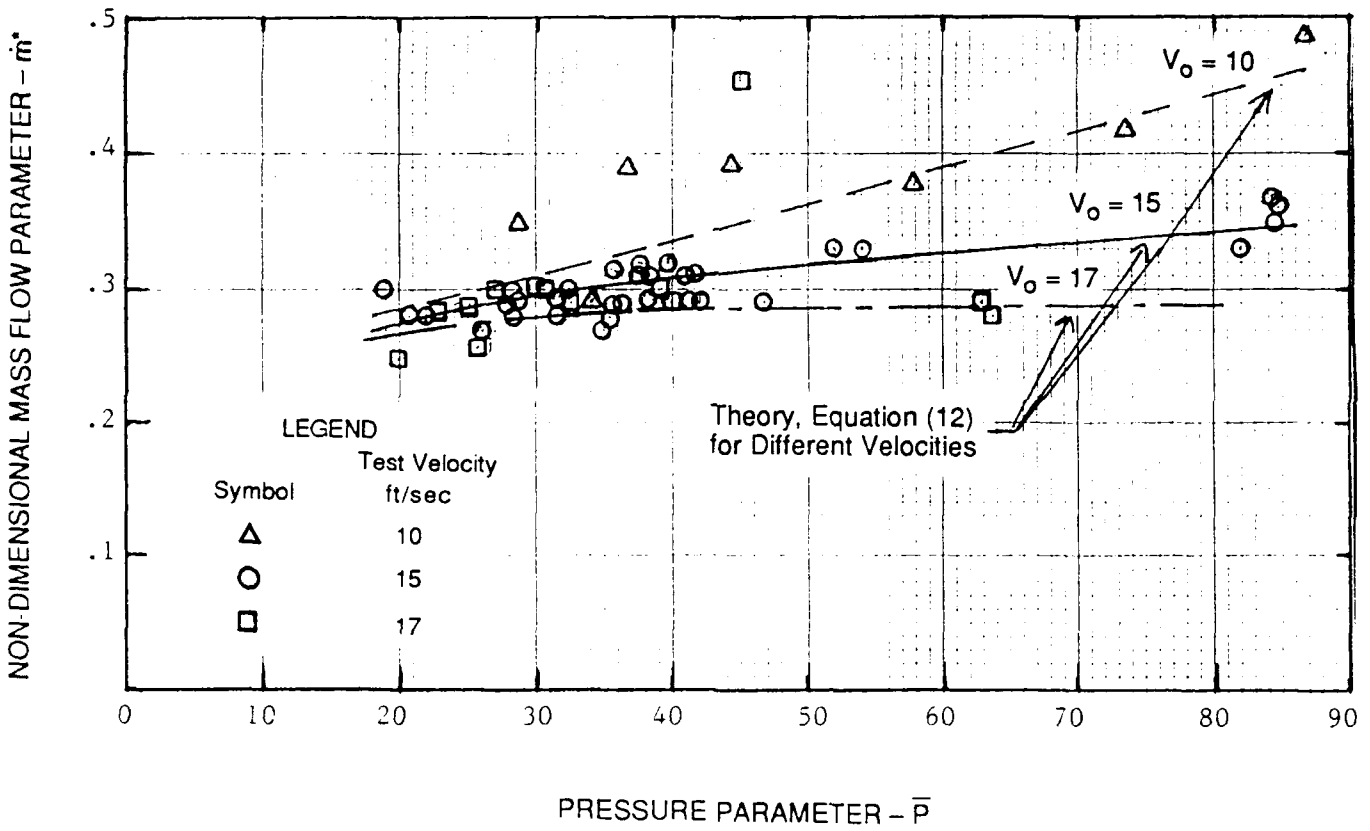

Figure 5-9. Variation of Non-dimensional Mass Flow Rate with Pressure Parameter, $\overline{P}$

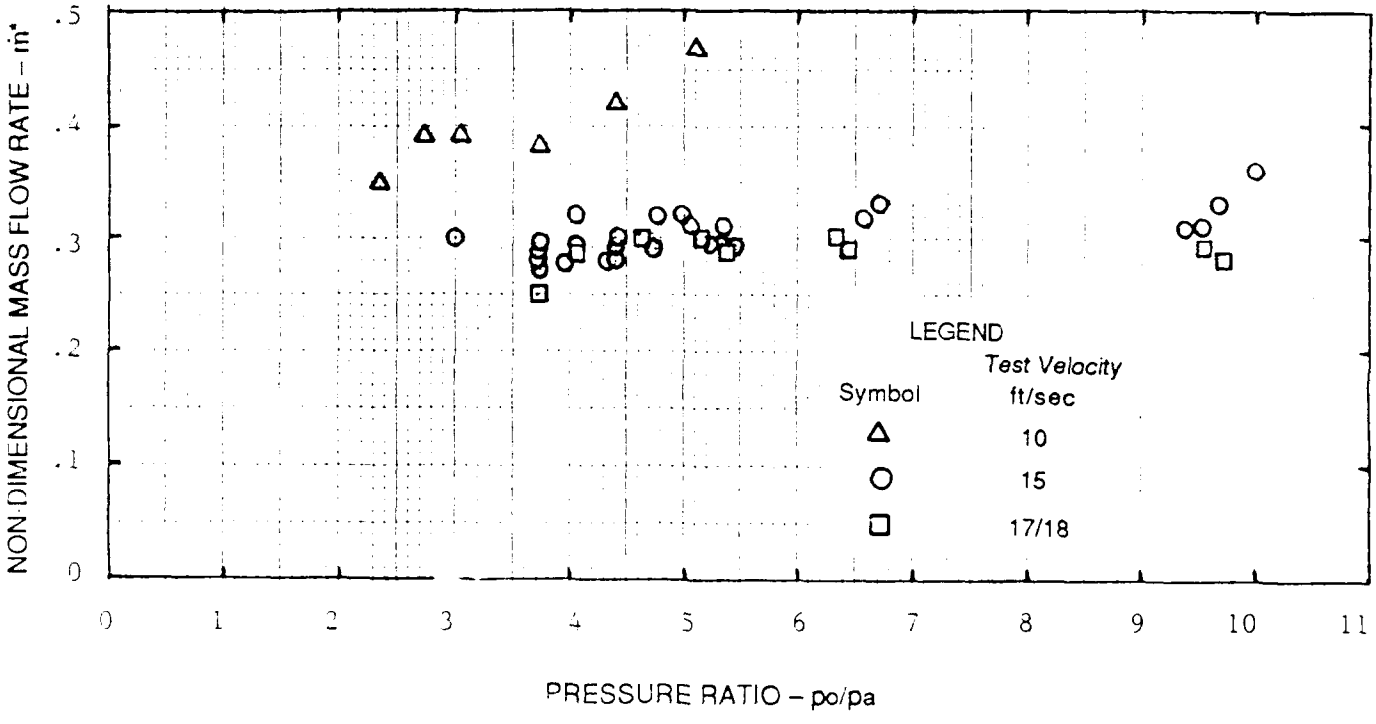

Figure 5-10. Variation of Non-dimensional Mass Flow Rate with Pressure Ratio

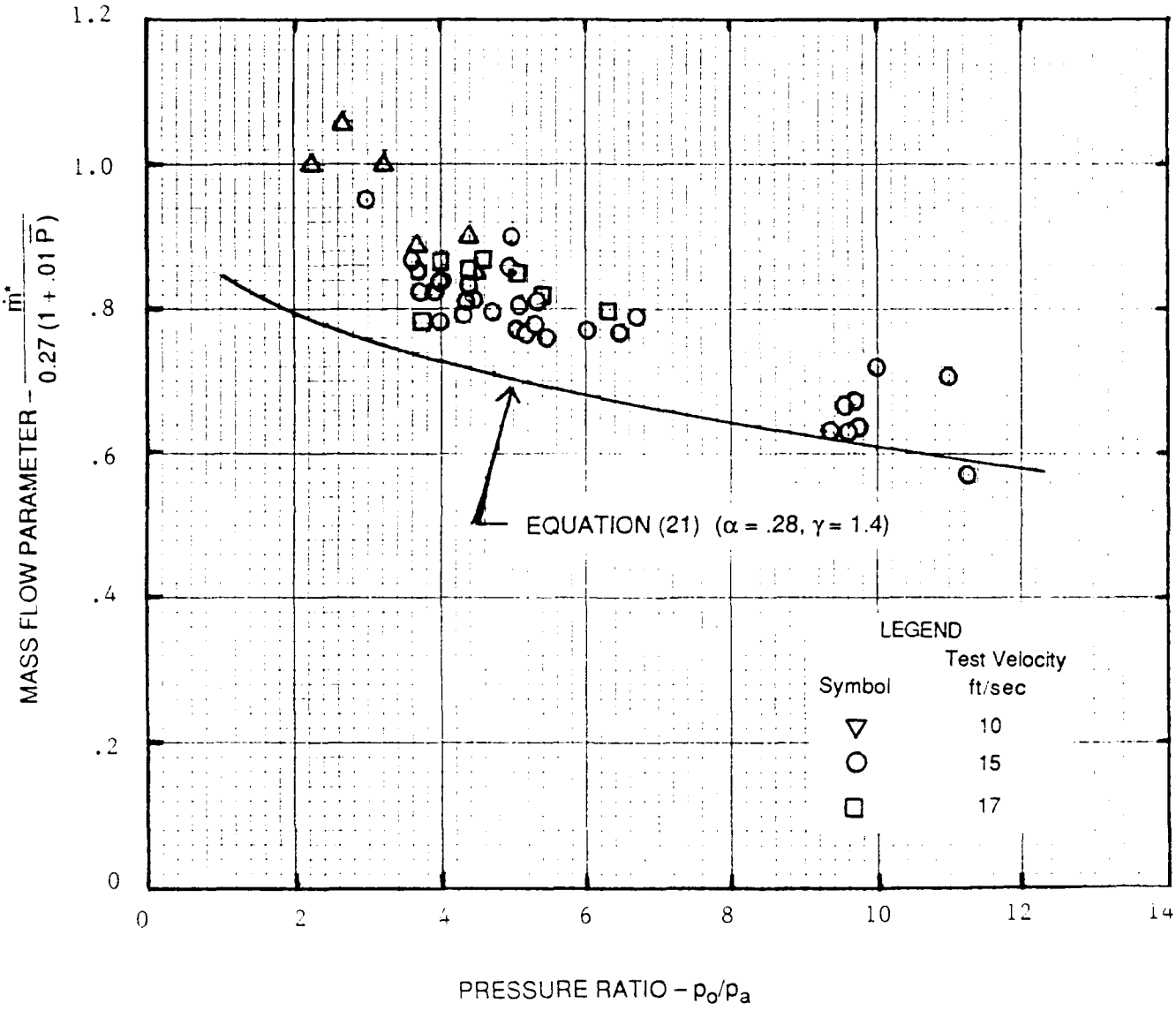

Figure 5-11. The Influence of Pressure Ratio and Pressure Parameter on the Mass Flow Parameter $\dot{m}^*$ – Comparison of Theory with Experiment for Cold Gas and Advance Coefficient of 3.15

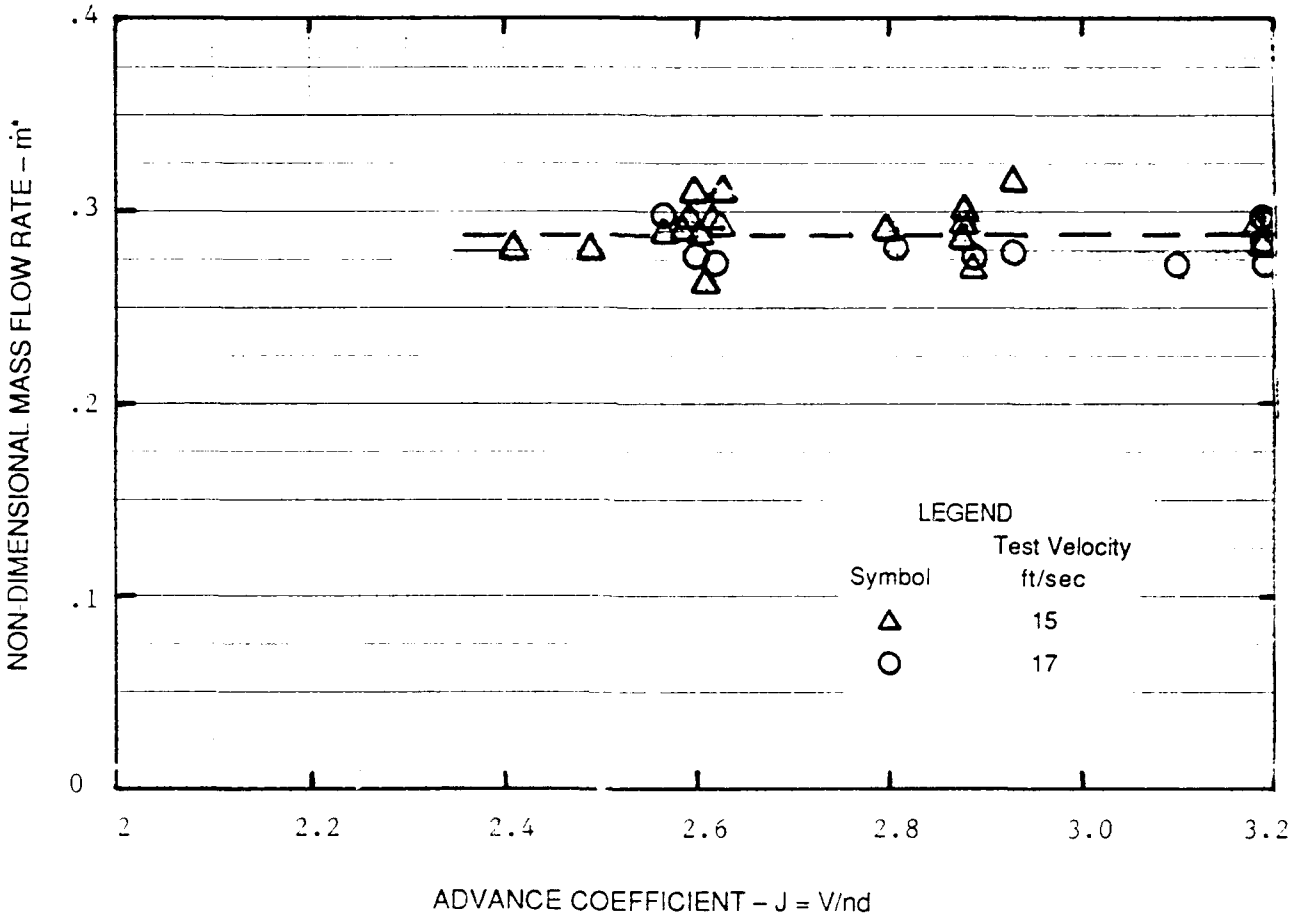

Figure 5-12. Measured Effect of Advance Coefficient on the Mass Flow Parameter, $\dot{m}^*$

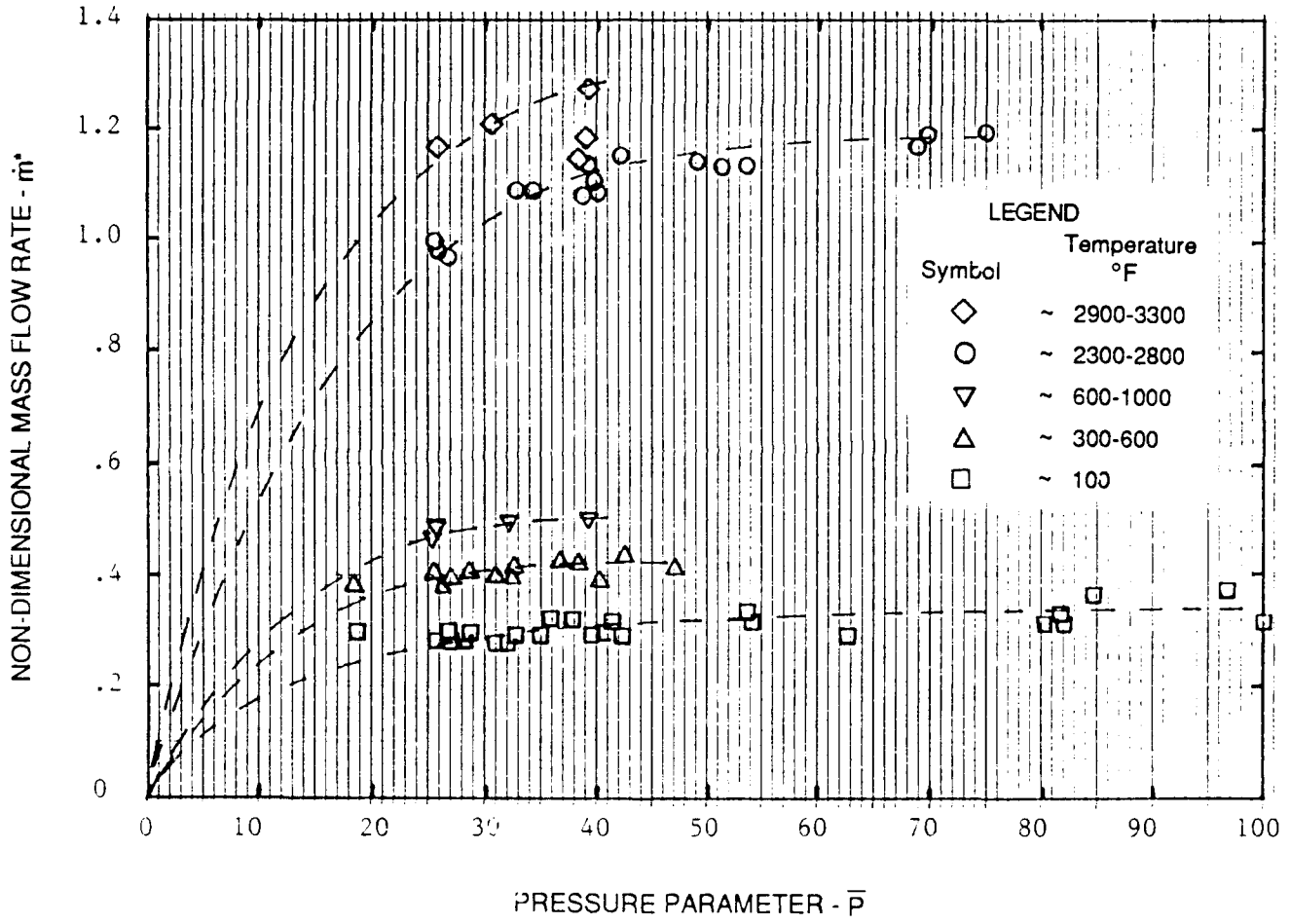

Figure 5-13. The Influence of Gas Temperature and Pressure Parameter, $\bar{P}$, on the Mass Flow Parameter, $\dot{m}^*$

representing the measured values of $\dot{m}^*$ using cold gas (T_o ~ 600° R). Figure 5-13 shows that the value of $\dot{m}^*$ for the combustion gas (3500° R) is approximately four times the measured cold gas values for all values of $\overline{P} \gtrsim 40$. This means that the high temperature efficiency of the WPP is only one-quarter of the adiabatic efficiency at this test speed or 75% of the available heat energy is lost.

Figure 5-14 presents measured values of $\dot{m}^*$ at design J = 3.14 and $\overline{P}$ = 35 for velocities of 10, 15, 17-18 and 18-22 feet per second over a range of gas temperatures from cold (525° R) to the hottest combustion gas (4900° R). The important point to note in this figure is the definite decrease in the value of $\dot{m}^*$ (at a given temperature) as the speed is increased. It then follows that the efficiency at a given temperature and $\overline{P}$ will increase as the speed increases - - the heat loss fraction, α_L, decreases with increase in speed.

5.1.3 Efficiency

Cold Gas

Figures 5-15 and 5-16 present measured efficiencies for the cold gas (T = 525 ° R) as defined in Equation (31) using a value of 1/3 for the compressor efficiency, η_c. Figure 5-15 shows the variation of the efficiency with the pressure coefficient $\overline{P}$ for speeds of 10, 15 and 17 fps. The estimated value of efficiency as given by Equation (35) for $K_{t,o}$ = .19 for $\overline{P}$ > 60 is also shown on this Figure. Equation (35) compares favorably with the measured values in the high $\overline{P}$ range. Figure 5-16 presents these same data plotted against the pressure ratio, p_o/p_a.

Hot Gas

Figures 5-17, 5-18 and 5-19 show the influence of the pressure ratio p_o/p_a on measured values of the efficiency for three nominal gas temperatures - - heated air T = (300-360° F) and (700-800° F) and combustion gas T = (3000° to 4000° F). Figure 5-17 presents the efficiency data for speeds of 15, 17-18, and 21 fps. As shown in Figure 5-18 data were obtained in the 700 to 800° F range at only one speed, V_o = 15 fps. Figure 5-19 shows that for the combustion gas the efficiency was measured at speeds of 10, 15, 17, 20 and 22 fps. The important points to note in Figures 5-17 through 5-19 are that the efficiencies decrease with an increase in temperature and that at a given temperature, there is an observable influence of water speed, V_o.

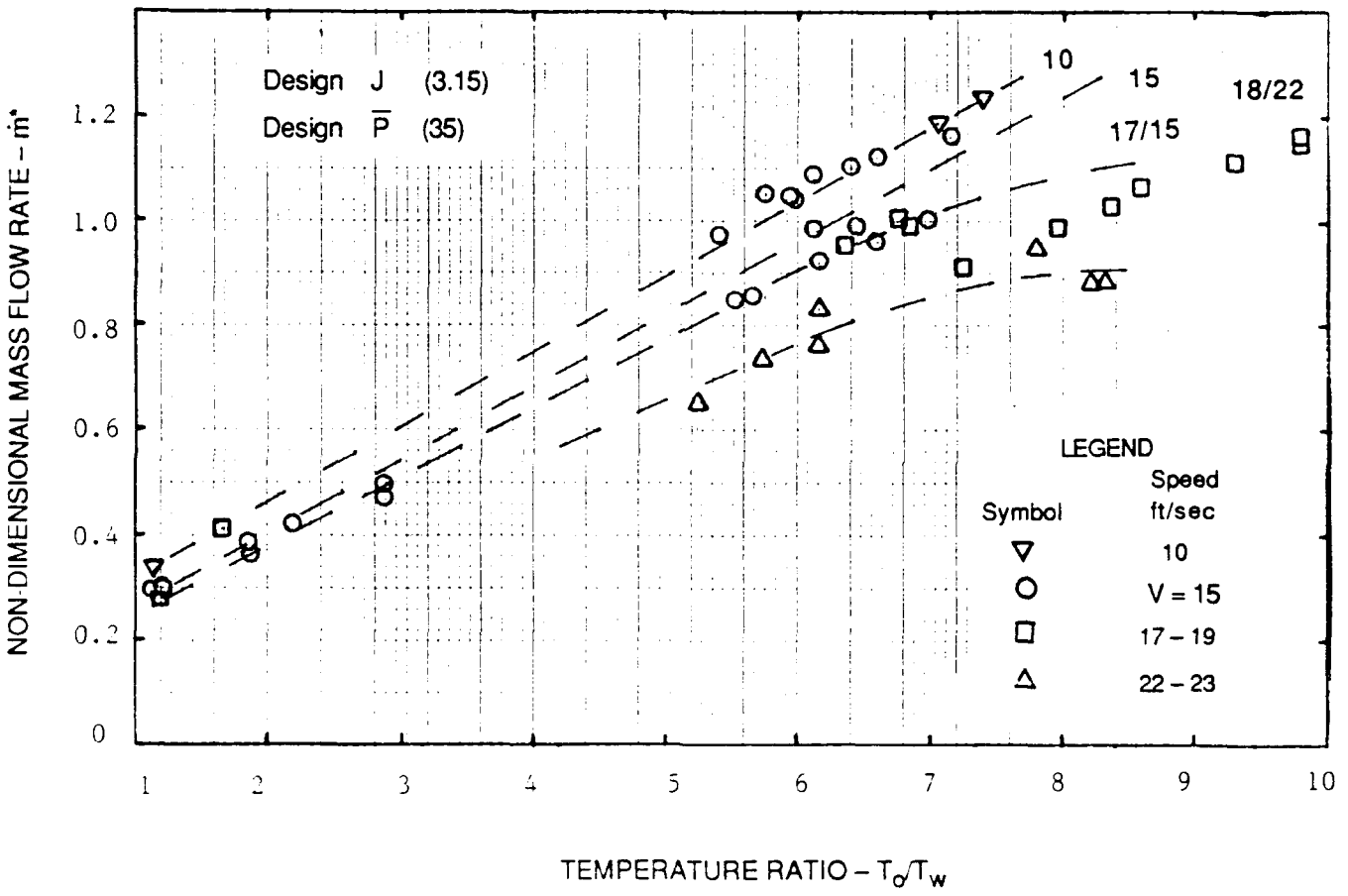

Figure 5-14. Variation of Non-dimensional Mass Flow Rate with Temperature Ratio at Nominal Design Point, $\bar{P}$ (35) and J (3.15)

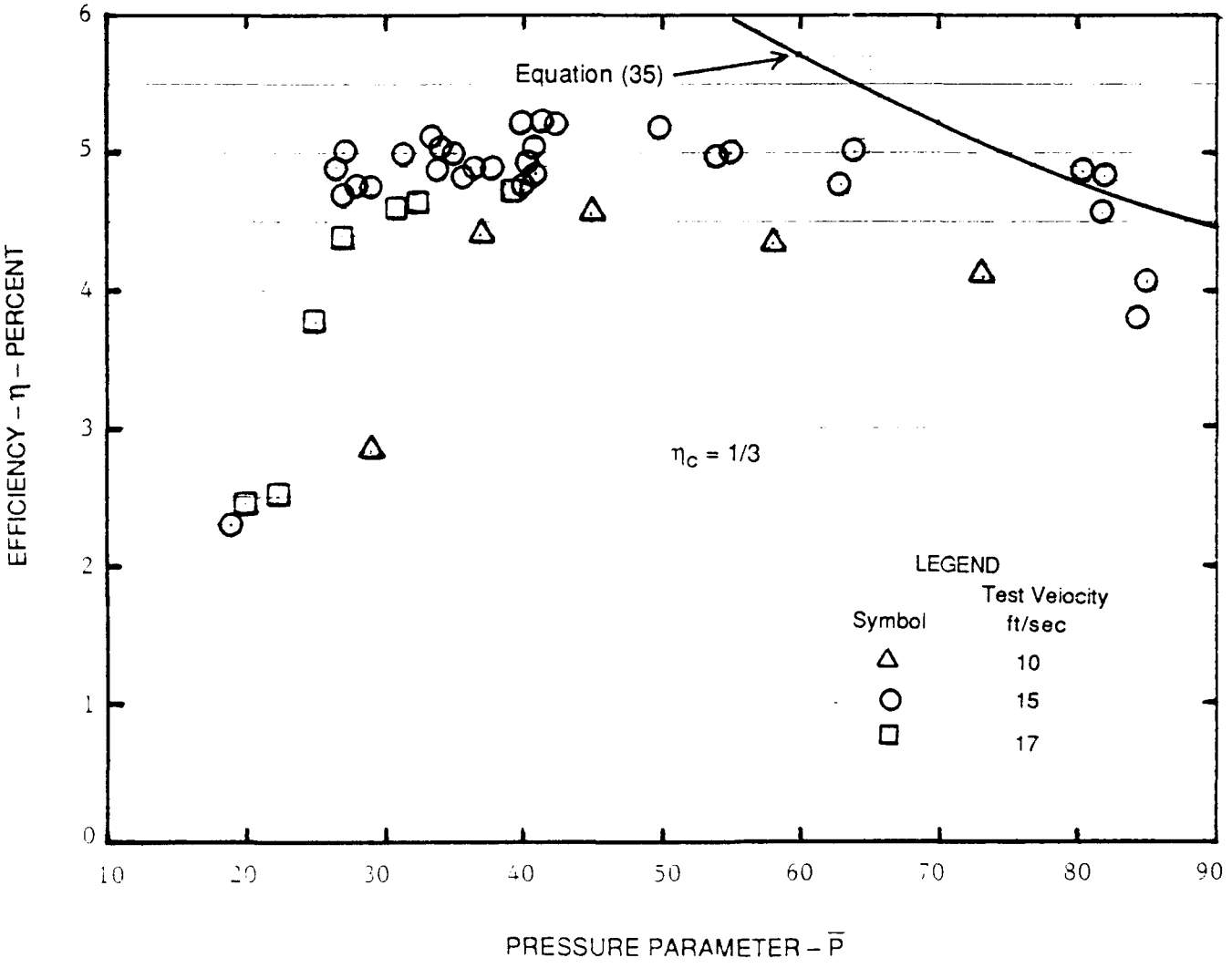

Figure 5-15. The Influence of Pressure Parameter, $\overline{P}$, on the Total Efficiency, η, for Various Speeds. Theory and Experiment, Cold Gas (T= 65°F), J = 3.15

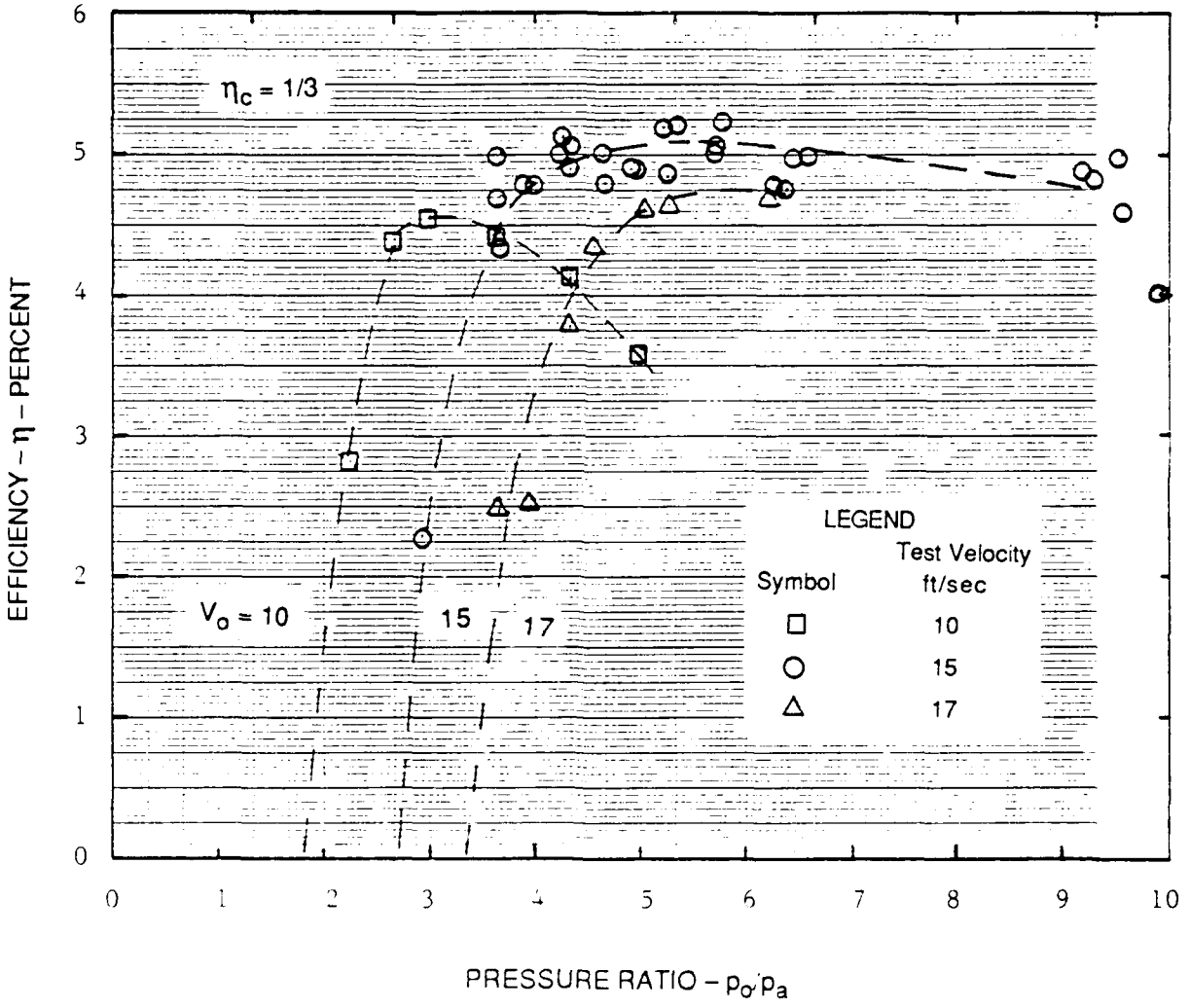

Figure 5-16. The Influence of Pressure Ratio on the Total Efficiency, η, for Various Speeds, Cold Gas (T = 65°F)

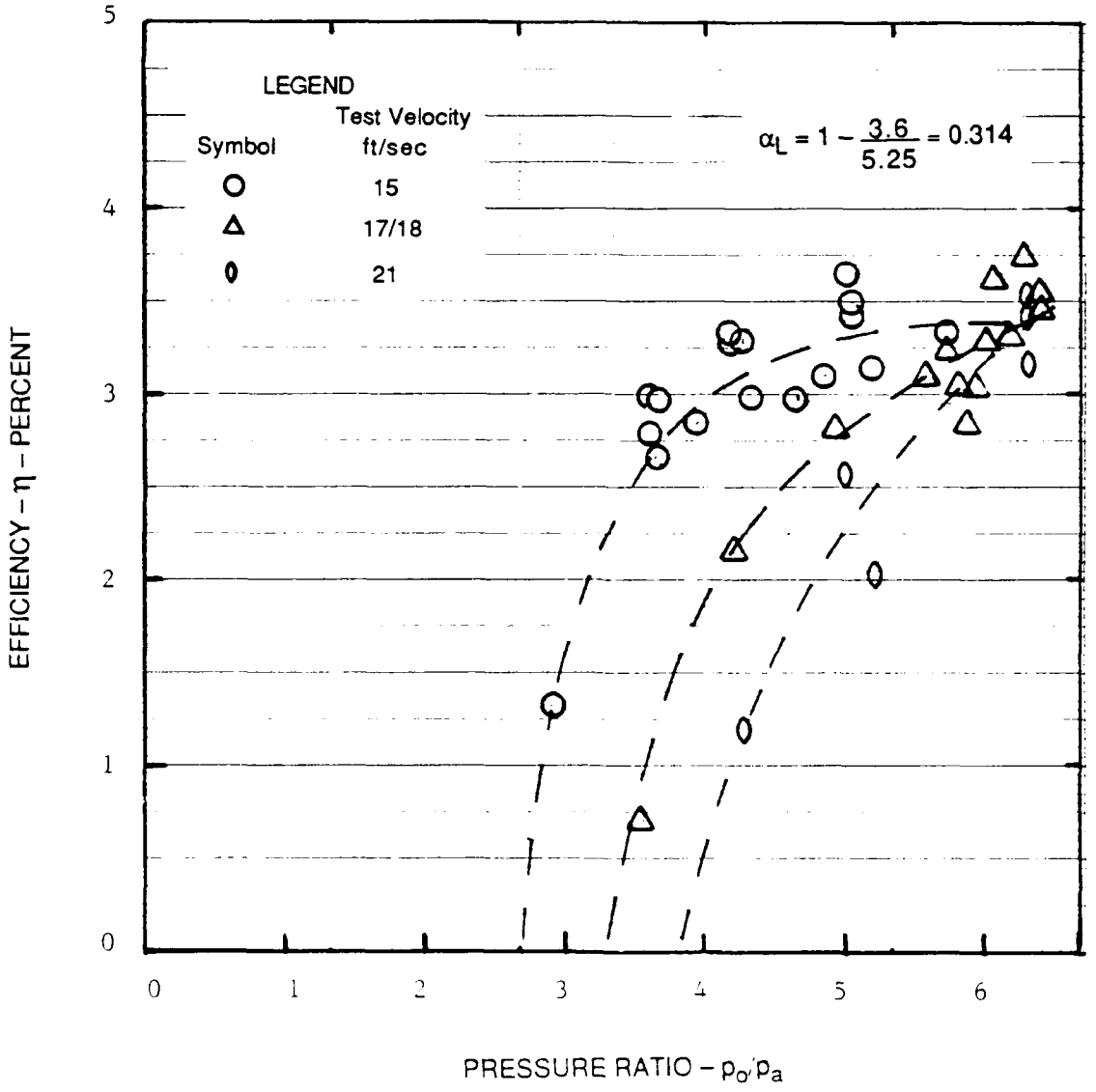

Figure 5-17. The Influence of Pressure Ratio on the Total Efficiency, η, for Various Speeds

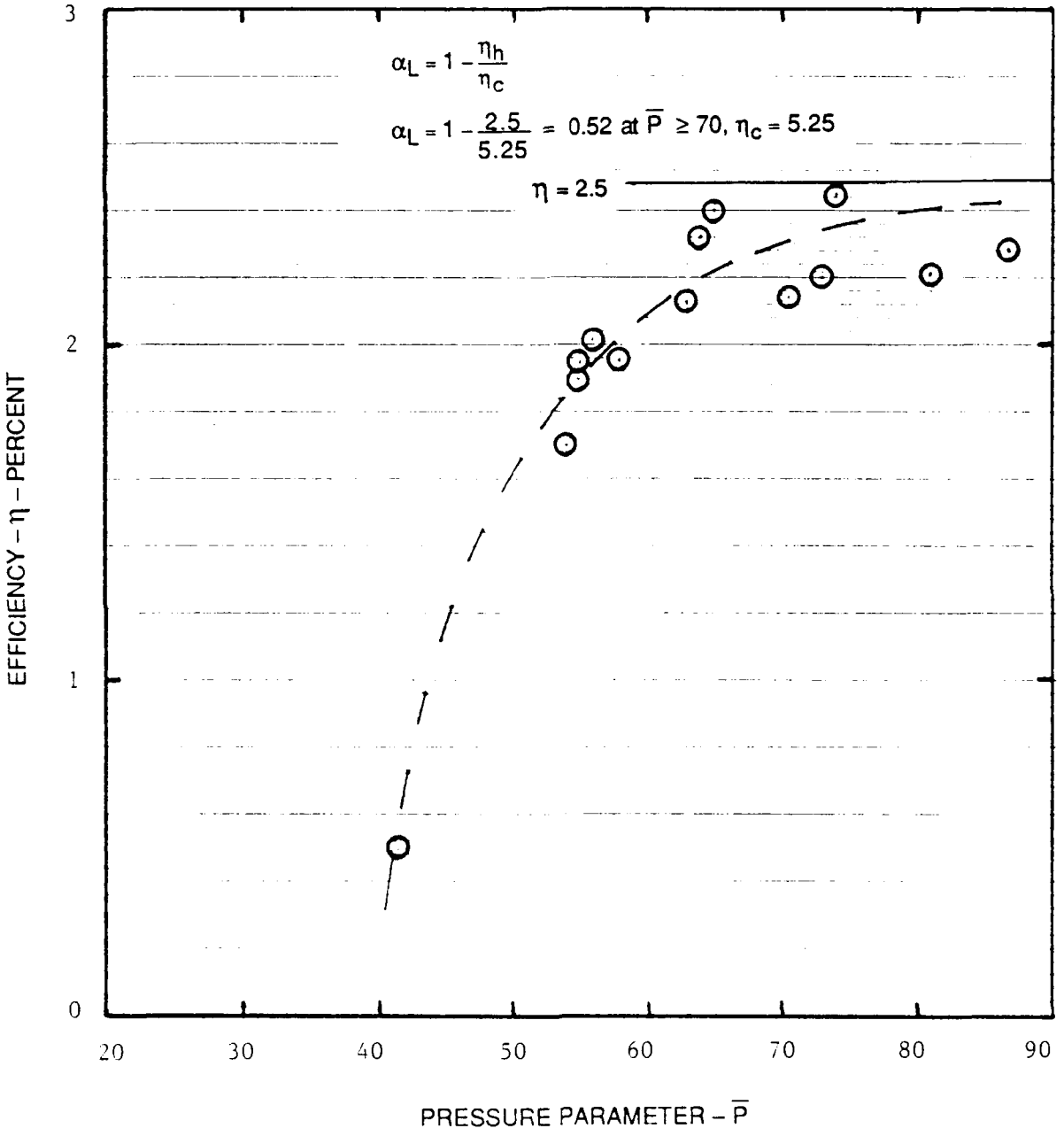

Figure 5-18. The Influence of Pressure Ratio on Total Efficiency for Different Speeds For Warm Air, T_o = 700° – 800°F

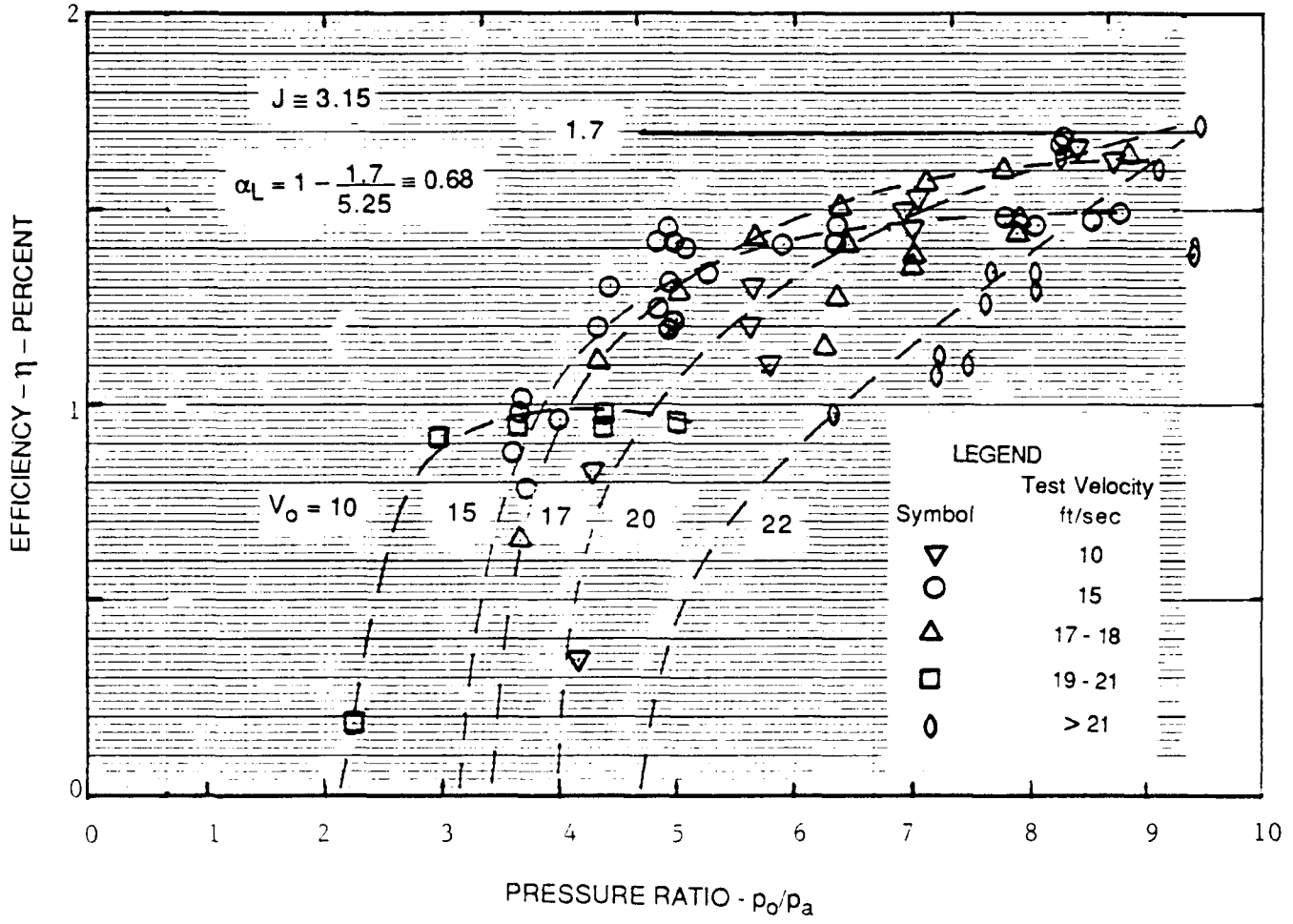

Figure 5-19. The Influence of Pressure Ratio on Total Efficiency for Different Speeds for Hot Gas

Figure 5-20 is a plot of all the efficiency data obtained at approximately the design advance ratio J = 3.15. The extremely rapid decrease in the efficiency with increasing gas temperature shown in Figure 5-20 illustrates the large heat losses that must be present. As gas temperature increases, heat transferred from the hot gas to the cold water greatly reduces the energy available to do work. Figure (5-20) includes all of the efficiency data together with the line representing the nominal values. Also shown in Figure (5-20) is the efficiency ratio, η_r, with η_a taken at its nominal value of 5% for $T_o = T_w$.

Figure 5-21 presents nominal values of β and α_L deduced from Figure 5-20 using Equation (60). Note that near $T_o/T_w = 1$, $\beta \rightarrow \infty$ so that detailed measurements of β near $T_o/T_w = 1.0$ will be expected to have significant error or scatter.

The effective inlet temperature may be deduced from the nominal efficiency measurements using Equations (27) and (28). This effective temperature normalized by T_o and T_w is presented in Figure 5-22. The effects of heat loss are dramatic.

An examination of the data show that Equations (53) and (56) does agree very well with the experimental data obtained if the coefficients, C_β, a, and C_Ω are taken as follows. It is assumed the $(P_r)^{1-b} = 1$; that is, $b \approx 1$

$$C_\beta = 7.1$$
$$a = .75$$
$$C_\Omega = 5.3$$

Figure 5-23 is a plot of the ratio of the measured value of β to the value of β given by Equation 48 with the values of $C_\beta = 7.1$, $a = .75$, and $C_\Omega = 5.3$. This ratio is near unity over the entire range of T_o/T_ω (1 to 6) measured except near $T_o/T_\omega = 1$ where β becomes singular and small errors in thrust and mass flow measurements will cause large scatter in the deduced values of β.

The fact that all of the measured data are satisfactorily predicted using the empirical constants specified means that the product $C_s\, C_h$ in Equation (48) is nearly constant because the values of η_h and P_r do not vary much for the conditions tested. Similarly the ratio ε/C_h in Equation (49) must be nearly constant because the value of P_r is constant.

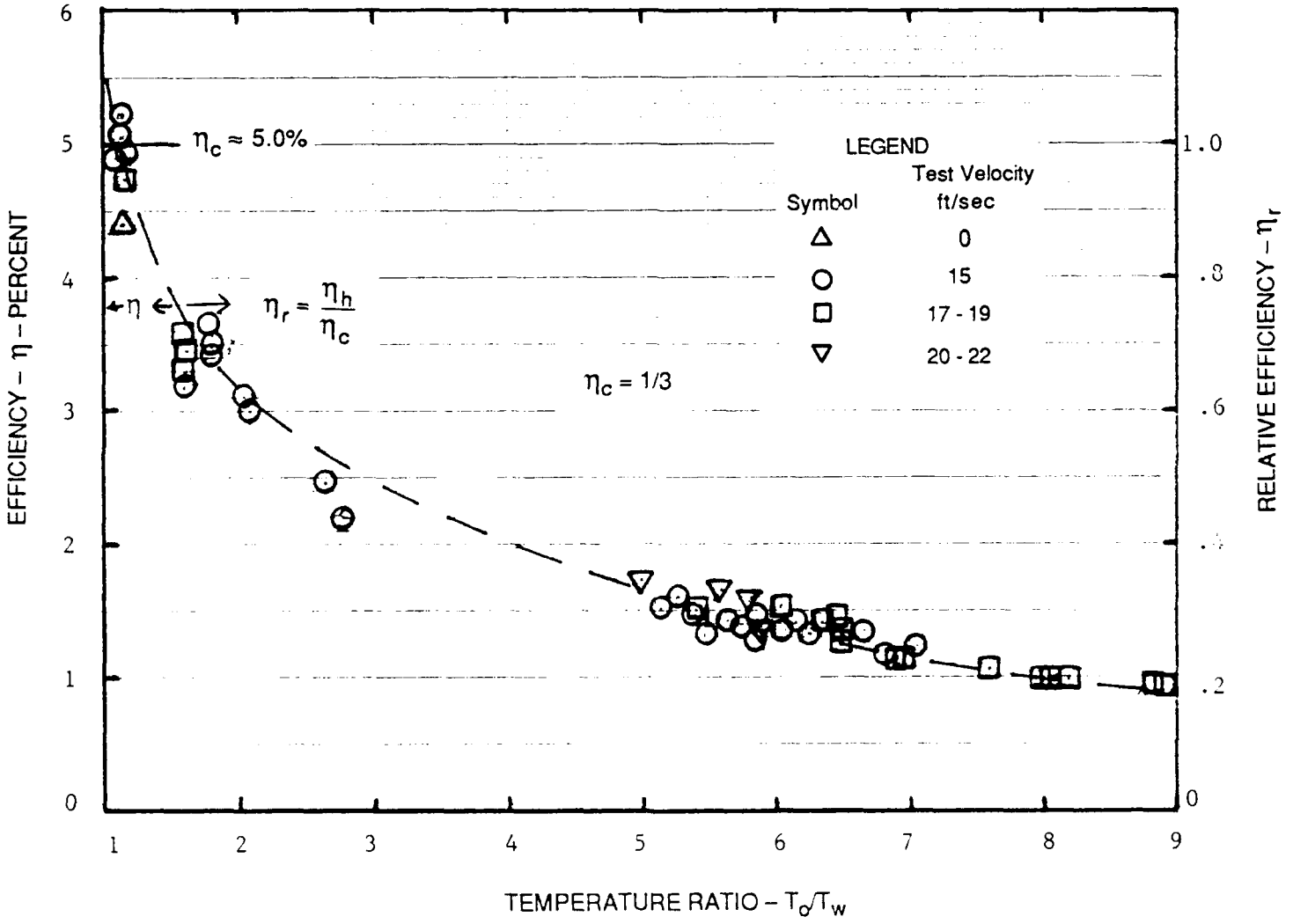

Figure 5-20. The Influence of Temperature Ratio on Total Efficiency for Various Speeds. $J = 3.15$, $\overline{P} \approx 35$, $\eta_c = 1/3$

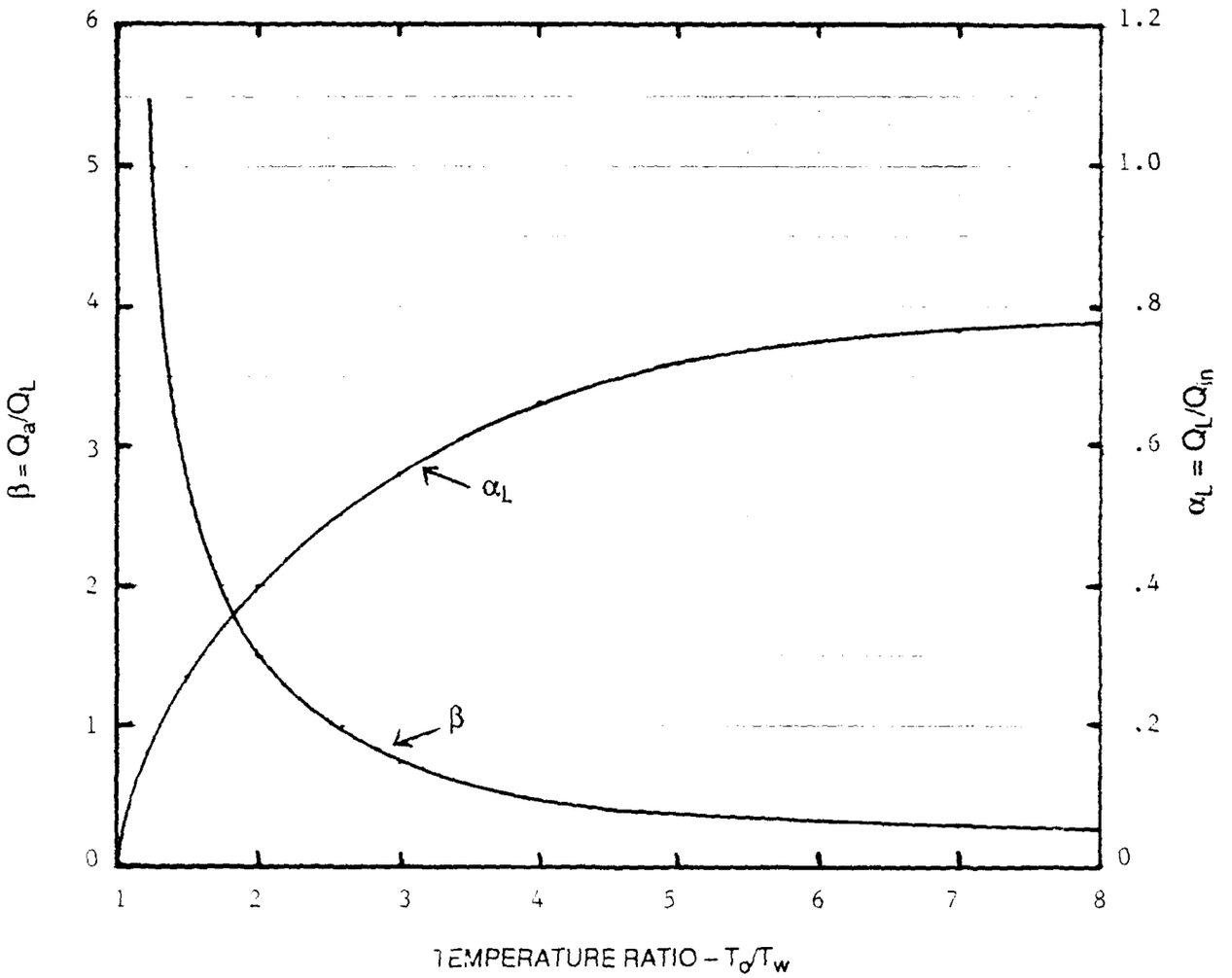

Figure 5-21. Nominal Values of Heat Loss Parameters α_L and β Deduced from Figure (5-20) Measured Efficiencies

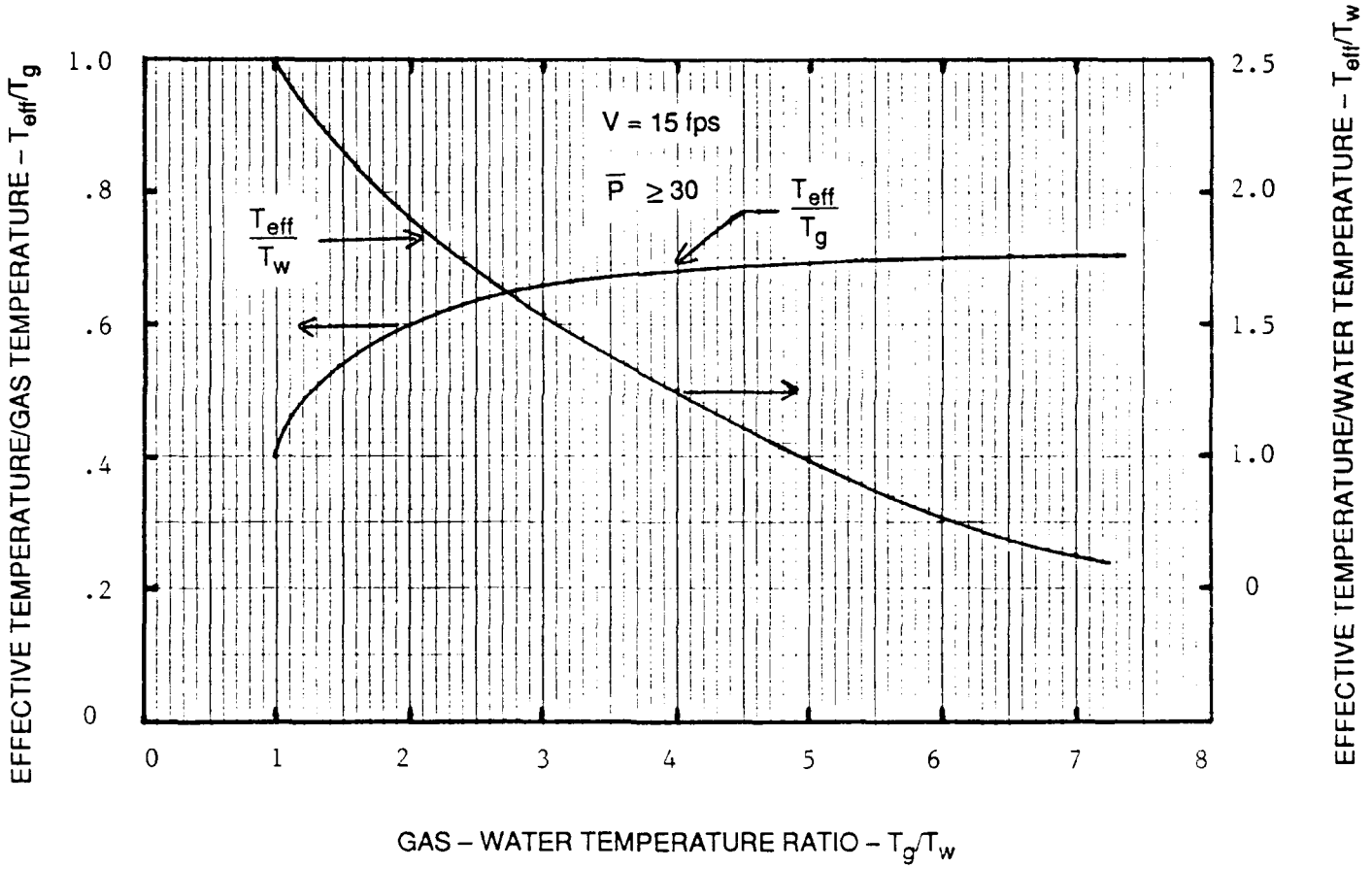

Figure 5-22. Nominal Values of Temperature Ratios Deduced from Figure (5-20) Measured Efficiencies

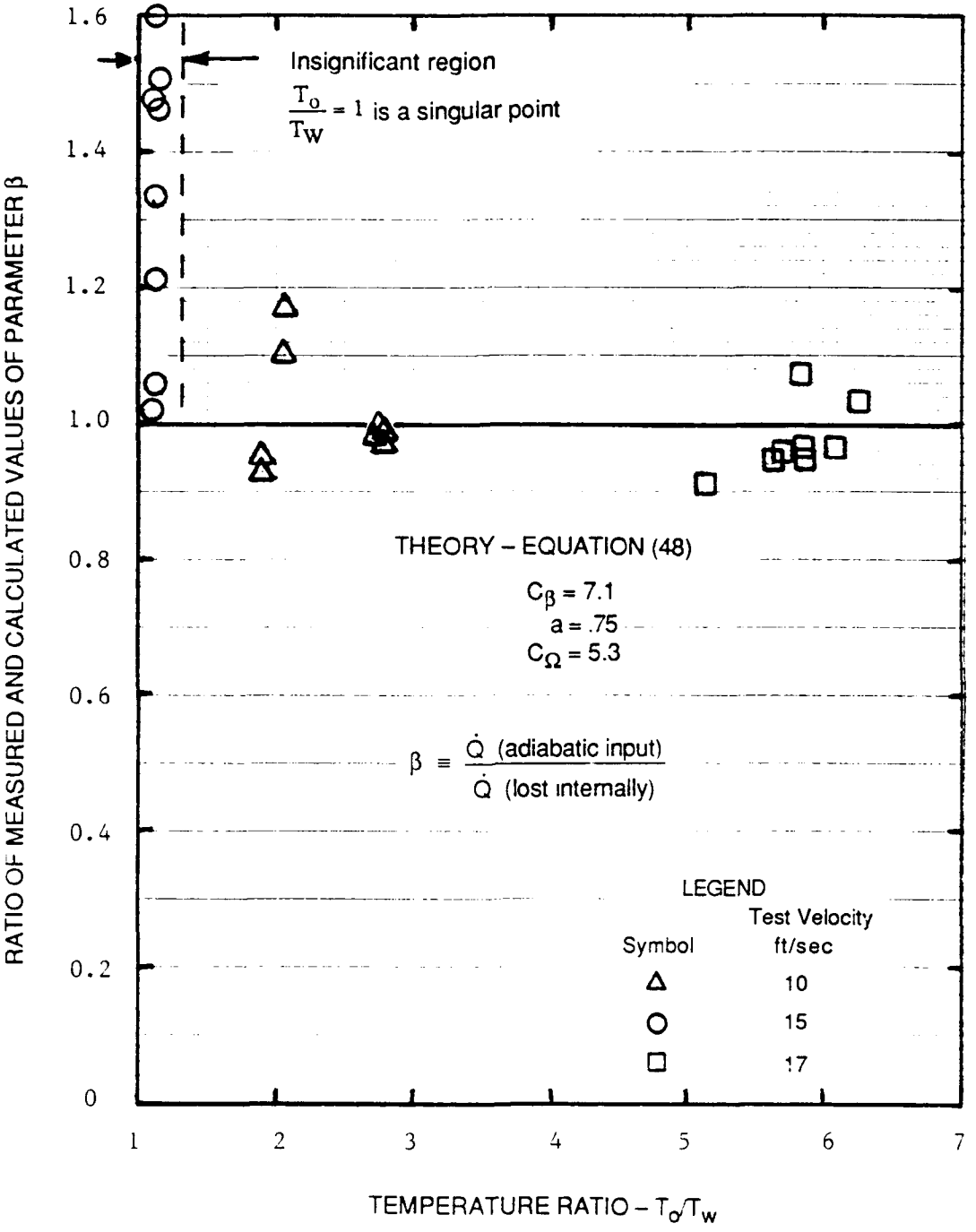

Figure 5-23. Comparison of Measured Values of the Parameter β and the Values Calculated from Equations (53) and (56)

The emissivity, ε, is a factor only for the combustor gas and should have a nearly constant value of approximately 0.03 (Reference 15). If the value of C_Ω is 5.3 and $\varepsilon \approx 0.03$ then the value of C_h may be deduced as 0,.04. Using C_h= 7.1, η_h= .4, and C_h = 0.4, the deduced value of C_s is 8.7.

Reference 15 gives C_h for convective heat transfer inside tubes as .023. The deduced value of C_h = .04 (based on ε = .03) is only about two times the Reference 15 value. Agreement can be achieved if ε= .016, however; such a large error in estimating ε is not likely. The deduction that the actual surface area is about10 times the reference surface area indicates that there must be an aerosol of water drops present and the model of heat transfer inside tube walls has no meaning for most of the heat transfer and so the value of C_h should not be expected to be the Reference 15 value of .023.

It is interesting to estimate the thickness of water film on the passage walls that will generate an aerosol of drops that are, say 10 μm in diameter with a total surface area 7.7 times the passage surface area. This thickness may be calculated to be 1.3 x (drop diameter) or 13 μm. It is believed that the very high heat loss fractions measured in the present tests are primarily caused by the greatly increased area resulting from the formation of a fog or aerosol. If the estimated increase in area of 8 times were eliminated so that C_s = 1. The value of C_β would increase by 8.7 and the measured heat loss fraction of .75 ($T_o \approx 3000°R$) would be reduced to .25.

During the experiments with the trapezoidal gas port, slots were provided in the seal face in the passage closure area (Figure 3-4) so that chemical additives that should alter the surface tension of the water could be injected. The motivation for injecting surfactants was to see if the observed values of β were altered and hence produce evidence of a high population of water drops. No significant changes in the value of $\dot{m}^*$ or b were observed. Since the drops are probably generated by the gas shear on the water film formed on the passage walls it is doubtful if the surfactants reached the passage walls in sufficient concentration to affect droplet formation.

The scaling of the experimental data to prototype conditions for the Marine Corps Amphibian is straightforward once the empirical coefficients C_β, C_Ω and a are established. For the prototype conditions

p_o = 220 psia

p_a = 15 psia

V_o = 29.33 fps

and thus

p_a/p_o = .068, p_o/p_a = 14.67

$$\frac{p_o - p_a}{1/2\ \rho V_o^2} = 34.3$$

Equation (12) and Figures 5-1 and 5-5 give $K_{t,o} = .195$. Therefore, the thrust produced will be 1,440 lbs., approximately one half the required full scale thrust required of 3,000 lbs. The overall efficiency without heat loss will be approximately 5%, about one half the desired value of approximately 10%.

Equation (48) gives a full scale value of $\beta = .49$ for a temperature ratio, $T_o/T_\omega = 6$, or for T_o = 3150°F and a water temperature of 525°R (65°F). The heat loss fraction is therefore .67 (compared to .75 measured in the present experiments at lower pressure and velocity. The efficiency ratio, η_r, is .33 and thus the predicted efficiency with the combustion gases is .33(0.05) or approximately 1.6%.

As noted previously if the value of C_s could be reduced to unity (no aerosol) the value of β would be increased to 8.7 (.49) = 4.2 and the heat loss fraction reduced to .19 and the efficiency increased to .81 (5) ≈ 4%. It is important to note that if Equation (53), with the empirical coefficients derived from the present test data, are generally applicable, the heat loss problem becomes much less significant as the product $p_o V_o$ increases. Such is the case for high speed missiles where this product may be 500 times the product typical for the present tests. For similar rotor geometry and gas temperature the value of Ω will be decreased by $(500)^{-.75}$ or by approximately 100 so that radiation losses are negligible compared with the convective losses even at somewhat higher temperatures. The value of β is increased by $(500)^{.25}$ or by approximately 5 so that the heat loss fraction will be .37 instead of .75. Since a water piston designed for a missile will have multiple ports, the passage geometry factor ($A_p/P_{er} \cdot L$) will be increased by about a factor of about 2 so that β will be further doubled and the heat loss fraction reduced to .23. Such values of heat loss fraction will probably be acceptable if the overall adiabatic efficiency is adequately high.

5.2 Summary and Conclusions

Based on the measured results described in this section and analysis presented in Section 5, certain conclusions about measured performance should be highlighted.

1. Measured thrust depends principally on the input and exhaust pressure and is generally independent of the gas input temperature.

The measured net thrust was approximately one half the value predicted by the Zonko-THI computer program for the rotor with smooth friction based on the pressure input to the combustion chamber. Thus the predicted full scale value of $K_{t,o}$ based on the measurements was 0.2 compared with a value of 0.4 required to propel the amphibian at 20 mph. The deficit of 0.2 may be partially accounted for as follows.

Forebody Fairing & Rotor External Drag	≈	0.04
Pressure drop in the Combustion Chamber	≈	0.005
Gas Port Tested Versus Original Design	≈	0.04
		0.13

The remaining deficit of 0.07 must be attributed to non-smooth friction, non-planar gas-water interface and pressure losses during gas injection.

The configuration tested must be supplied with gas at approximately 425 psia instead of the original design value of 220 psia in order to achieve the required thrust of 3,000 pounds per rotor.

2. Thrust is essentially the same for cold air (75%) and hot gas (3000°F) although thrust coefficients with hot (700° to 1100°F) air are somewhat lower than those with cold air or hot gas. Independence of thrust and gas temperature would be expected only with adiabatic expansion at the gas, which clearly was not the case for the hot gas tests.

3. The measured efficiency of the WPP tested using gas at approximately the water temperature (negligible heat loss) was about 60 percent of the originally expected value of 10%. This reduction in efficiency is undoubtedly a direct result of the reduced thrust.

4. The measured efficiency of the WPP when tested using hot gas decreased greatly with increasing temperature -- from about 5% at 75°F to 1.3% at 3000°F. Based on these results it can be shown that at full scale operating conditions, approximately 67% of the heat input should be lost by transfer of heat from the hot gas to the water inside the rotor passages.

5.3 Reliability and Failures

The system proved to be fairly reliable during most of the final set of tests. However, a major failure of four of the rotor vanes or webs occurred near the end of the test program, resulting in a significant degradation of performance and a clearly observable increase in vibrations and mechanical

noise. Seal wear at the end of testing was fairly significant. Severe oil/soot fouling of the combustion chamber and HSC water and structure also occurred.

Figures 5-24 shows several views of the observed failure of the rotor webs. Figures 5-24a and 5-24b show radial cracks of increasing severity over a significant portion of the web radial length or span, while Figures 5-24c and 5-24d show complete failure of portions of a web. This failure occurred well downstream of the rotor inlet face where the greatest pressure differences across a given web and resulting stresses in the web should occur. It is felt that these failures were due at least in part to inadequate plug welds in the middle of the rotor. The plug welds were used to join the rotor shroud and webs.

It should be noted that failure of the rotor webs could have started at any time during the tests, with potentially adverse effect on performance. Actual damage was probably discovered after disassembly only because of its severity of and the desire to find a cause for the severe vibrations observed during the later tests. Less severe damage with significant performance degradation might have well have gone unobserved.

Figure 5-25 shows the seal wear which occurred primarily on the closure or low pressure side of the seal. The maximum depth of wear at the closure edge of the seal after 35 hours of operation was approximately one-eighth inch at the shroud. It is not possible to predict from the observed wear an expected seal life. It should be possible to achieve longer seal life and satisfactory rotor seal with a harder seal material.

Additional minor damage beyond that observed at the completion of the first set of tests was observed inside the combustion chamber after completion of all tests. It seems unlikely that the observed damage had a significant adverse effect on combustion performance, but the life of the combustion chamber could be limited by continuing, progressive failure of the type observed.

Fouling around the combustion chamber fuel oil spray nozzle, as shown in Figure 5-26, was so severe that degradation of combustion efficiency during some or most of the tests seems likely. The suspicion of incomplete combustion and significant reduction of combustion efficiency was greatly increased by the rapid and severe fouling of the 23,000 gallons of water in the HSC by some combination of oil and soot. Following completion of the tests large amounts of oil/soot were found on structure throughout the inside of the HSC.

a. Initial Failure in Outboard Portion of Web

b. Failure in Inboard Portion of Web

Figure 5-24. Damage to Rotor Observed Upon Completion of Test Program

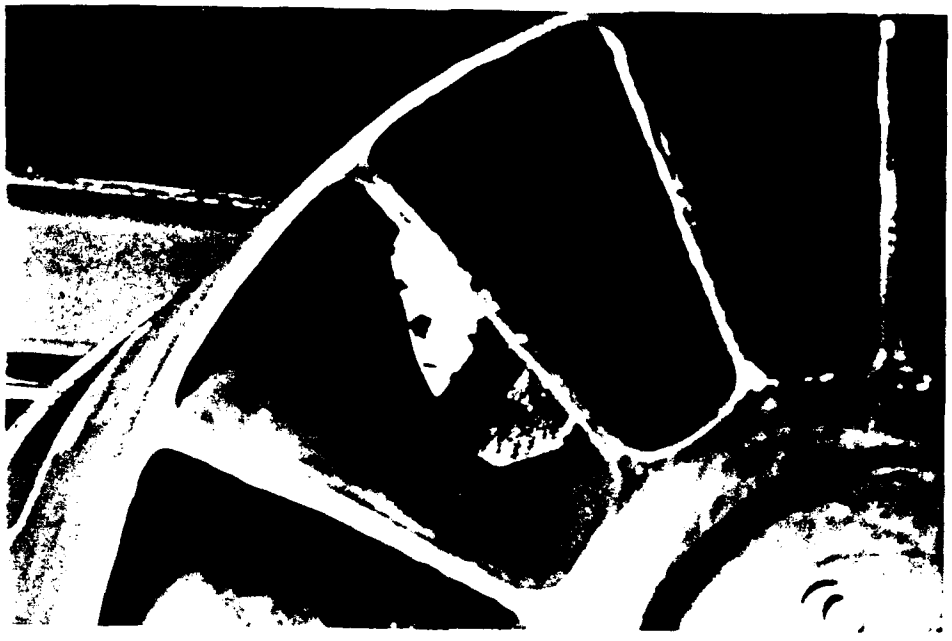

c. Complete Failure of Web

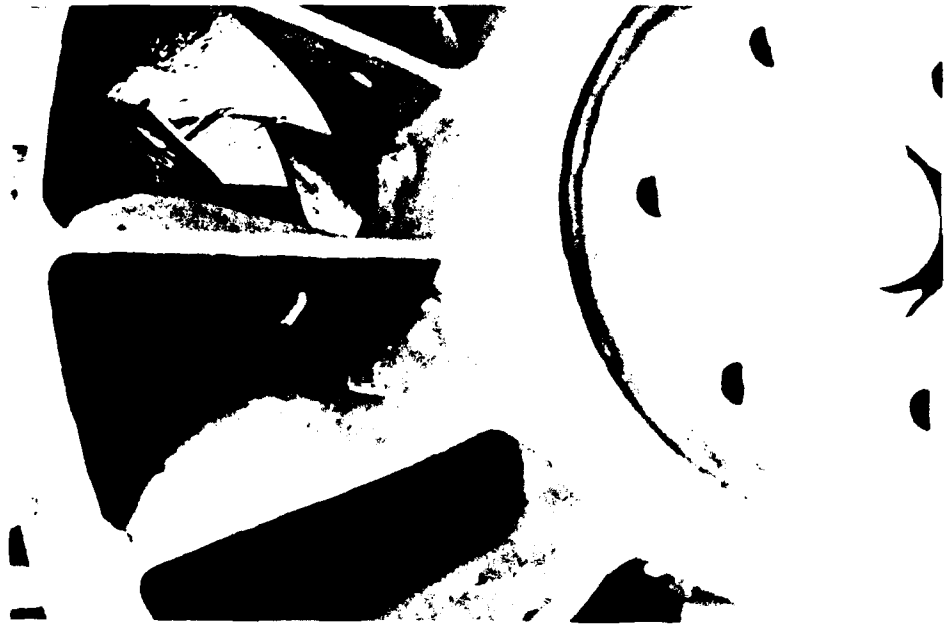

d. Complete Failure of Web

Figure 5-24 (Concluded)

a. Seal Before Testing

b. Seal After Testing Showing Light Scoring and Significant Wear at Outboard Edge of Rotor

Figure 5-25. Two Views of Bronze Seal with Trapezoidal Gas Port

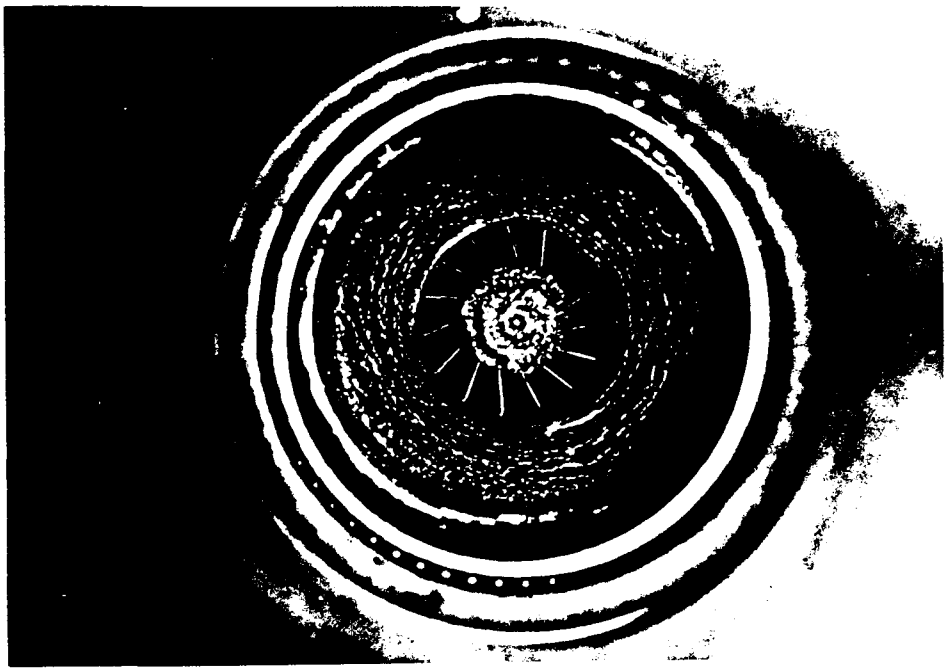

Figure 5-26. Interior of Combustion Chamber Showing Fouling of Nozzle and Area Surrounding Swirler

6.0 RESULTS OF INITIAL SET OF TESTS

The results of the first set of tests are generally similar in nature but more limited in scope than those of the second set of tests. Test velocities were limited to a maximum value of 17 feet per second and chamber pressure was limited to a maximum value of 90 psig.

As discussed in Section 5, the reduced data presented in this section generally do not reflect effects of reduced combustion efficiency or thrust tares due to higher drag of the test set-up than the actual water piston fairing. Inclusion of either of these factors will result in increased efficiency and inclusion of thrust tares will result in an increased net thrust.

6.1 Presentation of Measured Results

Figures 6-1 through 6-6 present a limited summary of results from the initial set of tests. These results are presented to document the principal findings of the initial set of tests and to indicate the changes in performance occurring between the initial and final set of tests. In most figures the trend lines of data from the final set of tests are shown for comparative purposes.

These figures present data for the rotor design advance ratio (nominally 2.65), except as noted. Figures 6-3 through 6-6 present data for the nominal design pressure parameter (P = 35-40), except as noted.

6.2 Discussion of Measured Results

Figures 6-1 and 6-2 present the measured variation of thrust coefficient (based on thrusts uncorrected for forebody drag tare) for combustion tests and air tests, respectively. These Figures indicate that thrusts are somewhat smaller and discrepancies between measured and predicted thrusts are somewhat greater than those found in the final set of tests. It should be noted that the data in these figures are primarily for the original design advance coefficient of about 2.6, where most initial tests were conducted, while most data in the final tests were obtained at an advance coefficient of approximately 3.15, the optimum operating advance coefficient deduced from the test data.

Figure 6-3 presents the variation of thrust coefficient with gas temperature. This variation is similar to that found in the final set of tests, Figure 5-6. As noted in Section 5, the reason for reduced thrusts for operation with warm/hot air cannot be explained.

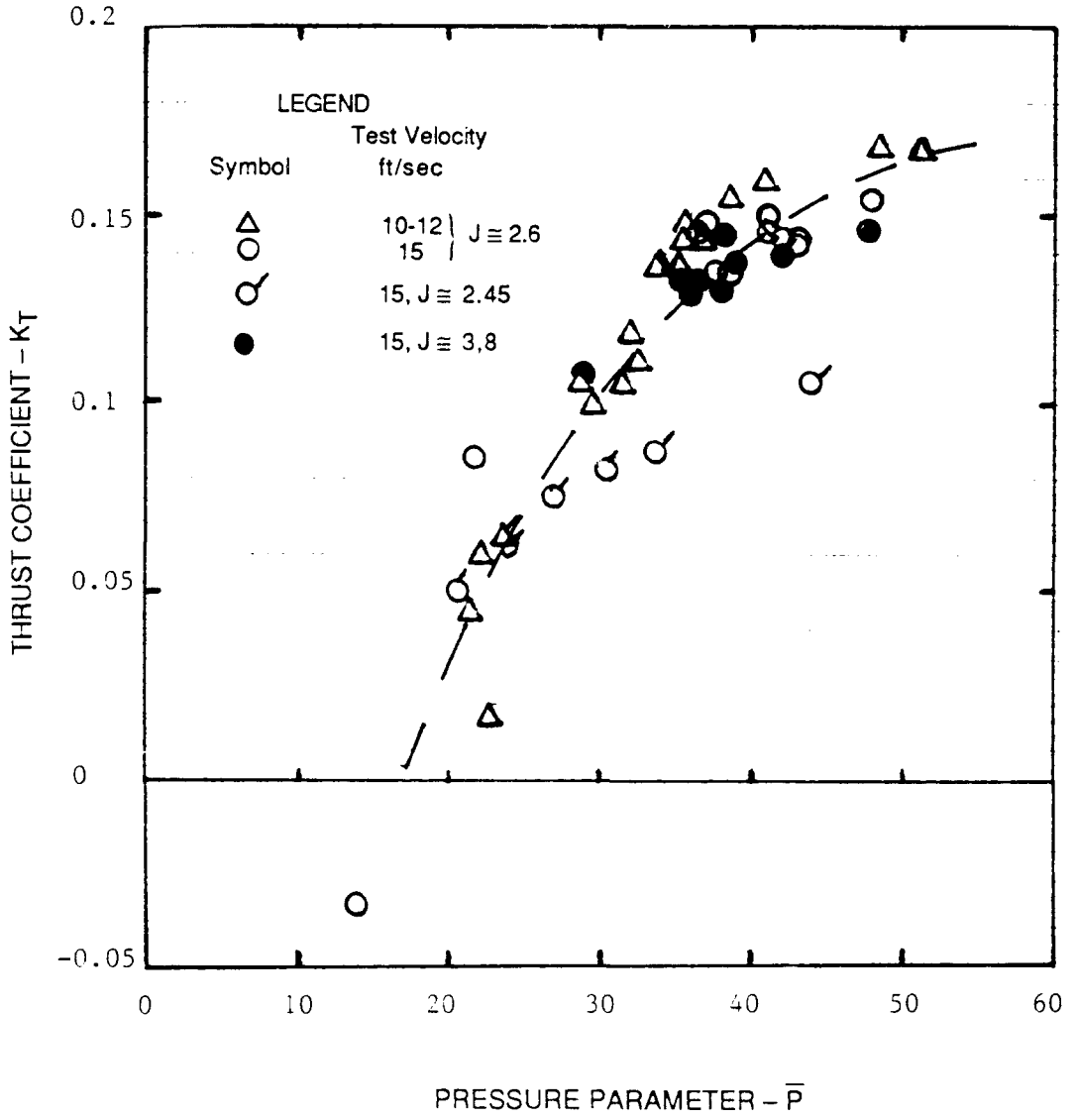

Figure 6-1. The Influence of Pressure Parameter on Thrust Coefficient – All Combustion Test Data for Initial Tests

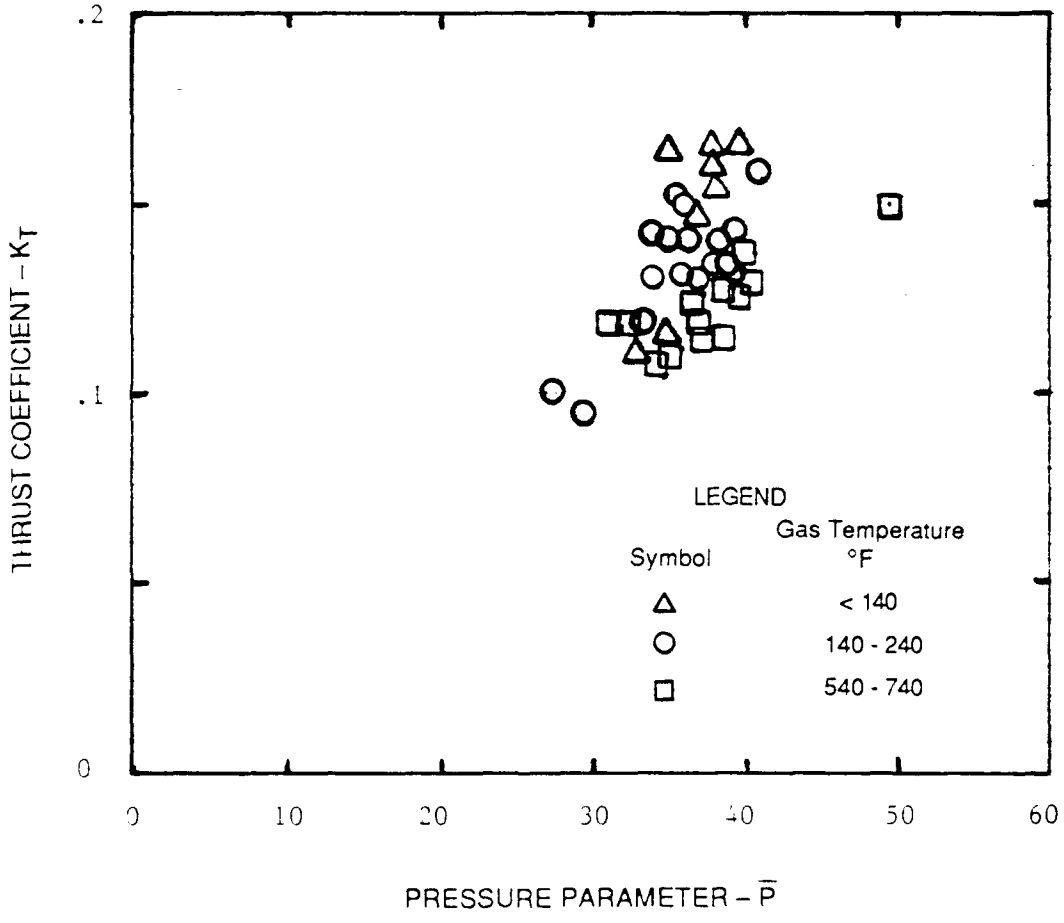

Figure 6-2. The Influence of Pressure Parameter on Thrust Coefficient – Cold and Warm Air Data for Initial Tests

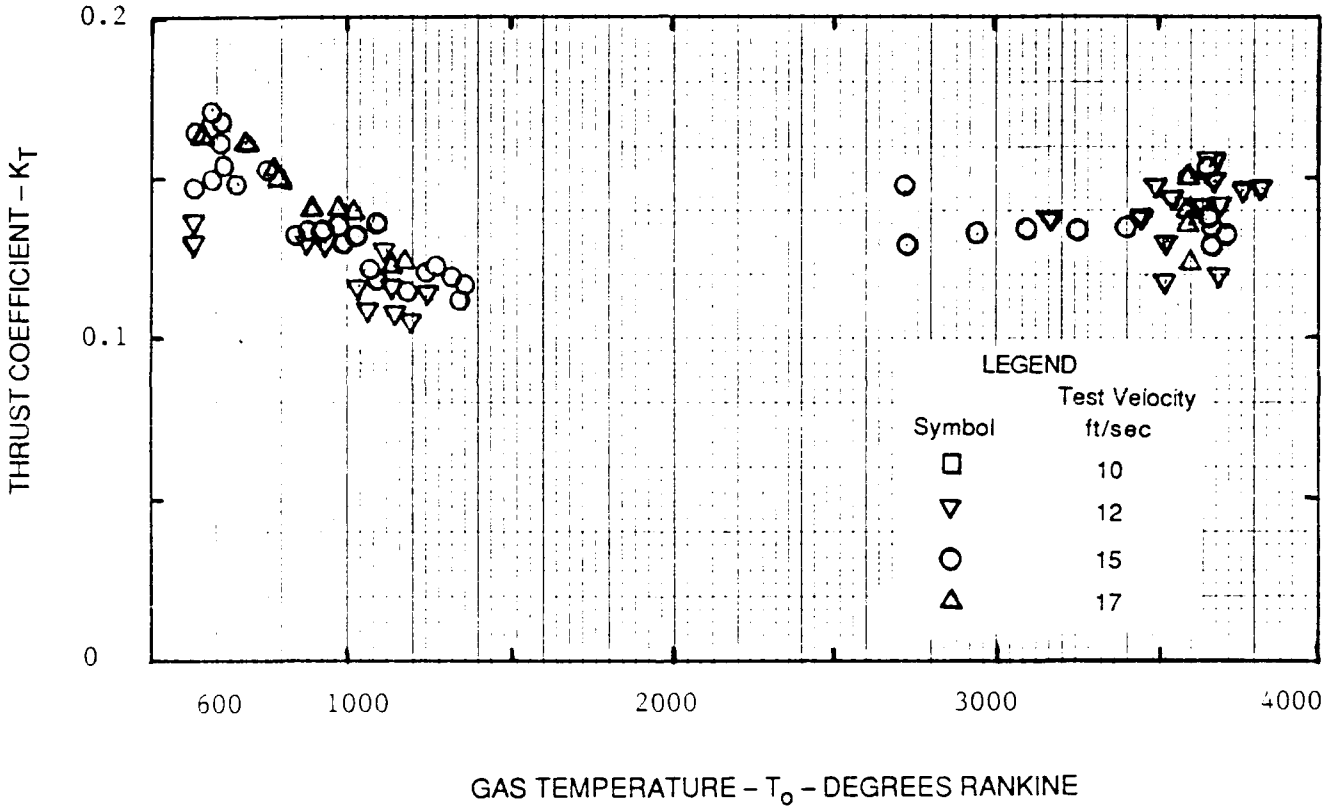

Figure 6-3. The Influence of Gas Temperature on Thrust Coefficient – Data for Initial Tests, $J \cong 2.6$, $\overline{P}$ = 35-40

Figure 6-4 presents the variation of thrust coefficient with advance coefficient for combustion tests. All data shown are for pressure parameters between 35 and 40, which correspond to the prototype design pressure parameter. This figure indicates that the maximum thrust occurs at an advance coefficient of about 3.1 to 3.2, a result that corresponds closely to the results for the final set of tests, Figure 5-8. This result confirmed the impression from the first tests that the rotor should operate at a higher than design advance coefficient or a lower than design RPM.

Figure 6-5 presents the variation of calculated overall water piston efficiency, including a compressor efficiency of one-third, with gas temperature ratio (ratio of propellant gas temperature to ambient or channel water temperature). This figure shows the same rapid decrease in efficiency with increasing gas temperature found in the final set of tests and discussed in Section 5. This figure indicates that efficiencies measured in the final set of tests were significantly greater than those in the initial set of tests. This difference is probably due to the combination of improved gas port geometry and the more efficient operating advance coefficient for the final test series data.

Figure 6-6 presents the variation of non-dimensional gas mass flow parameter with gas temperature. These results are similar to those for the final set of tests, but with calculated mass flow rates some 10 to 12 greater than those for the final set of tests, Figure 5-13, for combustion tests only. For the cold and warm air tests there was no significant difference between the two sets of results. These differences may be due to differences in advance coefficients for the two sets of data (2.65 for the initial set of tests and 3.15 for the final set of tests). The limited set of available results for the initial set of tests at an advance coefficient of 3.0 to 3.2 are shown on the figure.

A comparison of results from the two sets of tests indicates that the modifications to the gas port geometry resulted in some significant changes in measured water piston performance. Replacement of the round gas port of the initial tests with the trapezoidal gas port used of the final set of tests resulted in little change in thrust and selected operating advance coefficient, but a significant increase in the efficiency and a significant reduction in gas mass flow per passage fill for combustion tests only.

6.3 Reliability and Failures

Overall, the system proved to be fairly reliable during the tests. Two major failures were observed, one of the water piston rotor shaft and one of the graphite seals provided by Solar. Some minor damage inside the combustion chamber was also observed, but this damage did not appear to adversely effect the performance of the system. Significant deposits of oil/soot were observed within the combustion chamber and throughout the water channel following completion of tests. While these

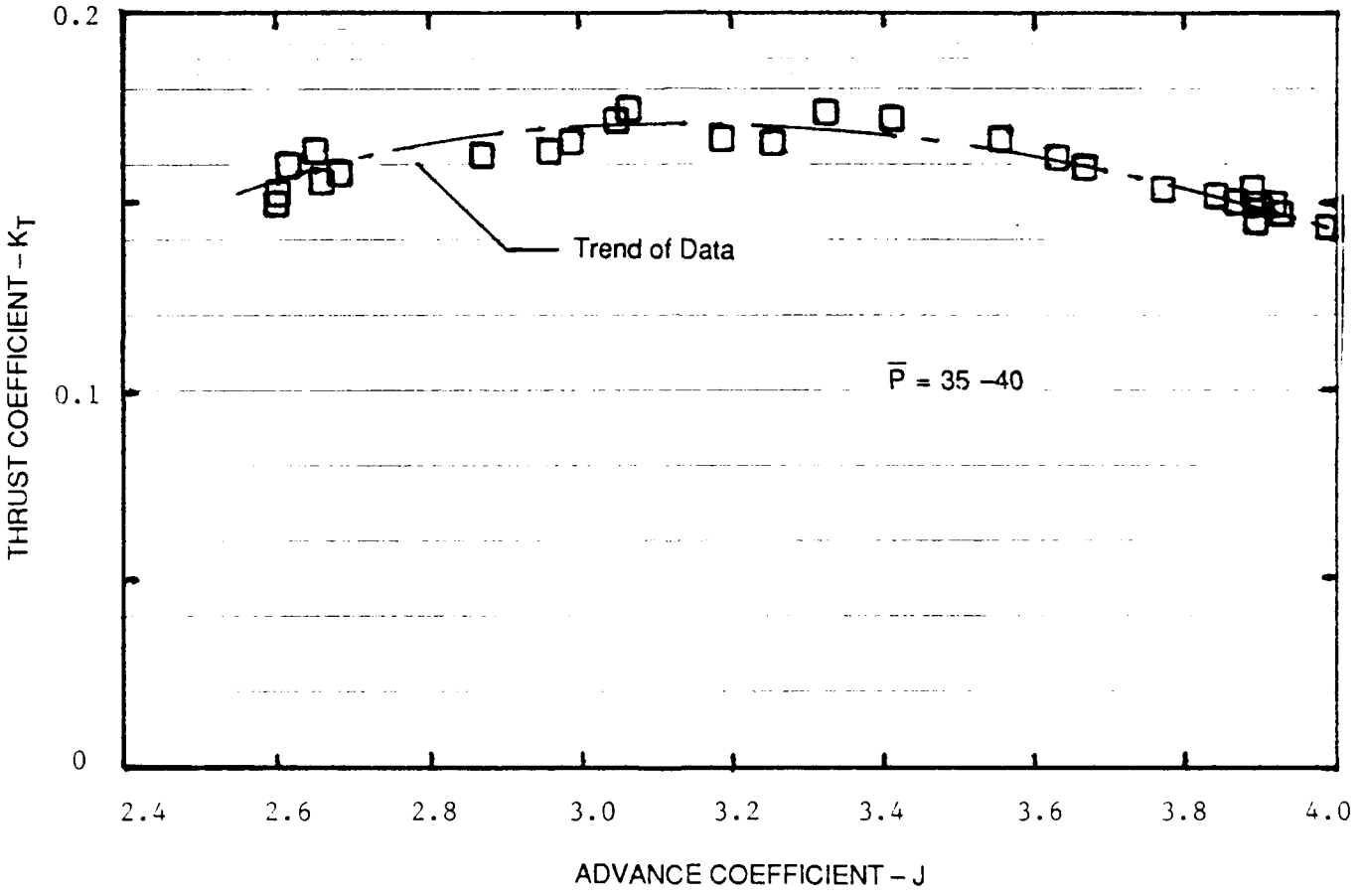

Figure 6-4. The Influence of Advance Coefficient on Thrust Coefficient – Combustion Data for Initial Tests, J ≅ 2.6, $\overline{P}$ = 35-40

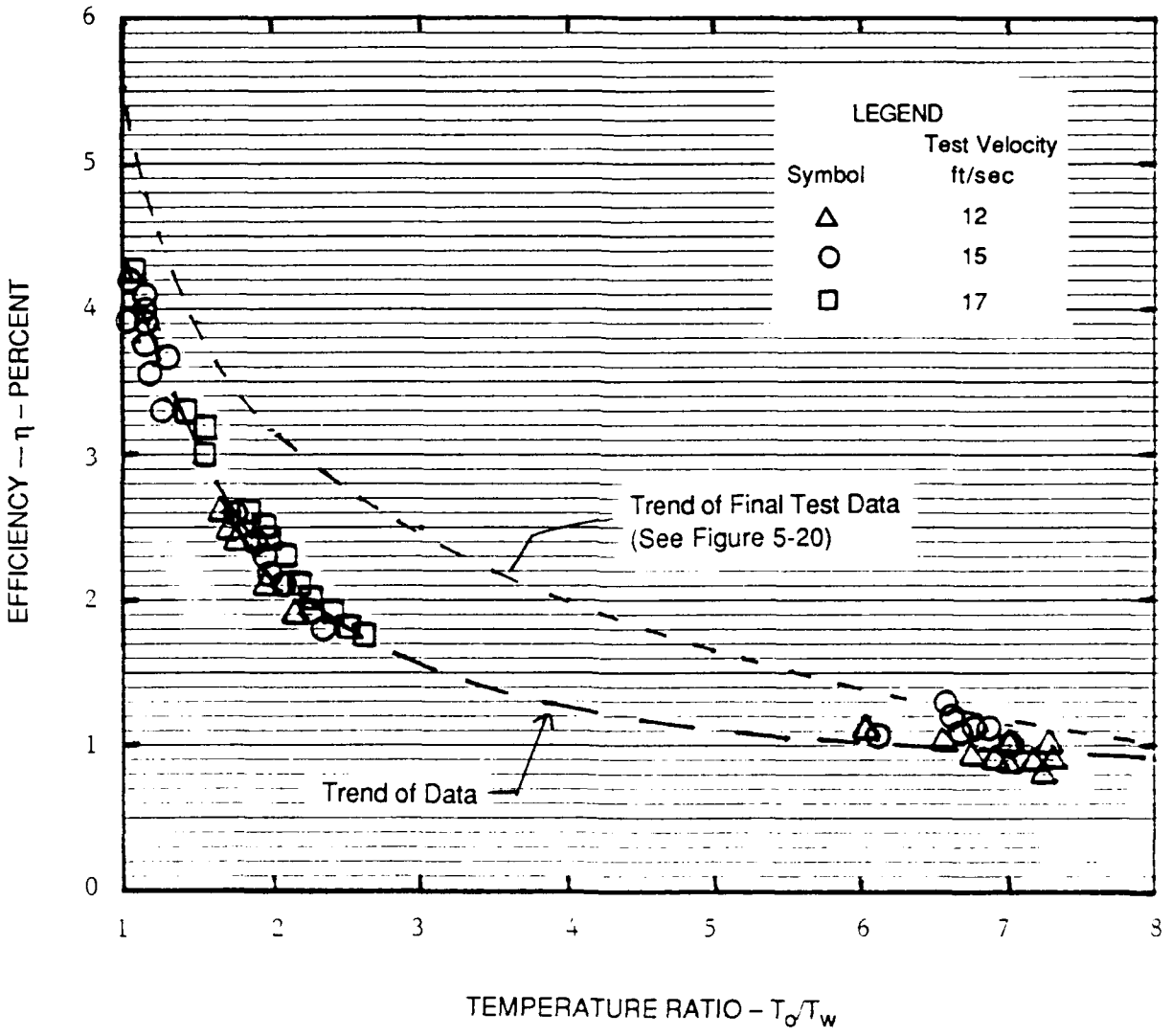

Figure 6-5. The Influence of Gas Temperature Ratio on Efficiency – Data for Initial Tests, $J \cong 2.6$, $\overline{P}$ = 35-40

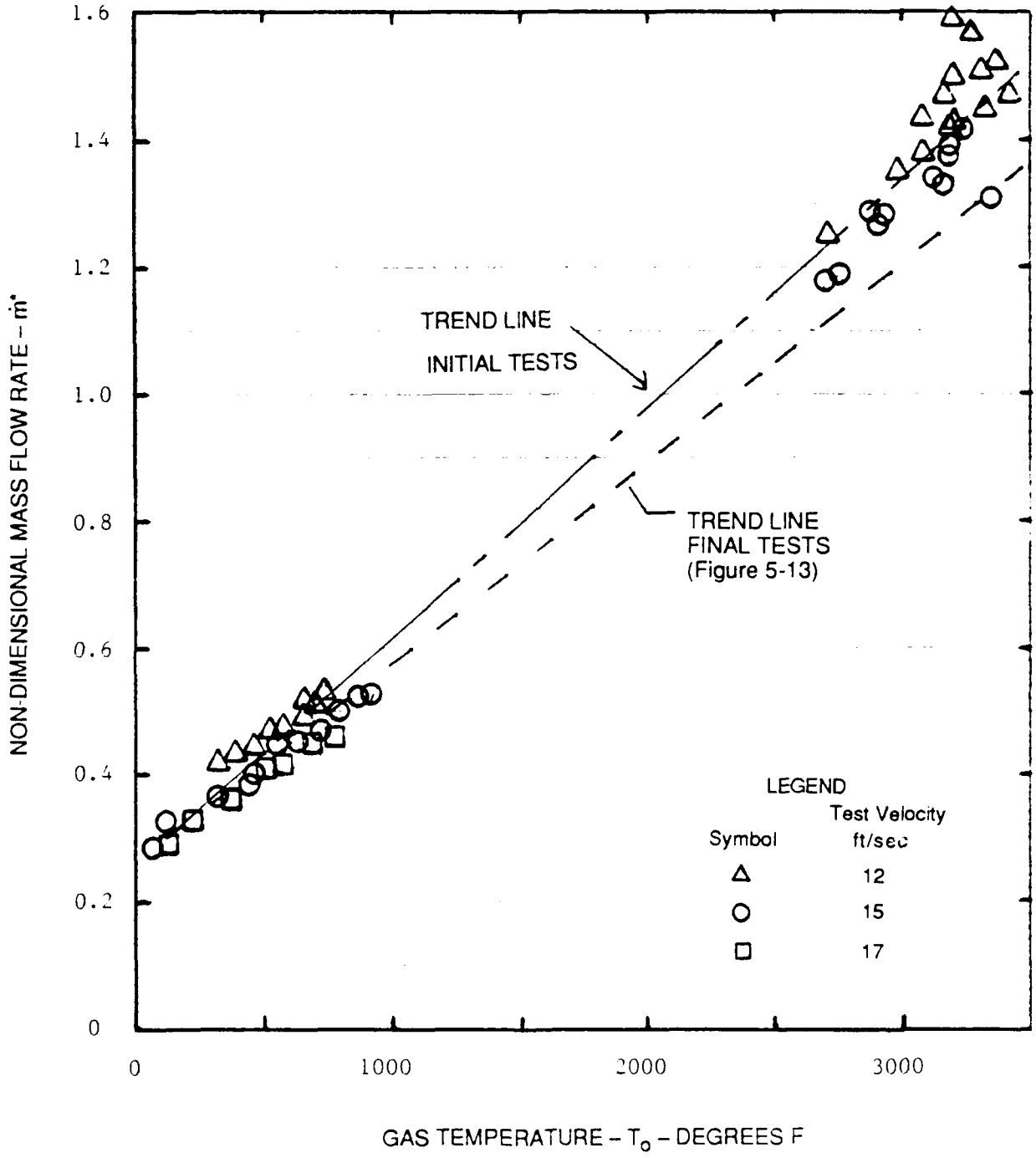

Figure 6-6. The Influence of Gas Temperature on Mass Flow Parameter – Data for Initial Tests, J as Noted, $\overline{P}$ = 35-40

deposits were not associated with any failure, they did indicate the possibility of incomplete or improper combustion of oil and resulting degradation of performance.

The forward rotor support shaft failed after only a few hours of testing. It was concluded that failure was due to a combination of flawed steel and the large oscillatory load imparted to the shaft by rotation and the use of a single gas port design. Rotor rotation produces a large, eccentric centrifugal acceleration of the water within the partially filled rotor. A large oscillatory force on the rotor results from the fact that the water always remains in the same physical position despite the rotation of the rotor. This oscillatory force will not exist when two or four gas ports are used and water is located symmetrically with respect to the rotor axis.

Damage in the form of local surface roughening, cracking and pitting of the seal surface was observed in the graphite seal installed in the combustion chamber assembly when this assembly was received from Solar (Figure 6-7). A new graphite seal was installed before initiation of testing. This seal began to show minor pitting after relatively little testing, as shown in Figure 6-8, and experienced severe pitting, shown in Figure 6-9, which necessitated its replacement after approximately thirty-five hours of operation or about one-half way through the tests. Another seal was installed and performed satisfactorily during the balance of the tests, although this seal showed surface roughness in areas where previous severe seal damage had been observed. It was concluded from this experience that the Solar provided graphite seals were probably not suitable for prototype operation or even for extended laboratory testing and that a more robust seal material was needed.

6.4 Summary

The results of the initial set of tests are generally similar in nature to those of the final set of tests. The primary difference in results were in the lower efficiencies and the somewhat greater heat losses observed in this initial set of tests. Based on a comparison of the results of the two sets tests it was concluded that the use of a round gas port rather than a trapezoidal gas port does have an adverse effect on water piston performance. Fouling of the combustion chamber and the HSC water appeared to be less severe during the first set of tests than during the final set.

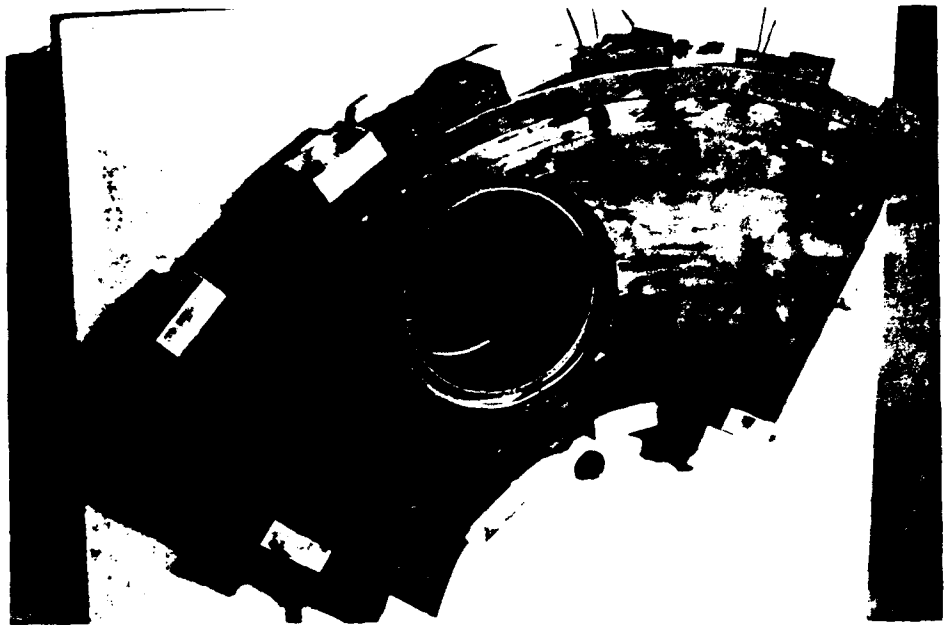

a. Overall View of Seal

b. Closeup of Crack and Pitting Damage

Figure 6-7. Damage to Seal Tested at SOLAR (Seal as received from SOLAR)

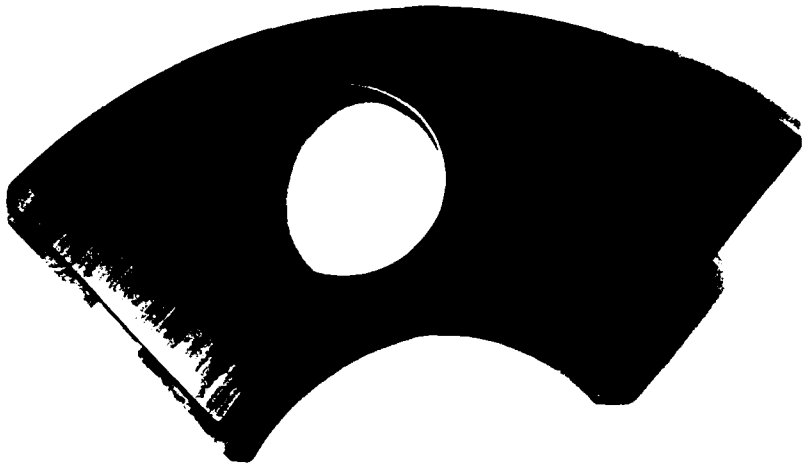

a. Evidence of Minor Scraping in Closure Portion of Seal (Upstream of Gas Port)

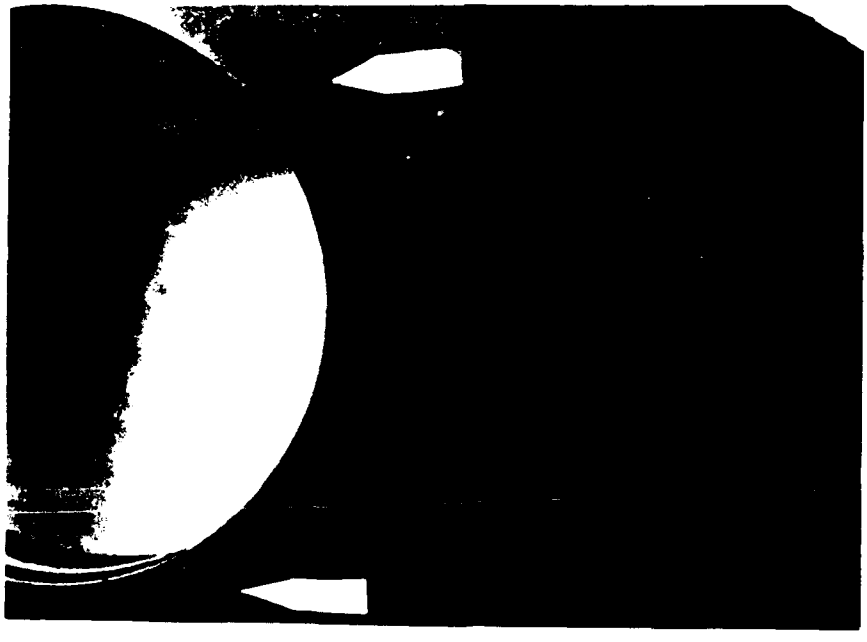

b. Small Pits in Expansion Portion of Seal (Downstream of Gas Port)

Figure 6-8. Minor Initial Damage to Seal Occurring During Initial Tests

a. Straight Lighting

b. Oblique Lighting

Figure 6-9. Two views of Serious Damage to Seal Used in Initial Tests at Tracor Hydronautics

7.0 CONCLUSIONS AND RECOMMENDATIONS

Based on the results of this study, a number of conclusions were reached and a number of recommendations for future study were suggested. These conclusions and recommendations are presented below.

7.1 Conclusions

The following conclusions were reached as a result of this study and the analysis of the data (primarily from the second set of tests) described in this report:

1. The rotor produced about 50 percent less thrust and about 40 percent less efficiency than predicted for cold gas with no heat losses when scaled to prototype conditions..

2. The rotor produced about 50 percent less thrust and about 83 percent less efficiency than predicted for gas at 3000 deg. F, with an estimated heat loss fraction of 0.67.

3. Gas leakage losses could not be measured directly but were estimated from indirect measurements to be small (approximately one percent) and thus were not a major reason for the poor measured performance.

4. Best performance was obtained at an advance coefficient approximately 14 percent greater than the design value, probably due to the smaller than design rotor inlet angle and the reduced inflow to and incomplete filling of the rotor flow passages due to significant inlet and flow passage losses and partial blockage of inflow by the fairing.

5. Performance was only modestly improved during the second set of tests in which the trapezoidal gas port was used.

6. None of the three additives injected into the flow passage had a measurable effect on performance.

7. There was significant circumstantial evidence that the combustion efficiency was relative low, probably due at least in part to the fact that the combustion chamber was designed to operate at the prototype pressure of 220 psia rather than the much lower pressures used in these tests.

8. Two graphite seals experienced significant damage after relatively few hours of operation while the bronze seal experienced measurable wear after relatively few hours of operation; based on observed damage during the tests the bronze seal appeared far more suitable for at-sea use.

9. Although no failure of or damage to the modified rotor shaft was observed, careful design will be required to prevent high-cycle fatigue failure of the rotor shaft resulting from the large eccentric loads on the rotor due to the use of a single gas port.

10. Tests data were highly repeatable and the variation of performance with operating parameters such as pressure coefficient and advance coefficient was in agreement with results of simplified analysis methods.

11. The present design is not suitable for the proposed design application due to its low thrust and efficiency and large heat losses, and it does not appear that a suitable water piston can be designed for this low speed application with current understanding and design tools.

12. Using the simplified theoretical analysis methods and empirical coefficients derived from the present test data it appears that the water piston will be an attractive propulsor for high speed applications such as torpedoes, where freedom to modify geometry is not severely limited and where heat losses should not exceed 25 to 35 percent.

7.2 Recommendations

Based on the results of this study and the conclusions presented above it is recommended that:

1. The water piston propulsion concept not be pursued for propulsion of the high speed amphibian until a more promising design approach can be developed.

2. Additional water piston tests and research should be conducted to explore its full potential and to determine:

a. The source(s) of the large observed discrepancies between measured and predicted performance
b. The attainable performance and heat losses for high speed, multiple gas port, small flow passage rotor designs suitable for underwater weapon applications
c. The performance gains attainable with variable area nozzles and small nozzle area ratios
d. The effect of other additives on heat losses
e. The effect of using low molecular weight gases such as hydrogen (the primary combustion of some liquid metal/seawater combustion processes) on heat losses and performance.

3. The performance analysis program be modified to provide a more accurate basis for predicting performance by more accurately accounting the effect of rotor inlet losses on the reduction of inflow velocity, the effects of passage shape and dimensions on internal flow losses, of varying of advance coefficient for a rotor of given inlet angle, of the large head losses that occur during the initial opening and closing of the gas port, and of time varying heat losses and non-adiabatic expansion of the gas.

Despite a number of recent water piston tests and studies conducted at Hydronautics, Incorporated and Tracor Hydronautics, knowledge about water piston performance remains very limited and incomplete. In order to properly assess the potential of this propulsion system for various applications it will be necessary to conduct well designed and experimental and theoretical research programs. The present program has clearly demonstrated the need to support tests with thorough theoretical analysis. Without such an analysis it would not have been possible to adequately understand the test results presented in this report.

8.0 REFERENCES

1. Zovko, C. T., "The Water Piston Propulsor," NOL Technical Note 66-222, January 1967.
2. Zovko, C. T., "The Water Piston Propulsor," NOL Technical Report 69-130, August 1969.
3. Zovko, C. T., "Several Unusual Propulsion Systems." Naval Engineers Journal, December 980, page 43.
4. Krishnamoorthy, V. and Johnson, Jr., V. E., "Investigation of a Water Piston Propulsor Powered by Compressed Gas," Tracor Hydronautics, Inc. Technical Report 8201-1, May 1983.
5. Krishnamoorthy, V. and Johnson, Jr., V. E., "Single Channel Tests of the Water Piston Propulsor," Tracor Hydronautics, Inc. Technical Report 82010.50-1, March 1985.
6. Krishnamoorthy, V. and Johnson, Jr., V. E., "Application of Water Piston Propulsor for Amphibious Vehicle Propulsion," Tracor Hydronautics, Inc. Technical Report 82010.24, May 1983.
7. Krishnamoorthy, V., "Water Piston Propulsor for Marine Corps Amphibious Assault Vehicle: An Exploratory Development Test Plan," Tracor Hydronautics, Inc. Technical Report 82010.36-1, April 1984.
8. Krishnamoorthy, V. and Johnson, Jr., V. E., "Conceptual Design Study of Water Piston Propulsion System for Marine Corps Tracked Amphibians," Tracor Hydronautics, Inc. Technical Report 83029-1, February 1984.
9. Swanek, R. and Johnson, Jr., V. E., "Status of the Water Piston Propulsor," Proceedings of ATTC August 1985 (Attached as Appendix A).
10. Johnson, Jr., V. E., Kobayashi, S., Bateman, R. and Krishnamoorthy, V., "Single Channel Investigation of Water Piston Propulsor Interface Stability and Heat Loss," Tracor Hydronautics, Inc. Technical Report 83012.07-1, December 1986.
11. Altmann, R., "A Test Plan to Characterize a Water Piston Propulsor," Tracor Hydronautics, Inc. Technical Report 86043-1, March 1987.
12. Kobayashi, S., "Water Piston Propulsor for Marine Corps Amphibious Assault Vehicles - On Adopting an Exit Nozzle of Variable Area Ration," Tracor Hydronautics, Inc. Technical Report 86043-2, September 1987.
13. Swanek, R. A. and Johnson, Jr., V. E., "Water Piston Propulsor for an Advanced Marine Corps Amphibian." Proc. of Intersociety Advanced Marine Vehicles Conference (AIAA), June 1988.
14. Perry's Chemical Engineers Handbook, Sixth Edition, McGraw-Hill Book Co.; 1984
15. McAdams, W. H. Heat Transmission, Third Edition, McGraw-Hill Book Co.; 1954